PREPARATION AND EVALUATION OF ACECLOFENAC LOADED MAGNETIC DEVICE FOR TARGETED DRUG DELIVERY SYSTEM

THESIS SUBMITTED FOR THE DEGREE OF
MASTER OF PHARMACY

JADAVPUR UNIVERSITY
2023

By
AMRITA DAS
Roll No. – 002111402030
Examination Roll No. – M4PHP23006
Registration No. – 160258 of 2021-2022

DEPARTMENT OF PHARMACEUTICAL TECHNOLOGY
FACULTY OF ENGINNERING AND TECHNOLOGY
JADAVPUR UNIVERSITY
KOLKATA – 700032
INDIA

JADAVPUR UNIVERSITY
KOLKATA – 700032

Title of the thesis

PREPARATION AND EVALUATION OF ACECLOFENAC LOADED MAGNETIC DEVICE FOR TARGETED DRUG DELIVERY SYSTEM

Name, Designation and Institution of the supervisor:

Dr. Kajal Ghosal, Assistant Professor

Department of Pharmaceutical Technology

Jadavpur University

Kolkata – 700032, India.

DEPARTMENT OF PHARMACEUTICAL TECHNOLOGY

FACULTY OF ENGINEERING AND TECHNOLOGY

JADAVPUR UNIVERSITY

CERTIFICATE OF APPROVAL

This is to certify that the thesis entitled "**PREPARATION AND EVALUATION OF ACECLOFENAC LOADED MAGNETIC DEVICE FOR TARGETED DRUG DELIVERY SYSTEM**" submitted by **Amrita Das**, of Jadavpur University, for the course of **Master of Pharmacy** is absolutely based upon his work under the supervision of **Dr. Kajal Ghosal**, Assistant Professor, Department of Pharmaceutical Technology, Jadavpur University, Kolkata and that neither his thesis nor any part of the thesis has been submitted for any degree/diploma or any other academic award anywhere before.

Kajal Ghosal
12.9.23

Dr. Kajal Ghosal
Assistant Professor
Department of Pharm. Tech
Jadavpur University
Kolkata - 700032

(Signature of M.Pharm thesis Guide)

Asst. Prof. Kajal Ghosal

Department of Pharmaceutical Technology

Jadavpur University, Kolkata – 700032.

12/9/23

Head
Dept. of Pharmaceutical Technology
Jadavpur University
Kolkata-700032, W.B. India

(Signature of Head of the Department)

Prof. (Dr.) Sanmoy Karmakar

Department of Pharmaceutical Technology

Jadavpur University, Kolkata – 700032.

Saswati Majumdar
12.9.23

(Signature of Dean)

Faculty of Engineering and Technology
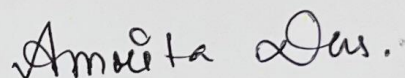
Jadavpur University, Kolkata – 700032.

DEAN
Faculty of Engineering & Technology
JADAVPUR UNIVERSITY
KOLKATA-700 032

DECLARATION BY THE CANDIDATE

I do hereby declare that the work incorporated in the thesis entitled "**PREPARATION AND EVALUATION OF ACECLOFENAC LOADED MAGNETIC DEVICE FOR TARGETED DRUG DELIVERY SYSTEM**" has been carried out by me in the Department of Pharmaceutical Technology, Jadavpur University under the supervision of Dr. Kajal Ghosal, Assistant Professor, Department of Pharmaceutical Technology, Jadavpur University, Kolkata – 700032. Neither the thesis nor any part therefore has been submitted for any other degree.

Date: 12/9/23

Place: Kolkata, India

Signature of the candidate

(AMRITA DAS)

Dedicated to my Guide and

My Family

ACKNOWLEDGEMENT

Date: 12/9/23   AMRITA DAS

PREFACE

The thesis presented here, titled **"PREPARATION AND EVALUATION OF ACECLOFENAC LOADED MAGNETIC DEVICE FOR TARGETED DRUG DELIVERY SYSTEM"** delves into the intricate realm of synthesizing magnetite using the co-precipitation method. Additionally, this research endeavors to create magnetic beads loaded, with the primary objective of facilitating targeted drug delivery while mitigating the potential side effects associated with drug administration.

- ❖ Chapter 1 introduces the fundamental concepts underpinning magnetic targeting, covers diverse approaches to magnetite preparation, discusses surface chemistry and modification, and explores various applications of MNPs. Additionally, it provides a list of commercially available micro and nano magnetic products.
- ❖ Chapter 2 presents a comprehensive literature survey on the relevant subject matter.
- ❖ In Chapter 3, the aims, objectives, and the planned work sequence are outlined.
- ❖ Chapter 4 catalogs the materials utilized in the project.
- ❖ Chapter 5 encompasses the procedures for magnetite and MNPs bead preparation, along with a description of the characterization techniques employed.
- ❖ Chapter 6 delves into the presentation and discussion of the results.
- ❖ Finally, Chapter 7 offers a summary and conclusion of the present work.

Contents

List of Tables

Table no.	Title
1.	Various green synthesis methods of magnetic nanoparticles.
2.	Various co-precipitation synthesis methods of MNPs.
3.	Different processes of synthesis of MNPs by thermal decomposition methods .
4.	Classes of coating materials
5.	Potentially therapeutic MNP coatings material.
6.	Commercially available micro and nano magnetic products.
7.	Magnetic nanoparticles beads formulation.
8.	Physical properties of aceclofenac .
9.	Absorbance of aliquots of aceclofenac at λmax 273.60nm.
10.	Percentage yield and entrapment efficiency result of the prepared formulations.
11.	%CDR Calculation of F1 formulation
12.	%CDR Calculation of F2 formulation
13.	%CDR Calculation of F3 formulation
14.	%CDR Calculation of F4 formulation
15.	%CDR Calculation of F5 formulation

List of Figures

List of Abbreviations

CFO - cobalt ferrite

CTAB - cetyltrimethylammonium bromide

Cup - N-nitrosophenyl hydroxylamine

DOX - Doxorubicin hydrochloride

EDTA - Ethylenediaminetetraacetic acid

EVAc - Ehylene-vinyl acetate copolymer

IONPs - Iron oxide nanoparticles

MDT - Magnetic drug targeting

MNPs - Magnetic nanoparticles

MRI - Magnetic resonance imaging

NDDS- Novel drug delivery systems

NSAID - Non-Steroidal Anti-Inflammatory Drug

NPs- Nanoparticles

PEG - Polyethylene glycol

PEI - Polyethylenimine

PEO- Polyethylene oxide

PLGA –Poly(lactic-co-glycolic acid

PPT- Precipitate

PVA - Polyvinyl alcohol

SDS - sodium dodecyl sulfate

SDT - switching duration time

SS -Summer Savory

SPIONs - Superparamagnetic iron oxide nanoparticles

TPP - Tripolyphosphate

TREG - Tri(ethylene glycol)

USPIONs- Ultrasmall superparamagnetic iron oxide nanoparticles

Chapter 1

Introduction

1.1 Introduction to NDDS

Novel drug delivery systems (NDDS) are a contemporary category of drug delivery systems that have several benefits in comparison to traditional dosage forms. Conventional dosage forms often encounter challenges pertaining to high dosage administration, limited bioavailability, instability, first-pass metabolism, fluctuation of plasma drug levels, and fast drug release. The issues mentioned may be effectively addressed by the use of NDDS, which aims to improve the effectiveness, safety, patient adherence, and lifespan of the product [1].

Nanoparticles (NPs) find use across a diverse range of applications and may be synthesised using several methods. NPs are defined as particles with dimensions ranging from 1 to 100 nanometres [2]. These entities possess a size that enables their interaction with cellular and tissue structures, while also providing sufficient capacity for the transportation of therapeutic substances. There are many different kinds of nanoparticles that can be used for drug delivery. Magnetic nanoparticles (MNPs) are a type of nanoparticle that has garnered growing attention due to their unique properties including size, magnetic behaviour, biocompatibility, chemical stability [3].

1.2 Introduction to Magnetic Nanoparticle

In the ever-evolving landscape of medical science and technology, the field of drug delivery has emerged as a pivotal avenue for revolutionizing the efficacy and specificity of therapeutic interventions. Traditional methods of drug administration often suffer from limitations such as non-specific biodistribution, suboptimal therapeutic concentrations, and systemic toxicities. To overcome these challenges, researchers have turned to nanotechnology to design innovative and precise drug delivery systems. Among these novel approaches, magnetic nanoparticles (MNPs) have garnered significant attention due to their unique ability to manipulate drug transport and distribution through the application of external magnetic fields.

Magnetic nanoparticles, often on the nanometre scale, possess distinctive physical properties that make them amenable to controlled drug delivery. These nanoparticles exhibit promising properties that can be leveraged in diverse fields such as magnetic fluid catalysis, biotechnology, MRI, biomedical sciences, healthcare, drug delivery systems, agriculture, food industry, textiles, defence and aerospace sectors, as well as environmental remediation efforts. [4]. Magnetic nanoparticles (MNPs) are a prominent class of nanoscale materials, typically ranging from 1 to 100 nm in size. These particles possess remarkable properties such as

superparamagnetism, ferrimagnetism, and ferromagnetism which can be manipulated using an applied magnetic field, offering numerous possibilities in the field of biomedicine. MNPs with superparamagnetic properties are particularly fascinating due to their ability to exhibit strong magnetic interactions when subjected to an applied magnetic field, while lose them in absence of the magnetic stimulus. This unique property opens up possibilities for the development of ferrofluids and also paves the way for their use in in vivo applications. For instance, they can serve as (i) cellular labelling agents [5], (ii) drug delivery systems guided by a magnetic stimulus [6], (iii) imaging enhancers [7], and (iv) heat generators in hyperthermia therapy [8].

The two primary constituents of MNPs are the nucleus and the shell. The nucleus comprises magnetic elements such as Fe, Co, or Ni and their related oxides, plays a significant role in the quantum effect and magnetic properties. On the other hand, the shell is essential for stabilising the core and shielding it from the chemical effects of the environment [9]. The coating also imparts unique characteristics to the nanoparticles. These nanoparticles can be functionalized with biocompatible coatings and loaded with therapeutic agents, allowing for targeted delivery to specific tissues or cells. Importantly, the application of an external magnetic field enables researchers to guide and enhance the transport of these nanoparticles, thereby directing the delivery of therapeutic payloads to desired sites within the body. This magnetic guidance system offers unprecedented precision, ensuring not only improved therapeutic efficacy but also reduced off-target effects and minimized systemic toxicity [10]. Drugs can either be attached to the surface of magnetic nanoparticles (MNPs) or incorporated within them, following which the MNP surface is coated with a protective layer and functionalized with ligands, enzymes, linkers, and active molecules. This enables targeted delivery of the drug to its intended location [11]. These nanoparticles can be functionalized with biocompatible coatings and loaded with therapeutic agents, allowing for targeted delivery to specific tissues or cells. Importantly, the application of an external magnetic field enables researchers to guide and enhance the transport of these nanoparticles, thereby directing the delivery of therapeutic payloads to desired sites within the body. This magnetic guidance system offers unprecedented precision, ensuring not only improved therapeutic efficacy but also reduced off-target effects and minimized systemic toxicity.

The utilization of magnetic nanoparticles for drug delivery holds immense promise across various medical domains. From treating localized diseases such as cancers, where site-specific drug release is imperative, to addressing neurodegenerative disorders that demand precise delivery across the blood-brain barrier, the versatility of MNPs offers a plethora of possibilities.

Additionally, magnetic nanoparticles can facilitate the controlled release of drugs over time, leading to prolonged therapeutic effects, reduced dosing frequencies, and enhanced patient compliance.

This thesis embarks on a comprehensive exploration of the fascinating realm of magnetic nanoparticles for drug delivery. By delving into the underlying principles of magnetic interactions, synthesis method, and surface functionalization or surface modification, this work aims to provide a thorough understanding of how these nanostructures can revolutionize the field of drug delivery. Furthermore, through an in-depth review of current research and cutting-edge advancements.

As we venture into this captivating realm of nanomedicine, the potential to reshape the landscape of disease treatment and patient care is immense. By harnessing the capabilities of magnetic nanoparticles, we have the prospect to usher in a new era of targeted and personalized therapeutics, ultimately improving the lives of countless individuals around the globe.

1.3 Advantages of Magnetic Nanoparticle based NDDS [12]:

Novel drug delivery systems offer several advantages compared to traditional methods of drug administration. These advancements aim to improve the efficacy, safety, and convenience of delivering medications to patients. Here are some of the key advantages:

Improved Therapeutic Efficacy: Novel drug delivery systems have the potential to increase the therapeutic effectiveness of drugs by providing controlled and targeted release. This ensures that the drug reaches the desired site of action in the body at the right concentration and for the appropriate duration, optimizing its effectiveness.

Targeted Delivery: These systems enable precise targeting of drugs to specific tissues, cells, or organs. This reduces the exposure of healthy tissues to the drug, minimizing side effects and enhancing the therapeutic index of the medication.

Reduced Side Effects: Controlled release and targeted delivery help minimize the systemic distribution of drugs, reducing the potential for adverse effects on non-targeted tissues and organs. This is particularly important for drugs with a narrow therapeutic window.

Improved Patient Compliance: Some novel drug delivery systems, such as transdermal patches or long-acting injections, can simplify the dosing regimen and improve patient

compliance. This is especially beneficial for patients who have difficulty adhering to complex medication schedules.

Steady Plasma Levels: Controlled-release systems maintain more consistent drug plasma levels over time. This can lead to a more predictable and stable therapeutic effect, avoiding the peaks and troughs associated with conventional dosing.

Prolonged Duration of Action: Some novel delivery systems can provide prolonged drug action, reducing the frequency of administration. This is advantageous for chronic conditions and can improve the patient's quality of life.

Reduced Dosage Frequency: Extended-release formulations and other novel methods can often allow for less frequent dosing, which can be especially beneficial for medications that need to be taken multiple times a day.

Minimized First-Pass Metabolism: For drugs that undergo extensive first-pass metabolism in the liver, novel delivery systems can bypass this process, leading to higher bioavailability and more effective drug delivery.

Enhanced Bioavailability: Drug formulations that enhance solubility and permeability can improve the bioavailability of poorly soluble drugs, making them more effective.

Customizable Release Profiles: Novel delivery systems can be engineered to release drugs with specific profiles, such as immediate, sustained, pulsatile, or triggered release, based on the therapeutic requirements.

Minimized Drug Interactions: By controlling the timing and location of drug release, novel delivery systems can minimize potential drug interactions that could occur when multiple drugs are taken together.

Suitable for Labile Drugs: Labile drugs (drugs prone to degradation) can be protected and delivered effectively using specialized delivery systems, preserving their therapeutic activity.

1.4 Basic concepts - The fundamental laws governing magnetic targeting.

The concept of magnetic targeting is based on the principle that magnetic nanoparticles are drawn towards an externally applied magnetic field. When a magnetic material is subjected to

a magnetic field with a strength denoted as H, the combined response of the individual atomic moments in the material is referred to as magnetic induction, denoted as B.

$$B = \mu_0(H + M)$$ (Equation 1)

Where, μ_0 = magnetic permeability

M = Intensity of magnetization

In the presence of a magnetic field gradient, a translational force is exerted on the particle-drug complex, causing it to be attracted towards the magnet. Consequently, this force traps the complex within the designated region at the target site, ensuring its confinement in that specific area. (figure 1) [13].

$$F_{mag} = (x_2 - x_1) * v * 1/\mu_0 * B(\nabla B)$$ (Equation 2)

Where, B = magnetic field strength

∇B = field gradient, which can be reduce to $\partial B/\partial x$, $\partial B/\partial y$, $\partial B/\partial z$

$x_2 - x_1$ = is the effective magnetic susceptibility of the particle relative to the medium.

$x_1 < x_2$, thereby x_1 takes no account in the case of biological system.

v = volume of the particle
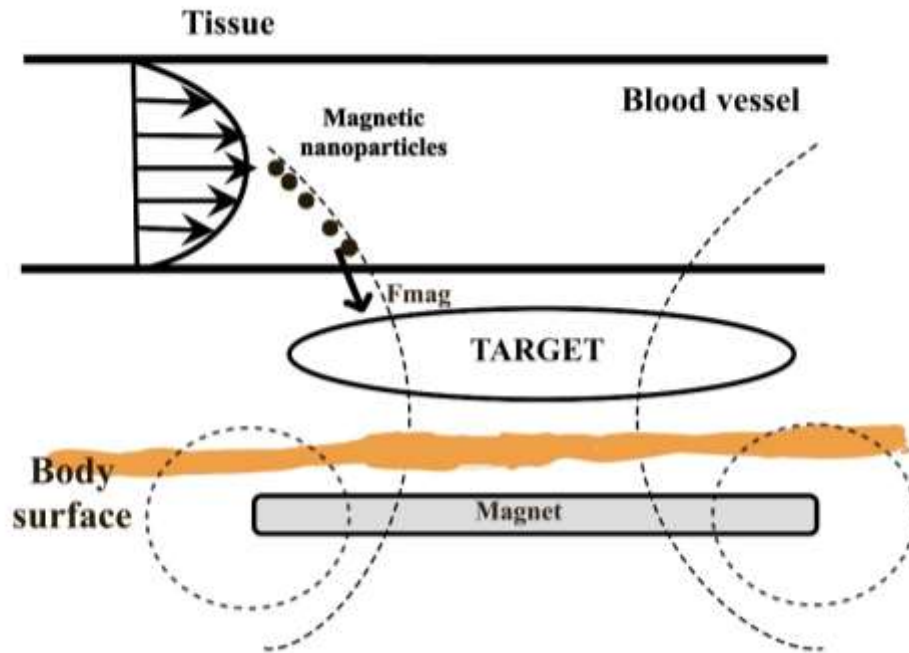
Figure 1: A simplified representation of drug delivery via magnetic nanoparticles. Figure redrawn after Jon Dobson [14]

From equation ii., It can be inferred that magnetic properties and size of nanoparticles, as well as the strength and gradient of the magnetic field, play significant roles in ensuring effective nanoparticle capture. Moreover, there is a clear correlation between the ability to trap nanoparticles and the intensity of the magnetic field. If the field strength decreases, the capability to capture nanoparticles diminishes. [13].

1.5 Factors to be considered during synthesis

When developing a magnetic nanoparticle-based targeting system, several factors must be considered, including both physical and physiological parameters. Physical parameters encompass the magnetic properties, field strength, size and shape of the carrier particles, geometry of the magnetic field, as well as the capacity of the particles to bind drugs or genes. Physiological parameters, on the other hand, involve factors like the rate of blood flow, blood supply, the depth of targeted region within the body, the individual's body weight, age and gender [14].

1.6 Synthesis method of Magnetic nanoparticles

Various strategies for synthesizing magnetic nanoparticles (MNPs) have been extensively described in numerous publications. These include well-known techniques like green synthesis, precipitation from solution, microemulsion, co-precipitation, thermal decomposition, and several other methods. Moreover, apart from the mentioned methods, magnetic nanoparticles (NPs) can also be prepared using additional processes like electrochemical synthesis, microorganism or bacterial synthesis (particularly magnetostatic bacteria and iron reducing bacteria), and even through laser pyrolysis techniques and so on. and so on. Many new and promising techniques have been established for synthesising Fe_3O_4 nanomaterials with various geometric forms, including nanorods, nanotubes, and hierarchical superstructures [15].

A. Green synthesis of MNPs

Green synthesis of magnetic nanomaterials (MNP) has garnered a great deal of interest in researchers. This approach involves the utilization of bioactive agents, such as inactivated plant tissue, plant extracts (e.g., Tridax procumbens), exudates[16,17], fungi, algae (such as Kappaphycus alvarezii), and bacteria, to facilitate the transformation of metal ions into their elemental form, leading to the formation of metal nanoparticles with sizes ranging from 1 to 100 nm [18,19].To synthesize magnetic MNP various methods (table 1) can be employed which are less costly , environment friendly, scaled up easily for large scale, and this method is not subjected to high pressure, temperature, energy and toxic chemical [16]. Plant components are known to contain various bioactive compounds, including alkaloids, flavonoids, carotenoids, starch, carbohydrates, proteins, essential oils, and amino acids, which serve as stabilizing agents, capping, and reducing. For instance, P.K. Dhar (2021) reported the utilization of Lathyrus sativus peel extract for the green synthesis of Fe_3O_4-NPs (iron oxide nanoparticles) [20].

Equations (1) and (2) provide a concise summary of the chemical reaction involved in the formation of Fe_3O_4-NPs:

Equation 1- Lathyrus sativus peel extract + Fe^{2+} + Fe^{3+} (aq) + $H_2O_{(l)}$ → stirring→[Lathyrus sativus -Fe^{2+}/Fe^{3+}]

Equation 2- [Lathyrus sativus -Fe^{2+} +Fe^{3+}]+$8OH^-$(aq)× → Stirring Δ→ [Lathyrus sativus -/Fe_3O_4](s)↓ + $4H_2O$(aq)

The peel extract of Lathyrus sativus contains phytochemicals that effectively reduce iron salts, facilitating the formation of Fe_3O_4-NPs. This natural process offers several advantages, including simplicity, speed, and cost-effectiveness, without the need for the incorporation of harmful chemicals.

To develop biomedical applications for NPs, methods need to be reliable, biocompatible, biodegradable, non-toxic, and eco-friendly (figure2).

Chin et al. used the thermal decomposition method to make Fe_3O_4 NPs without involving toxic organic surfactants or harmful organic solvents [2]. To obtain Fe3O4 nanoparticles with precise particle size and a narrow size distribution, using polyethylene oxide (PEO) as both a solvent and surfactant. PEO is commonly employed as a green solvent due to its low toxicity and minimal environmental impact. Moreover, PEO demonstrates efficacy as a surface-active

agent, effectively preventing the agglomeration of the nanoparticles during the synthesis process [2,10]
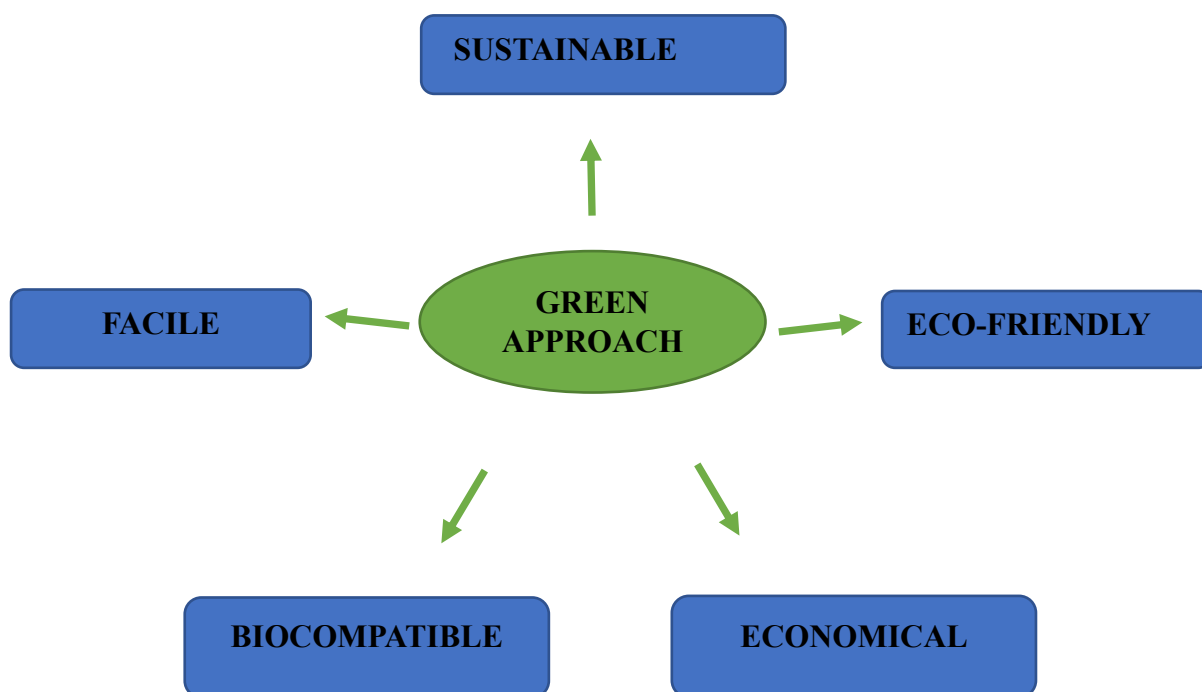
Figure 2 : The benefit of green MNPs.

Table 1 : Various green synthesis methods of magnetic nanoparticles.

Main reagent(s)	Green regent(s)	Aim	Process condition(s)	MNP size	References
$FeSO_4.7H_2O$ and Fe $(NO_3)_3.9H2O$	Eucalyptus leaves	Design and validation of an eco-friendly approach for synthesizing molecularly imprinted polymers using environmentall	Green nanoparticle was synthesized in a water bath at 70^0C under inert atmosphere with N_2	20−40 nm.	[16]

		y friendly nanoparticles			
$FeCl_3.6H_2O$	tea residue	Arsenic removal from aqueous solution	$FeCl_3.6H_2O$ pre-treated with tea extracts and was heated in a furnace at 450^0C for 6 h.	5–25 nm	[21]
$Fe(NO_3)_3.9H_2O$	green tea extract	To synthesize Fe_3O_4 MNPs by a modified greener method.	The $Fe(NO_3)_3.9H_2O$ and green tea extract were mixed in a 1:2 ratio. The mixer was kept in the furnace at 180^0C, 200^0C and 220^0C for 2 hours	25-30nm	[22]
$Fe(NO_3)_3 \cdot 9H_2O$, Cobalt nitrateis $(Co(NO_3)_2 \cdot 6H_2O)$	Okra (A. esculentus) extract	To synthesize nanoparticles that demonstrate remarkable antimicrobial efficacy against a wide range of bacterial and fungal strains.	A mixture of $Co(NO_3)_2 \cdot 6H_2O$ and $Fe(NO_3)_3 \cdot 9H_2O$ was prepared in a 1:2 molar ratio. Okra extract was then added dropwise to the mixture at room temperature and stirred.	300-500nm	[23]

Ferric III chloride (FeCl$_3$)	Cinnamomum verum bark extract	synthesise and characterise Fe-NP utilising the extract of Cinnamomum Verum	FeCl3 solution and bark extract were mixed 1:1 to synthesise Fe-NPs. The reaction mixture then was centrifuged at 10,000 rpm for 15 min.	20− 50 nm	[24]

B. Precipitation from solution

The precipitation of products from solutions is an ancient method to produce NPs. The precipitation method has been widely employed for the synthesis of magnetite (Fe3O4) nanoparticles from a solution. This method involves the controlled mixing of iron(II) and iron(III) salts in an aqueous solution, followed by the addition of a base to induce precipitation. The formation of magnetite occurs through a redox reaction between the iron(II) and iron(III) ions. The pH of the solution plays a critical role in controlling the size, morphology, and magnetic properties of the resulting magnetite particles. By carefully adjusting the pH to a range between 9 and 10, a favorable environment is created for the nucleation and growth of magnetite crystals. The continuous stirring of the solution for an extended period allows the particles to form and reach the desired size. Optionally, the reaction temperature can be elevated to accelerate the reaction kinetics. Once the precipitation is complete, the magnetite particles are separated from the solution by decantation or centrifugation, followed by thorough washing to remove any residual impurities. The collected magnetite nanoparticles can then be dried and utilized for various applications in fields such as biomedicine, environmental remediation, and magnetic data storage. The versatility and simplicity of the precipitation method make it a popular choice for the synthesis of magnetite nanoparticles with tailored properties. [2].

C. Co-Precipitation

Co-precipitation is an uncomplicated and practical way for synthesising iron oxides from aqueous solutions containing Fe^{2+}/Fe^{3+} salt. In this method, a base is added under an inert atmosphere at ambient or elevated temperatures to facilitate the synthesis process [25, 26]. Table 2 presents the synthesis of magnetic nanoparticles (MNPs) using the co-precipitation method under various conditions. The size, structure, and composition of the magnetic nanoparticles formed are profoundly influenced by key factors, including the Fe^{2+} to Fe^{3+} ratio, reaction temperature, pH value, and ionic strength of the media. By establishing and maintaining specific synthesis conditions, the production of magnetite nanoparticles becomes highly reproducible, ensuring consistency in their properties [5,27]. In co-precipitation, produced particles are polydisperse type. Controlling the initial burst of nucleation followed by a controlled, gradual growth process is pivotal in achieving monodisperse iron oxide magnetic nanoparticles. Organic additives, serving as stabilizers and/or reducing agents at suitable concentrations, are employed to create monodisperse MNPs with diverse sizes. Ethylenediaminetetraacetic acid (EDTA) is widely utilized to effectively stabilize magnetite nanoparticles, safeguarding them from aggregation under specific conditions.

In a closed system, oxygen may be removed from the solution by bubbling nitrogen gas through the reaction medium. Nanoparticles formed in this way may be extracted from the solution using centrifugation, magnetic decantation, or both [28]. Figure 3 illustrates the synthesis process of magnetic nanoparticles (MNPs) using the co-precipitation method.

The following is a potential reaction chain that leads to Fe_3O_4 nanoparticle formation:
$Fe^{2+} + 2Fe^{3+} + 8OH^- \rightarrow Fe(OH)_2 + 2Fe(OH)_3 \rightarrow Fe_3O_4\downarrow + 4H_2O$ [27].
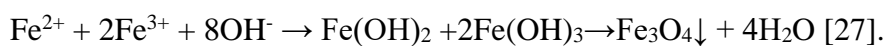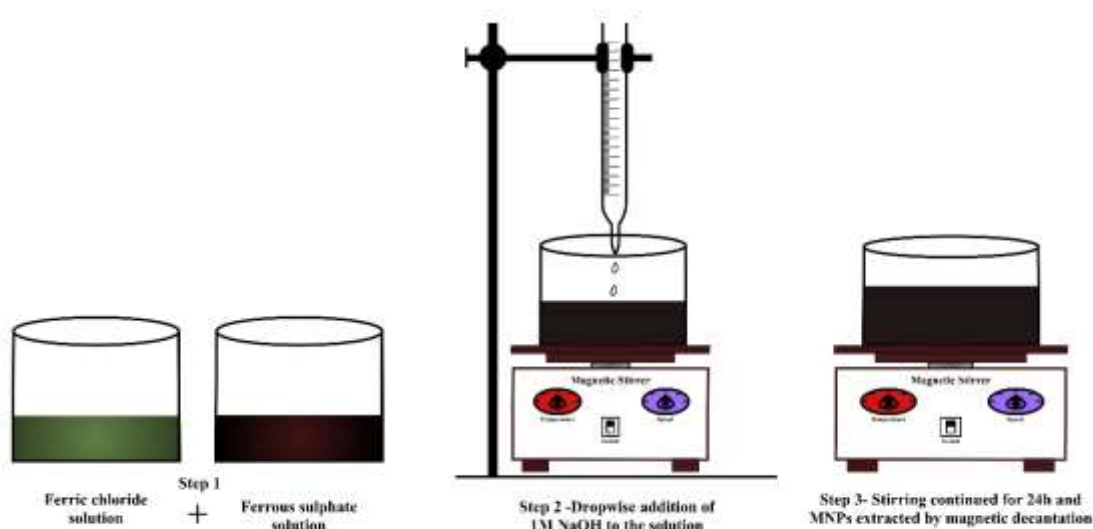
Figure 3: Co-precipitation method for the synthesis of magnetic nanoparticles. Step1: Mixing of FeCl$_3$ solution and FeSO$_4$, step 2: stirring the solution at 80-85°C, and dropwise addition of NaOH, step 3: stirring continued for 24hrs and then precipitated MNPs are extracted either by magnetic decantation or centrifugation or both. Further the extracted MNPs are dried and ground.

Table 2: Various co-precipitation synthesis methods of MNPs.

Main reagent(s)	Other reagent(s)	Aim	Process conditions	size	References
FeCl$_2$.4H$_2$O, FeCl$_3$.6H$_2$O, Fe(NO$_3$)$_3$.9H$_2$O, FeSO$_4$.7H$_2$O, Fe$_2$(SO4)$_3$	NaOH	To synthesize and investigate the MNPs formed by different precursor of Fe^{2+} and Fe^{3+}	A solution of Fe^{3+} and Fe^{2+} ions was treated with NaOH solution and stirred for a duration of 3 minutes. The resulting precipitate was then subjected to a	12 nm and 5 nm	[29]

			drying process at 80°C for 12 hours.		
FeCl$_2$.4H$_2$O, FeCl$_3$.6H$_2$O	Polyethylene Glycol (PEG)4000, Oleic Acid (OA), Tetra ethoxysilane (TEOS), Iso-butanol, NH$_3$ and NaOH	Estimation Toxicity NP by the MTT assessment	In Fe salt solution NaOH solution was added and stirred. To synthesize MNPs, PEG solution was introduced and continuously stirred at a speed ranging from 400 to 700 rpm.	10 nm	[30]
FeCl$_3$.6H$_2$O, FeCl$_2$.4H$_2$O	NH$_4$OH	To utilize the co-precipitation method for the formation of MNPs.	NH$_4$OH was added to the solution of FeCl$_3$.6H$_2$O and stirred at different speeds of 300, 400, and 500 rpm. The temperature was gradually increased to 40°C, 60°C,	2.7 to 3.3 μm	[19]

			and 80°C. The resulting precipitate was filtered and subsequently dried at 100°C for a duration of 150 minutes.		
$FeCl_3$ and $FeCl_3.6H_2O$, $Fe(NO_3)_3.9H_2O$	NaOH, ammonia solution, potassium iodide (KI) and PVA	Synthesis of MNP using iron(III) salts as Precursors.	3:1 M ratio sol. of iron salt and KI solution. Iodine formed was filtered out and hydrolysed with NaOH. Ppt was filtered and dried at 250^0C	7.8 ± 0.05 nm	[31]
Fe(NO3)3·9H2O, Holmium(III)nitrate pentahydrate	Ethanol, NH_3 solution	To evaluate the optical and magnetic properties of nanocrystalline $HoFeO_3$.	Magnetite formed was dried in room temp.	25-30 nm	[32]
Iron (III) chloride, iron (II) chloride	Sucrose $(C_{12}H_{22}O_{11})$, NaOH	To compare MNPs obtained via	$C_{12}H_{22}O_{11}$ was added to Fe salt	4nm	[33]

		co-precipitation and hydrothermal methods.	solution. Then NaOH was dropwise added to it. Ppt was separated by centrifugation at 3000rpm for 10mins and then dried at 50^0C		
$FeCl_3 \cdot 6H_2O$, $FeSO_4$	Chitosan	To synthesize magnetic composites below 1 μm in size using biodegradable polymers through the co-precipitation method.	A solution containing Fe3+ and Fe2+ ions was stirred at 70°C under a nitrogen atmosphere for 25 minutes. Subsequently, NaOH was added to the solution to precipitate.	498nm	[34]

D. Thermal decomposition

NPs with precise size control and a high level of monodispersity can be synthesized through the thermal decomposition of organometallic precursors, including $[Mn^{n+}(acetylacetonate)_n]$ (where M represents metals like Fe, Mn, Co, Ni, Cr, and n is 2 or 3), $M^X (Cup)_X$ (where Cup refers to N-nitrosophenyl hydroxylamine), and carbonyls (such as iron pentacarbonyl). This decomposition process is carried out using organic solvents and surfactants such as fatty acids, hexadecylamine , and oleic acid [35]. Notably, maghemite nanocrystals have been successfully synthesized by introducing $Fe(Cup)_3$ solutions in octylamine into long-chain amines at temperatures ranging from 250°C to 300°C, as demonstrated by Alivisatos and colleagues. Nanocrystals ranging from 4 nm to 10 nm in size demonstrate excellent dispersibility in organic liquids [5].

The size and shape of magnetic nanoparticles primarily relies on the proportions of the initial chemicals, which encompass organometallic substances, surfactants, and solvents [36]. Additionally, accurate regulation of size and shape may be influenced by the reaction temperature and reaction time [37].

Direct thermal decomposition of metal antecedent (iron pentacarbonyl) to produce metal nanoparticles is not achievable owing to the zero-valency of the metal in the precursor.
However, by decomposing iron pentacarbonyl in octyl ether and oleic acid at 100°C, and subsequently adding trimethylamine oxide $(CH_3)_3NO$ as a mild oxidant at high temperatures, homogeneous dispersion of γ-Fe_2O_3 nanocrystals is obtained with an average size of approximately 13 nm (as shown in figure 4). Cationic metal-complexes such as $[Fe(acac)_3]$ can be decomposed directly into metal nanoparticles like Fe_3O_4. This can be achieved by combining 1,2-hexadecanediol, oleylamine and oleic acid in presence of phenol ether [5]. Table 3 lists a few more instances of MNPs synthesised using the thermal decomposition approach, along with the aim and synthesis process.

Fe(CO)$_5$+Oleic Acid + Octyl Ether + (CH$_3$)$_3$NO   Hydrophobic Iron Oxide Nanoparticles
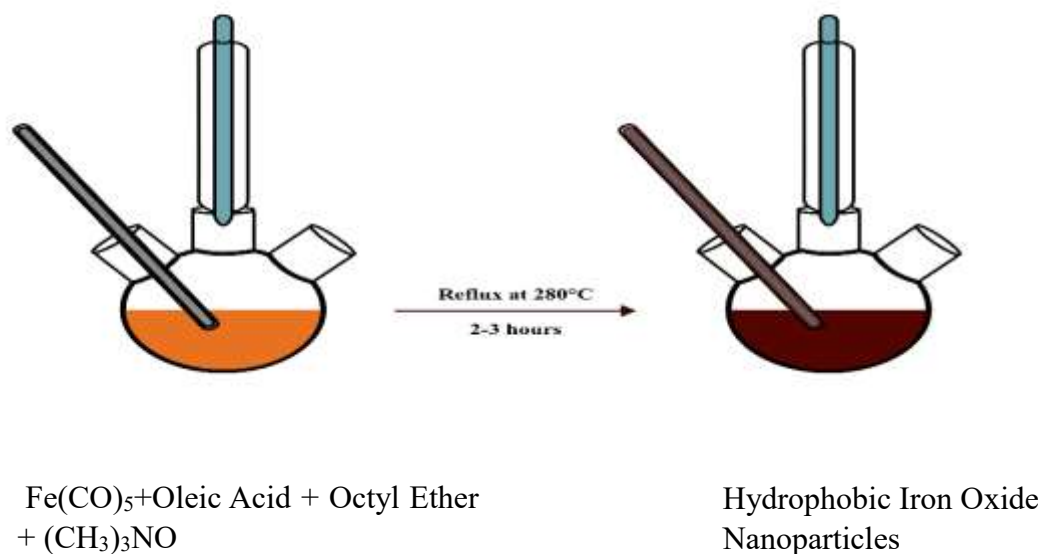
Figure 4: Synthesis of -Fe$_2$O$_3$ nanocrystals via thermal decomposition of iron pentacarbonyl.

Table 3: Different processes of synthesis of MNPs by thermal decomposition methods.

Main reagent(s)	Other reagent(s)	Aim	Process	size	References
Iron(III) acet-ylacetonate (Fe(acac)$_3$)	Ethanol, ethyl acetate, Tri(ethylene glycol) (TREG, 99%)	To study of MNP synthesized by thermal decomposition.	A Fe(acac)$_3$-TREG solution was dehydrated at 1200°C for 1 hour. Then solution was heated to 280^{0}C for 2hrs to from the black ppt.	11 nm	[38]
Fe(acac)$_3$	oleic acid and	To develop a thermal	A surfactant mixture was	5nm	[39]

	oleylamine	decomposition method for the solvent-free synthesis of high-quality MNPs	used to dissolve $Fe(acac)_3$. The solution underwent dehydration at 120°C for 1 hr, followed by heating at a specific temperature for 2 hrs, resulting in the formation of a black precipitate.		
$Fe(acac)_3$	Ethanol, hexane, 1-Octadecene, Oleylamine, Phenyl ether, Oleic acid, Benzyl ether	To synthesize MNP by thermal decomposition	A surfactant mixture was used to dissolve $Fe(acac)_3$. The solution underwent dehydration at 120°C for 1 hr, followed by heating at a specific temperature for 2 hrs, resulting in the formation of a black precipitate.	3, 5, 9 and 24 nm	[40]
$Fe(NO_3)_3 \cdot 9H_2O$	$C_6H_8O_7 \cdot H_2O$	Synthesise MNP with highly-	A solution of $Fe(NO_3)_3 \cdot 9H_2O$ and	20 nm	[41]

		controlled phases and magnetic properties via single-step reduction.	$C_6H_8O_7 \cdot H_2O$ was stirred at 20 $r \cdot s^{-1}$ and heated for 30mins to 40 °C. It was then autoclaved for 20mins at 600^0C to obtain brown powders.		
Fe(acac)$_3$	oleic acid, dibenzyl ether, Oleylamine, n-hexane and acetone	to synthesize MNPs using a cost-effective surfactant through the thermal decomposition method, while achieving a short reaction time.	Fe(acac)$_3$, OA and OLA dissolving in dibenzyl ether was stirred for 30mins at room temp. and was further heated at different temp for different time interval.	13 nm	[42]

E. Microemulsion method

The microemulsion method is a widely employed technique for preparing magnetic nanoparticles. It involves the formation of a stable and isotropic phase by combining two immiscible liquids (oil and water) with an amphiphilic surfactant. This surfactant plays a critical role in stabilizing the microemulsion system and controlling the size and shape of the resulting nanoparticles. By creating a confined environment, the surfactant-stabilized microemulsion facilitates the formation of nanoparticles [43]. The surfactant molecules orient themselves with the hydrophilic head groups facing the water phase and the hydrophobic tails residing in the oil phase. This arrangement enables the surfactant molecules to form a

monolayer at the interface between the oil and water [44, 45]. To synthesise the required nanoparticles, the emulsion's microdroplets serve as nanoreactors and undergo a co-precipitation chemical process [46].

The microemulsion method is adaptable since it as allows for the modification of particle characteristics such geometry, size distribution, morphology, purity, surface area, and The large surface area of superparamagnetic nanoparticles has made them attractive for usage in both biomedical (drug administration, MRI, and hyperthermia) and environmental settings. homogeneity [45].

The large surface area of superparamagnetic nanoparticles has made them attractive for usage in both biomedical (drug administration, MRI, and hyperthermia) and environmental settings [47,48].

The microemulsion technique yields nanoparticles with characteristics that are sensitive to the surfactant's type and structure. The choice of surfactant is also critical as it influences the stability of the nanoparticles. Cetyltrimethylammonium bromide (CTAB), Tween 80, and sodium dodecyl sulphate (SDS) are only a few examples of the surfactants employed in the production of magnetic nanoparticles. CTAB is a cationic surfactant that has been extensively employed in the manufacture of magnetic nanoparticles owing to its ability to stabilise the microemulsion system and regulate the shape and size of the NPs generated [46].

1.7 Surface chemistry and surface modification

Uncoated MNPs possess high surface area-to-volume ratios, aggregation propensity and hydrophobic surfaces [48]. Prior to clinical applications, it is essential to modify the surface of manufactured MNPs, as IONPs without surface modifications frequently exhibit elevated toxicity in both in vitro and in vivo models. It is possible to increase the stability of iron oxide MNPs by modulating their surface chemistry with appropriate surface coating agents (figure 5) [48]. Surface chemistry is significant because it modulates particle size, biodistribution, dispersion state and magnetization values, solubility, immune response and cell recognition mechanisms [48]. Therefore, the surface coating of MNPs customises functionality, enhances biocompatibility, and shields cells against the fast biodegradation of MNPs as well as the generation of reactive oxygen species (ROS) [49].
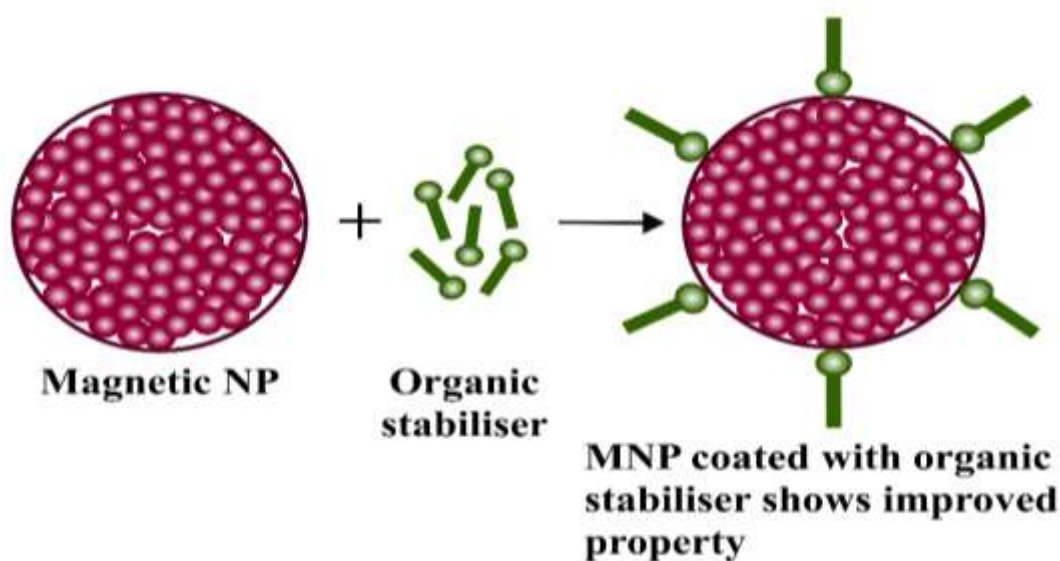
Figure 5: MNP with an organic stabiliser coating. Figure adopted from Monica Cîrcu et al. [50]

In biomedicine, it is often desirable to separate certain therapeutic/diagnostic element from their native environment in order to produce concentrated samples for testing and other purposes. This can be accomplished, for example, by utilising magnetic nanoparticles that are biocompatible. The first stage is to attach a magnetic tag or label to the target entity biological entity; the second is to use a magnetic separation system in a liquid medium to isolate the tagged entities. Magnetic nanoparticles are tagged by chemically modifying their surface with

biocompatible molecules. Several promising agents, such as dextran [51], PVA, PEG, and phospholipids are use to coat MNPs. Tagging allows them to associate with or to desired target biomolecule [13]. The chemical composition of the surface of MNPs can be changed by applying any of the coating materials enumerated in Table 4, but advantages and disadvantages must be evaluated prior to selection [4].

Table 4: Classes of coating materials [4,48]:

Class of coating materials	Examples
Organic polymer	dextran, PVA, chitosan, polyethylene glycol (PEG), polysorbate 80, Polyethylenimine (PEI), polyaniline
Organic surfactant	sodium oleate, dodecylamine
inorganic metals	gold
Inorganic oxides	silica and carbon
Bioactive molecules and structures	liposomes, peptides and ligands/receptors

The remarkable affinity of naturally derived polymers, such as biodegradable dextran and carbohydrate derivatives to iron oxides and their widespread application as plasma expanders have made them the choice for clinical usage of MNPs.

The hydrophilicity and low antigenicity of polyethylene glycol (PEG) make it popularly used polymer [52]. PEG not only provides steric stabilization to MNPs but also impedes their opsonization in plasma and prevent PEG coated MNPs uptake by macrophages, thereby enhancing their circulation within the body. The effective uptake of PEG-coated MNPs by cells is facilitated by fluid-phase endocytosis and the amphiphilic attraction to lipid bilayers on cell membranes, contributing to their cellular internalization [48, 53]. However, it is worth noting that frequent injections of PEGylated NPs can elicit an immune response and cause rapid blood clearance. Nevertheless, PEG remains the optimal choice for surface coating of MNPs [4]. Polyvinyl alcohol (PVA) is a polymer known for its remarkable ability to produce thin coatings, facilitate emulsion formation, and possess strong adhesion properties. The concentration of PVA is crucial factor to consider when coating drug-loaded MNP. At higher concentrations of PVA, the magnetization saturation of the MNP decreases swiftly. This is due to a decrease in

the magnetization saturation of the MNP, which makes it more challenging to control the drug delivery via an external magnetic field [54]. Although the use of PVA for intravenous (i.v.) administration is limited due to its poor stability and tendency to agglomerate in ferrofluids, PVA can be cross-linked to form a magnetic gel, making it suitable for vitreous eye replacement. This particular characteristic of cross-linked PVA holds potential for applications in biosensors, biological tissue engineering, and targeted delivery of drug [48].

Polyethylenimine (PEI) is regarded as the best nanoparticle coating material for gene (DNA) delivery. PEI is aliphatic polymers characterized by their high basicity and positive charge. They consist of primary, secondary, and tertiary amino groups in a 1:2:1 ratio. It exhibits remarkable transfection efficiency in both in vitro and in vivo setting through the formation of polyplexes. Polyplexes refer to the complexes formed by the binding of nucleic acids and polymers together [55]. PEI is a positively charged polymer that can bind to DNA through electrostatic interactions. This forms PEI/DNA complexes that have a net positive charge. The positive charge of the complexes allows them to interact with the negatively charged cell membrane, facilitating their delivery into the cell nuclei. Once inside the nuclei, the complexes can regulate the expression of the encapsulated gene. It is important to note that However, it is essential to note that cytotoxicity is a drawback of PEI modification [49]. However, studies showed this can be mitigated by coating it extensively with PEG.

Poly(lactic-co-glycolic acid) (PLGA) is a biodegradable polymer that has gained approval from regulatory agencies, the Food and Drug Administration and the European Medicines Agency. It is widely used in various medicinal applications due to its exceptional biodegradability, biocompatibility, and controlled release properties. PLGA nanoparticles are synthesized by employing techniques such as precipitation polymerization, emulsion solvent evaporation, interfacial polymerization, and emulsion polymerization, using lactide and glycolide monomers. These techniques allow for the production of PLGA nanoparticles with different polymer structures (linear, branched, or globular) and size control, enabling the desired release profile to be achieved [56]. However, its applicability in some lesions that are difficult to treat, such as those in the brain, is severely limited due to its low drug loading and strong drug burst release [4,57].

Theoretically, magnetic targeting has a lot of benefits for the delivery of drugs. It has the potential to deliver drugs more effectively and with fewer side effects by targeting them to the

target sites in the body. This could reduce the amount of drug that is needed, making treatment more affordable and less toxic. It is challenging to attain these goals in actual practice. Preparation methods, advantages, and medical applications of coating materials are listed in table 5.

Table 5: Potentially therapeutic MNP coatings material.

Coating	Source/Production/ Preparation	Advantages	Medical applications	References
PEG	Synthesize through the reaction of C_2H_4O with H_2O, ethylene glycol, or ethylene glycol oligomers	Blood circulation time increased, improved water solubility, and decreased phagocytosis	MRI, tumor diagnosis, and treatment	[58, 59]
PVP	Obtain from polymerization of N-vinylpyrrolidone	Particle aggregation reduced, enhanced stability,blood circulation time increased	MRI, targeted eradication of cancerous breast cells , and bioseparation	[60, 61, 62]
PEI	Post-modification of polymers like poly(2-oxazolines) or N-substituted polyaziridines yields linear PEI, whereas aziridine ring-opening polymerization yields branched PEI.	Biocompatible	Cancer cell isolation, tissue engineering, thermal therapy	[55, 63, 64]

Chitosan	Extracted from the cell walls of shellfish or fungi.	Biocompatible	regenerative medicine, thermotherapy, and radiotherapy	[65, 66, 67]
Liposome	Made from cholesterol and natural non toxic phospholipid	Biocompatible	Tumor treatment, thermotherapy, and MRI	[68,69,70,71]
Dextran	lactobacilli produce dextran.	Biocompatible	In vivo drug delivery systems for cancer treatment, contrast agent for MRI scans	[51,52]
Alginate	Extracted from brown algae	Biocompatible, biodegradability, strong bioadhesion , innert nature	Drug-targeted controlled release, MRI, adsorbent	[52,72]

1.8 Applications

MNPs have been used in magnetic resonance imaging (MRI), targeted medication and gene delivery, tissue engineering, cell tracking, and bio-separation due to their unique propensity to be steered by an external magnetic field [73] .

Magnetic nanoparticles (MNPs) are unique in their ability to be steered by an external magnetic field. This property has rendered them useful for numerous applications (figure 6), such as magnetic resonance imaging (MRI), targeted drug delivery, delivery of genes, biofabrication, cell monitoring, and bioseparation [73]. Functionalizing MNPs with pharmaceuticals and bioactive substances such as peptides and nucleic acids to generate one-of-a-kind particulate system that can overcome cell and tissue barriers, offering organ-specific therapeutic and diagnostic capabilities. The functionalization and magnetic responsiveness of MNPs have positioned them as valuable tools in the field of theragnostics. Theranostics is the integration of therapeutic and diagnostic technologies [48,74]. Some of the commercially available micro and nano magnetic products are listed in table no. 6

MAGNETIC NANOPARTICLES APPLICATIONS

THERAPY

- Drug delivery
- Hyperthermia
- Radiotherapy combined with MRI
- Musculoskeletal system associated diseases
- Anemic chronic kidney disease

DIAGNOSIS

In vivo

- MRI

In vitro

- Sensing
- Cell sorting
- Bio-separation
- Enzyme immobilization
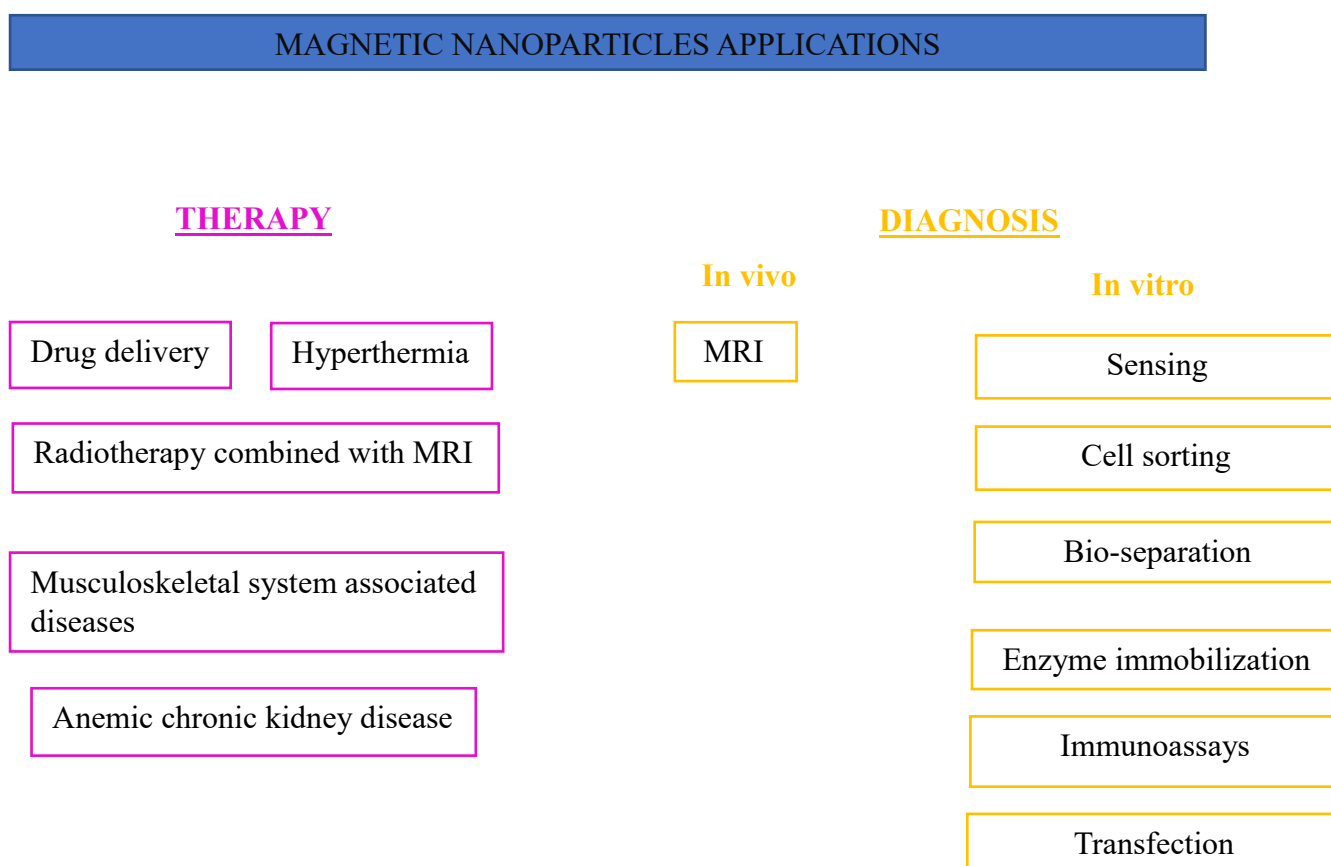- Immunoassays
- Transfection

Figure 6. Applications of magnetic nano-particles.

A. Drug Delivery

Typically, conventional medications are not very specific, which means that they can affect the target tissue as well as other tissues in the body. This can result in adverse effects as well as a reduction in the amount of the drug reaching the targeted region. In order to obtain an adequate concentration of drug at the target site, conventional medications often require high doses[74].

In 1960, it was proposed that magnetic nanoparticles (MNPs) could be guided to specific body locations using a magnetic field [11]. MNPs facilitate targeted and controlled drug release by adhering cleavable linkers or polymeric compounds to drug. These MNPs can be targeted using an external magnetic field (figure 7), and drug release can be triggered by enzymatic cleavage or environmental changes, such as fluctuations in temperature or pH [75]. In addition to smart drug delivery, MNPs find applications in hyperthermia treatment, magnetic bio-separation, lab-on-a-chip technology, and emerging imaging techniques [74].

Cancer cells exhibit unique structural and molecular features owing to inadequate blood flow, resulting in conditions such as hypoxia and increase in level of acid in body. These factors render cancer cells highly sensitive to heat. Hyperthermia is a therapeutic approach that involves gradually raising the body temperature to 40-43 °C. Hyperthermia is a therapeutic approach involving the application of heat, that is used to target and kill cancer cells. It is done by gradually increasing the body temperature to a range of 40-43 degrees Celsius. It aids in cancer treatment by enhancing the effectiveness of chemotherapy and radiation therapy by killing cancer cells. The problem with this strategy is that it cannot target cancer cells with pinpoint precision. However, this problem can be sidestepped by magnetic hyperthermia that is administering MNPs intravenously to specified areas and using an external magnetic field to create heat locally. The main advantage of magnetic hyperthermia is that it can be used to heat specific desired parts of the body. The MNPs can be linked to specific molecules that target cancer cells. This indicate that heat will be produced only in the area where cancer cells are located, which minimizes damage to healthy tissue. Although magnetic hyperthermia is still in its early stages of development, promising results have been observed in clinical trials. It holds potential as a novel cancer treatment that can enhance the safety and effectiveness of hyperthermia therapy [11,76].
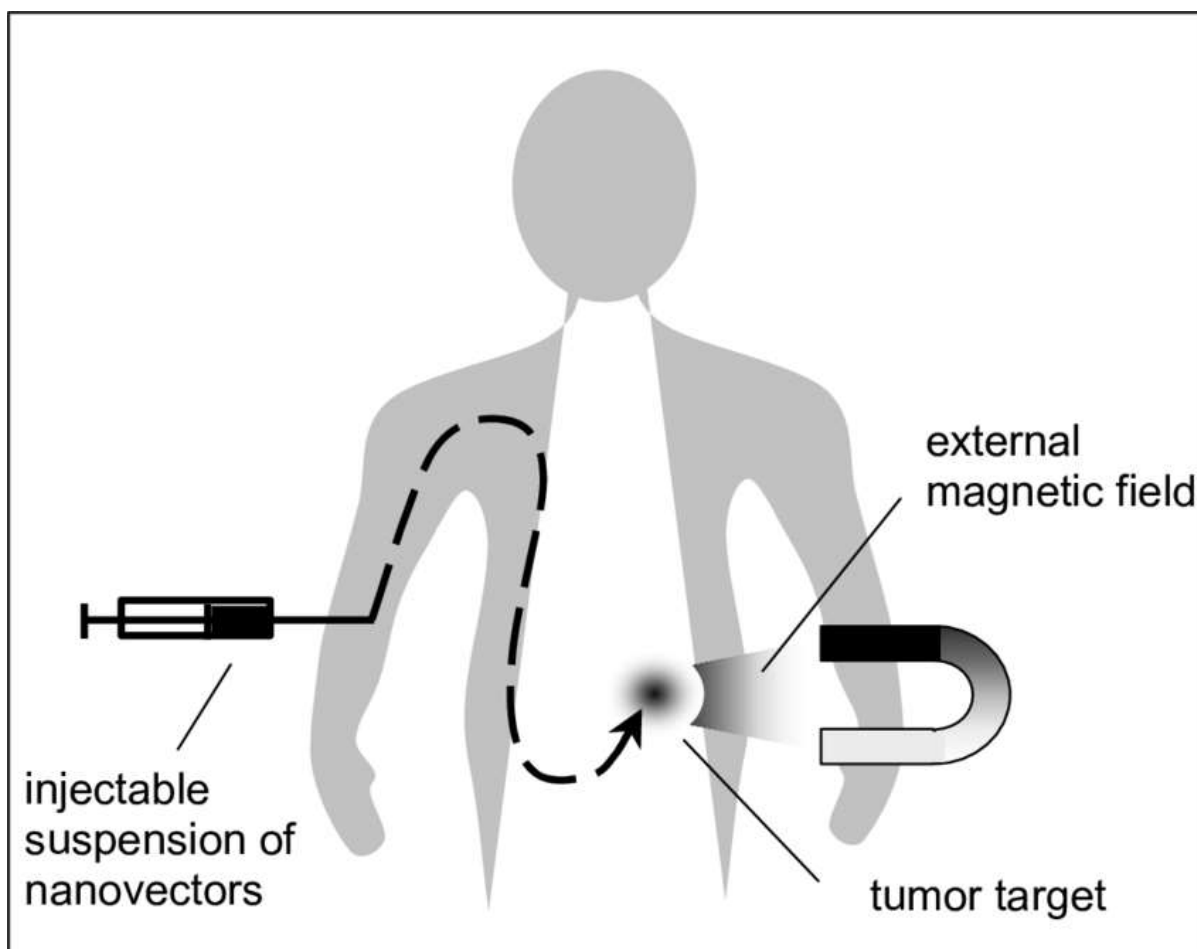
Figure 7- Magnetic Drug Targeting

B. Magnetic Nanoparticles in Diagnosis

Early identification of maladies such as cancer is an important healthcare objective, but it is difficult to attain. In health care units, a variety of diagnostic tools, including MRI, CT scan, and X-rays, are utilised to detect disease conditions. Among these techniques, MRI has gained prominence due to its ability to provide detailed and high-resolution images of soft tissues without the need for surgical interventions. Despite MRI's broad use, scientists are still looking at methods to enhance the technology for more precise tissue detection [77].

Superparamagnetic iron oxide nanoparticles (SPIONs) and ultrasmall superparamagnetic iron oxide nanoparticles (USPIONs) are two different category of iron oxide nanoparticles which can enhance the sensitivity of MRI. SPIONs exhibit a rapid alteration in proton alignment when subjected to an externally applied magnetic field. SPIONs shows higher degree of relaxivity, thus improving the sensitivity of MRI. Upon injection into the body, these magnetic

nanoparticles activate the reticulo-endothelial system, triggering macrophages to engulf and remove the particles.

The size of the nanoparticle has a significant role in determining whether or not the immune system will recognise it. USPIONs are made up of iron oxide cores coated with a variety of functional coatings agents, including carbohydrates or polymers. The particle's functional group prevents it from aggregating together, and it also serves as a hook for attaching drugs and other ligands for specific targeting. The smaller size of USPIONs allows them to remain in the bloodstream for a longer period of time than SPIONs. Due to their small size, USPION particles are less likely to be attacked by the immune system, extending their half-life. Several varieties of SPIONs and USPIONs have been authorised for usage in the past. Feridex I.V., Resovist, Sinerem, and Clariscan are some of the most popular types that have been used in the past [11,78].

The nanoparticle's size plays a significant function in determining whether or not it will be recognized by the immune system. USPIONs consist of iron oxide coated with various chemical coating agents, such as carbohydrates, polymers etc. The functional group of these coating agents prevents USPIONs from aggregating together, and it also serves as a hook for attaching drugs and other ligands for specific targeting. The smaller size of USPIONs enables them to circulate in the bloodstream for an extended duration compared to SPIONs. Several types of authorized SPIONs and USPIONs such as Feridex I.V., Resovist, Sinerem, and Clariscan, have been successfully used in the past.

C. Magnetic bioseparation

The technique of magnetic bioseparation leverages the distinct magnetic characteristics of magnetic particles in order to separate different biological molecules when subjected to an external static magnetic field. In order to ensure their suitability for biological applications, it is imperative to purify DNA, proteins, antigens, and antibodies from their respective libraries [79]. For example, the process of DNA detection and separation plays a crucial role as a preliminary step preceding the polymerase chain reaction (PCR) in order to assess the expression of specific genes [80]. Hei and Cai [81] have documented a technique for the purification and concentration of RNA from the novel coronavirus (SERS-CoV). This RNA is subsequently subjected to amplification using polymerase chain reaction (PCR) in order to

identify the viral nucleic acid's genome sequence. In their study, Schwaminger et al. presented findings on the utilisation of bare iron oxide nanoparticles (BIONs) for the purpose of isolating proteins tagged with a short peptide (Glutathione6), specifically focusing on the Green fluorescent protein [82]. The Green fluorescent protein (GFP) can be effectively identified and isolated from a crude cell lysate by employing the peptide tag. A citrate buffered system was employed to recover bare magnetic nanoparticles, resulting in the binding of 0.2 g of proteins per gramme of nanoparticles. In a further study, Schwaminger and colleagues (year) conducted a further investigation on the separation of hexahistidine (His6) tagged GFP protein utilising BIONs with a diameter of 12 nm [83]. The researchers found a protein purity of 91% in the recovered proteins obtained from Escherichia coli cell lysate. Furthermore, the purification and removal of Bovine haemoglobin (Bhb) can be achieved through the utilisation of Fe_3O_4-SiO_2 nanoparticles coated with 3-methacryloxypropyltrimethoxysilane (MPS) [84]. After the attachment of bovine haemoglobins to the particles, a static magnetic field is employed to separate the bovine haemoglobin from the cell lysate. Subsequently, the elution process is executed to retrieve the Bhbs. The researchers reported the equilibrium adsorption capacity to be 87.7 mg g−1 of particles [85].

Table 6: Commercially available micro and nano magnetic products.

Company	Products	Applications	References
Bangs Laboratories, Inc	Magnefy™	Isolation of DNA, immunoassays and molecular assays	[86]
	ProMag® HP	immunoassay	[87]
	COMPEL	miniaturized bioassays and separations	[88]
	BioMag® & BioMag®Plus Unconjugated Particles	assays , Cell separation and purification of biomolecules.	[89]

	BioMag® & BioMag®Plus Binding Proteins	immunoprecipitation or PCR product clean-up	[90]
	MAGNETIC SEPARATORS	Isolation of cells and biomolecules such as antibodies, nucleic acids, and polypeptides.	[91]
Polysciences, Inc.	Magnefy™ COOH	Magnetic isolations & assay development	[92]
	PROMAG® MICROSPHERES	assays and isolations.	[93]
	BioMag® Amine Magnetic Immobilization Kit	Conjugates proteins to magnetic amine particles	[94]
	BioMag®Plus Carboxyl	Magnetic isolations of protein & assay development	[95]
	BioMag® Goat anti-Human IgG (Fc Specific)	Magnetic Ab affinity isolations	[96]
Micromod Partikeltechnologie GmbH	synomag-D, Cross-linked dextran (nanomag-CLD®®), Bionized NanoFerrite (BNF particles), Silicate-reinforced dextran (nanomag-silica®®)	Stem cell tracking, MRI tracers, biomolecules and metal ions separation, hyperthermia, and MPI	[97]

	Cross-linked dextran (nanomag-CLD-F, synomag-CLD-F®®), Bionized nanoFerrite (BNF-F particles)	Magnetic fluorescent tracers	[98]
Ademtech SA	Magnetic Particles	concentration, separation, purification and identification of molecules and specific cells.	[99]
Invitrogen Corp.	MagMAX™ Plant DNA Isolation Kit	qPCR, next-generation sequencing	[100]
	MagMAX™ Cell-Free DNA Isolation Kit	manual and automated isolation of cfDNA, Next-Generation Sequencing, Real-Time PCR, PCR	[101]
Nano Research Elements	Magnetite Iron Oxide Nanoparticles-polyimethylsiloxane $(C_2H_6OSi)_nFeO_4$	Assay	[102]

Chapter 2

Literature Survey

Literature review

1. **Joseph Kost et al. (1987)** conducted a study focused on investigating the controlled release of insulin from ethylene-vinyl acetate copolymer (EVAc)-protein matrices containing magnetic beads. This research intended to enhance the rate of insulin release. They devised the magnet-polymer system by the solvent casting method. To induce diabetes in the experimental rats, streptozotocin was injected. In a study, diabetic rats were implanted with polymer matrices containing insulin and embedded magnets. The polymer matrices released insulin passively, which lowered the rats' blood sugar levels. When the rats were exposed to an oscillating magnetic field, their blood sugar levels were further lowered by nearly 30%. This effect was not observed in control rats that were not exposed to the magnetic field. The authors' findings suggest that they have successfully increased the release of insulin and reduced blood glucose levels [103].

2. **Ting –Yu Liu et al., (2007)** created a novel intelligent magnetic hydrogel (ferrogel). It was synthesized by combining poly(vinyl alcohol) (PVA) hydrogels with Fe_3O_4 magnetic particles through a series of freezing-thawing cycles. Upon application of an external direct current magnetic field, the ferrogel exhibited drug accumulation in its vicinity. Conversely, immediate cessation of the magnetic field led to instantaneous release of the accumulated drug into the surrounding environment. Modulation of drug release kinetics from the ferrogel was achieved by altering the magnetic field state, allowing for a spectrum of release rates ranging from swift to gradual. This release behavior was notably affected by the size of Fe_3O_4 particles under a specific magnetic field strength. Notably, ferrogels containing larger Fe_3O_4 particles demonstrated heightened magnetic sensitivity attributed to their greater saturation magnetization and reduced coercive force. Furthermore, the amount of drug released could be finely tuned by adjusting the switching duration time (SDT) through externally controllable on-off manipulation within the magnetic field setting. Optimal burst drug release quantities and a favourable closely-configured arrangement of the ferrogel were achieved at SDTs of 10 and 5 minutes, respectively. The distinctive magnetic-responsive attributes exhibited by these newly developed ferrogels suggest their potential utility in creating drug release profiles that are controllable and customizable, aligning with practical clinical requisites [104].

3. **N.H. Sulaiman et. al., (2015)** synthesized calcium ferrite nanoparticles ($CaFe_2O_4$ NPs) for targeted drug delivery applications. It was prepared through a sol-gel technique. Initially, the proposed nanoparticles were created by blending calcium and iron nitrates with citric acid to prevent agglomeration. Subsequent calcination at 550°C yielded small particle sizes. The resultant nanoparticles underwent characterization via X-ray diffraction (XRD), which unveiled orthorhombic structures of the $CaFe_2O_4$ nanoparticles. The application of Scherer's formula revealed a crystallite size of approximately 13.59 nm. Vibrating Sample Magnetometer (VSM) analysis was employed for magnetic evaluation, demonstrating super-paramagnetic behaviour in the synthesized particles with a magnetization saturation of around 88.3 emu/g. A thorough examination using scanning electron microscopy (SEM) depicted the spherical morphology of the calcium ferrite nanoparticles. In the study calcium ferrite nanoparticles for side specific drug delivery was successfully prepared [105].

4. **Dong-Hyun Kim et al., (2010)** reports the synthesis and characterization of multifunctional magnetic nanoparticles composed of $MnFe_2O_4$ encapsulated in chitosan. The nanoparticles were synthesized by a co-precipitation method and then modified with meso-2,3-di-mercaptosuccinic acid (DMSA) to develop stable aqueous dispersions. The nanoparticles were coated with chitosan, and their magnetic properties, heat generation, and hydrodynamic size were evaluated for various linker concentrations and pH conditions.

The results showed that the nanoparticles had a spinel crystal structure and were superparamagnetic. The saturation magnetization of the nanoparticles was 44.1 emu/g. The chitosan coating was successful in forming a thin layer on the surface of the nanoparticles. The DLS results showed that the average size of the chitosan-coated nanoparticles was larger than that seen in TEM, which is due to aggregation. The loading of drug was most effective for the nanoparticles synthesized using 0.9% EDC. In summary, this study successfully synthesized multifunctional magnetic nanoparticles composed of $MnFe_2O_4$ encapsulated in chitosan. These nanoparticles have potential applications in magnetically-triggered drug delivery, localized hyperthermia, and MRI contrast imaging [106].

5. In a study by **Wang et al. (2011),** multiwalled carbon nanotube (MWCNT)/cobalt ferrite ($CoFe_2O_4$) magnetic hybrids were synthesized by a solvothermal method. The reaction temperature was found to have a significant effect on the structure of the hybrids, with 6 nm $CoFe_2O_4$ nanoparticles uniformly coated on the nanotubes at 180°C and agglomerated $CoFe_2O_4$ spherical particles threaded by MWCNTs and forming necklace-like nanostructures at 240°C.

   The MWCNT/$CoFe_2O_4$ hybrids prepared at 180°C (MWCNT/$CoFe_2O_4$-180) showed promising biomedical applications. They have a high T(2) relaxivity of 152.8 Fe mM(-1)s(-1) in aqueous solutions, which makes them effective magnetic resonance imaging (MRI) contrast agents. They also exhibit a significant negative contrast enhancement effect on cancer cells, making them potential candidates for cancer therapy.

   In addition, the MWCNT/ $CoFe_2O_4$ 180 hybrids have low cytotoxicity and negligible hemolytic activity. This means that they are safe to use in the body. The hybrids can also be loaded with the anticancer drug doxorubicin (DOX) and subsequently released in a sustained and pH-responsive way. This allows for the controlled delivery of DOX to cancer cells, which can improve the efficacy of chemotherapy.

   Overall, the results of this study suggest that MWCNT/ $CoFe_2O_4$ 180 hybrids have the potential to be used as both effective MRI contrast agents and anticancer drug delivery systems for simultaneous cancer diagnosis and chemotherapy [107].

6. In a study by **K. Sriram et al., (2018)**., hybrid nanoparticles of vanillin-chitosan coated with super paramagnetic calcium ferrite were developed for curcumin delivery. The vanillin-chitosan was modified by the Schiff base reaction to enhance the hydrophobic drug encapsulation efficiency. Calcium ferrite nanoparticles were added to the vanillin-chitosan to improve the biocompatibility. The hybrid nanoparticles were obtained by ionic gelation method. The characterization of the hybrid nanoparticles was performed by XRD, FTIR, 1H NMR, TGA, AFM, and SEM techniques. The results showed that the hybrid nanoparticles had a good dispersion, narrow size distribution, and high encapsulation efficiency of 98.3%. The drug release from the hybrid nanoparticles was studied at various pH, initial drug loading concentrations, and magnetic fields. The drug release mechanism was found to be dependent on the pH and magnetic field. The release followed the Higuchi model under most conditions.

   The biocompatibility of the hybrid nanoparticles was tested using L929 fibroblast cells. The results showed that the hybrid nanoparticles were non-toxic to the cells. The

cytotoxicity test against MCF-7 breast cancer cell line showed that the hybrid nanoparticles had significant anticancer activity.

Overall, the results of this study suggest that the hybrid nanoparticles of vanillin-chitosan coated with super paramagnetic calcium ferrite are a promising new carrier for curcumin delivery. The nanoparticles have high encapsulation efficiency, good biocompatibility, and controlled drug release. They could be used for the treatment of cancer and other diseases [108].

7. In a study by **Guangshuo Wang et al (2018)**., monodisperse and superparamagnetic manganese ferrite (MnFe2O4) nanoparticles were synthesized by a one-pot sonochemical method using polyvinylpyrrolidone (PVP) as stabilizer. The nanoparticles were characterized by TEM, XRD, FTIR, XPS, SQUID, and MTT.

The TEM results showed that the nanoparticles had a uniform dispersion with a narrow particle size distribution. The FTIR results showed that the PVP coating was successful. The XPS results showed that the nanoparticles were composed of manganese, iron, and oxygen. The SQUID results showed that the nanoparticles were superparamagnetic. The MTT results showed that the nanoparticles were non-toxic to cells.

Doxorubicin hydrochloride (DOX), an anti-cancer drug, was loaded onto the surface of the nanoparticles. The drug loading capacity was 0.45 mg/mg. The DOX release from the nanoparticles was pH-dependent.

The results of this study suggest that the PVP-coated MnFe2O4 nanoparticles are a promising new carrier for controlled drug delivery. The nanoparticles are non-toxic, have a high drug loading capacity, and exhibit pH-dependent drug release. They could be used to deliver drugs to cancer cells in a controlled manner [109].

8. **Meysam Ghanbari et al., (2021)** stated that the cobalt ferrite (CFO) nanoparticles have attracted considerable attention due to their unique properties, such as high saturation magnetization, good chemical stability, and biocompatibility. These properties make them promising candidates for a variety of applications, including magnetic recording media, catalysis, and drug delivery. In this study, the authors synthesized CFO nanoparticles using a modified sol-gel method. The nanoparticles were characterized using X-ray diffraction (XRD), Fourier transform infrared spectroscopy (FTIR), field-emission scanning electron microscopy (FE-SEM), transmission electron microscopy

(TEM), and vibrating sample magnetometer (VSM). The XRD results showed that the nanoparticles had a single-phase spinel structure. The average crystallite size was calculated to be about 33 nm. FE-SEM showed that the nanoparticles had a cubic morphology. The VSM results showed that the nanoparticles had a high saturation magnetization of 64 emu.g−1.

The authors then coated the CFO nanoparticles with tripolyphosphate (TPP) and chitosan polymer (Cs) to improve their biocompatibility and drug delivery properties. The coated nanoparticles were then loaded with the anticancer drug doxorubicin (DOX). The release of DOX from the coated nanoparticles was evaluated at different pH levels. The results showed that the coated nanoparticles had good biocompatibility and non-toxicity. They also showed that the DOX-loaded nanoparticles could effectively kill breast cancer cells in an acidic medium.

Overall, this study demonstrated a facile and efficient method for the synthesis of CFO nanoparticles with good biocompatibility and drug delivery properties. The coated nanoparticles could be used for the targeted delivery of DOX to cancer cells [110].

9. In a study **(2020), Amiri M et al.,** developed a novel magnetic liposome nanocomposite system for the delivery of the anticancer drug imatinib. The nanocomposites were prepared by loading imatinib into liposomes that were coated with zinc ferrite (ZnFe2O4) nanoparticles. The $ZnFe_2O_4$ nanoparticles were synthesized using a green synthesis method, which involves the use of Teucrium polium, an extract from the sage plant.

The in vitro cytotoxicity of the nanocomposites was evaluated using the MTT assay on U87 cell lines. The results showed that the nanocomposites had a lower cytotoxicity than free imatinib, indicating that they are well-tolerated by cancer cells.

The in vitro release of imatinib from the nanocomposites was also studied. The results showed that the alternating magnetic field significantly enhanced the release of imatinib from the nanocomposites. This is due to the fact that the alternating magnetic field causes the $ZnFe_2O_4$ nanoparticles to rotate, which disrupts the lipid bilayer and releases the imatinib.

The in vivo biodistribution of the nanocomposites was also studied. The results showed that the nanocomposites were rapidly accumulated in the tumor tissue after alternating magnetic field treatment. This suggests that the nanocomposites can be used to deliver imatinib to tumors in a targeted manner.

Overall, the results of this study demonstrate that the magnetic liposome nanocomposites are a promising new drug delivery system for cancer therapy. They are well-tolerated by cancer cells, they can be targeted to tumours using alternating magnetic field, and they can release the drug in a controlled manner [111].

10. According to **Arshadi et al. (2021),** magnetic drug targeting (MDT) is an auspicious approach in cancer treatment whereby magnetic nanoparticles are used to facilitate the targeted delivery of medications specifically to tumour sites. The goal of this research was to create a mathematical model that would allow the researchers to investigate how changing certain MDT operational parameters would affect the effectiveness of a treatment for glioblastoma.

The growth of the tumour was mathematically represented using partial differential equations. The equation governing the mobility of the medication was combined with equations describing tumour development and magnetism. In the drug targeting situations, a magnetic field with oscillating characteristics was used. has been conducted to examine the impact of various factors on the efficacy of treatment. The evaluation of therapeutic success included the assessment of the tumour volume index, which represents the ratio between the tumour volume in MDT and the tumour volume in conventional chemotherapy.

The findings indicate that the effectiveness of MDT is closely influenced by the dispersion of the drug inside the surrounding tumour tissue. By increseing the frequency of oscillations, the tumour volume index was seen to fall to a value of 0.95. However, the tumour Volume Index exhibited a further growth above a certain threshold. This implies that there exists an ideal frequency of oscillations for MDT treatment.

Additionally, the investigation revealed that the therapeutic efficacy is substantially influenced by the particle size of the magnetic nanoparticles. At the optimal particle size, the tumour Volume Index exhibited a drop to 0.94. This implies that the selection of particle size should be conducted with great consideration in order to optimise the effectiveness of MDT treatment.

Ultimately, the research findings indicate that the efficacy of therapy is influenced by the quantity of treatment cycles. The tumour volume index shown a drop to 0.87 as the number of treatment cycles increased. This implies that the efficacy of MDT treatment may be enhanced with an extended duration of administration [112].

Chapter 3
Aim and objectives

Aims and objectives

1. To synthesize magnetite by co-precipitation method.
2. Develop drug loaded magnetic nanoparticle alginate beads for magnetic targeted drug delivery.
3. Characterizations of the prepared magnetite and MNP beads.

Plans of work

➢ To identify various physical and chemical properties of drug (aceclofenac) as a part of pre-formulation study.

➢ Understand the various physicochemical controlling parameters to formulate stable magnetite by co-precipitation method. Examples: temperature of the reacting solvents, setting the correct speed of mechanical stirrer, height from which magnetite + drug solution is added to $CaCl_2$ solution and speed at which it is added and etc.

➢ Attempt to develop a scale-up method for the optimized formation of drug loaded MNP beads in laboratory scale.

➢ Characterization of magnetite and MNP beads.

Chapter 4

Materials

4.0 Materials and Reagents

Pure Aceclofenac was purchased from Yarrow Pharma Ltd. $FeCl_3$ (iron(III) chloride), $FeSO_4$ (iron(II) sulfate) were obtained from . Sodium hydroxide pellets, di sodium hydrogen phosphate dihydrate, postassium dihydrogen phosphate were purchased from Merck life science private limited. All the chemicals used were of analytical reagent grade.

4.1 Aceclofenac [113,114,115,116]

Drug class	Non-Selective COX 1&2 Inhibitors NSAID
Description	Aceclofenac is a non-steroidal anti-inflammatory drug (NSAID) that is chemically related to diclofenac. It is a monocarboxylic acid that is the carboxymethyl ester of diclofenac. It is used to treat osteoarthritis, rheumatoid arthritis, and ankylosing spondylitis. It has strong anti-inflammatory and analgesic properties, and is reported to be as effective as or even more effective than other NSAIDs in double-blind studies. Aceclofenac is a BCS Class II drug, which means that it has poor aqueous solubility and high permeability.
Chemical formula	$C_{16}H_{13}Cl_2NO_4$

Chemical structure
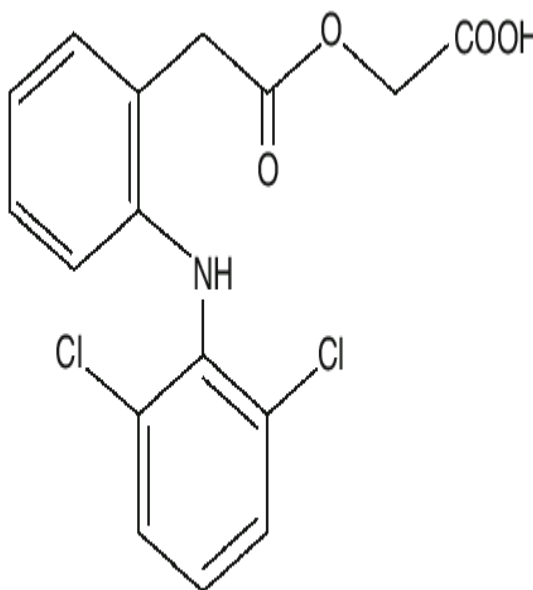
IUPAC name	2-[2-[2-(2,6-dichloroanilino)phenyl]acetyl]oxyacetic acid
Molecular weight	354.2 g/mol
Brand name	Acecgen (Generics UK), Aflamin, Airtal/Biofenac (Gedeon Richter Plc.), AklofEP (ExtractumPharma) and Flemac (Aramis Pharma)
Melting point	149-153^{0}C
Route of administration	Oral, Intramuscular, Intravenous, tropical
Half life	approximately 4 hours
Mechanism of action	Aceclofenac works by inhibiting the action of cyclooxygenase (COX) that is involved in the production of prostaglandins (PG) which is accountable for pain, swelling, inflammation and fever.
Metabolism	Aceclofenac is metabolized by the enzyme CYP2C9.
Metabolites	Main metabolite- 4'-hydroxyaceclofenac

other minor metabolites-diclofenac, 5-hydroxyaceclofenac, 5-hydroxydiclofenac, and 4'-hydroxydiclofenac

LogP   2.17

Adverse effects   gastro-intestinal disorders (dyspepsia, abdominal pain, nausea), rash, ruber, urticaria, symptoms of enuresis, headache, dizziness, and drowsiness. Oral LD50-130mg/kg [MSDS]

4.2 Sodium alginate [117]

Sodium alginate is the sodium salt of alginic acid. Alginic acid is a polyuronic acid composed of reduced mannuronic and glucoronic acids, which are obtained from the algal growth of the species of family Phaeophyceae. The common species are Macrocystis pyrifera, Laminaria hyperborea, Lami-naria digitata, Ascophyllum nodosum and Durvillaea lessonia. It is a purified carbohydrate extracted from brown seaweed (algae) by treatment of dilute alkali.

Synonyms: Algin, Alginic acid sodium salt, Sodium polymannuronate, Kelgin, Minus, Protanal.

Chemical Structure:
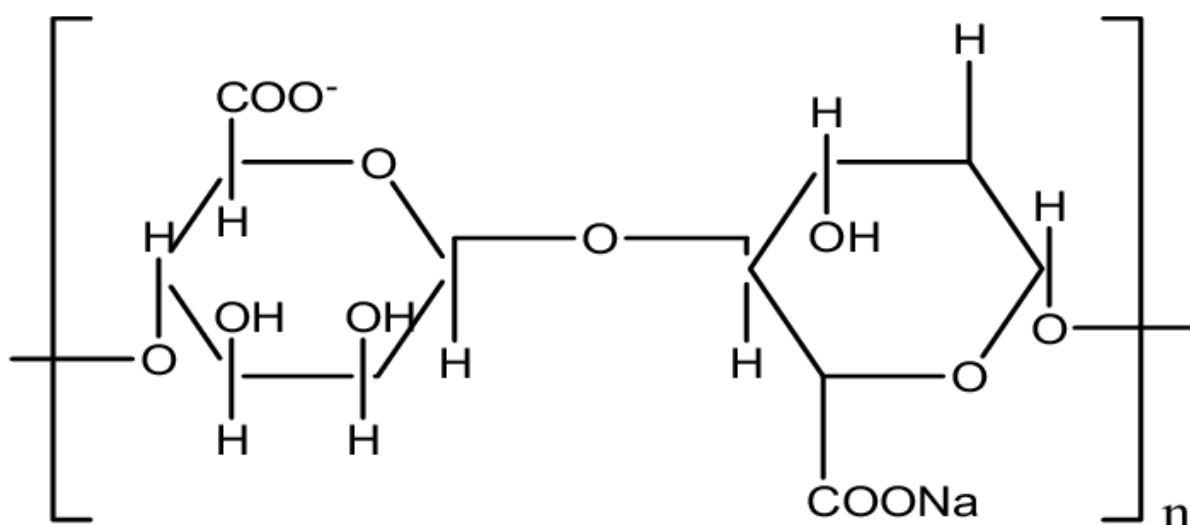
Physical state: Solid, coarse to fine powder.

Colour: White to buff coloured powder.

Odour: Odourless.

Taste: Tasteless.

Melting point: 300ºC

Solubility: Readily soluble in water forming viscous colloidal solutions and insoluble in alcohol, chloroform, ether and strong acids. 1% solution of gum at 20ºC may have a viscosity in the range of 20-400 centipoises.

4.3 Iron(III) chloride [118, 119]

Iron(III) chloride is a chemical compound with the formula $FeCl_3(H_2O)_x$. It is also known as ferric chloride. Iron(III) chloride is available in anhydrous (water-free) and hydrated (water-containing) forms. Both forms are hygroscopic, which means they absorb water from the air.

Synonyms: Iron trichloride.

Chemical Structure:
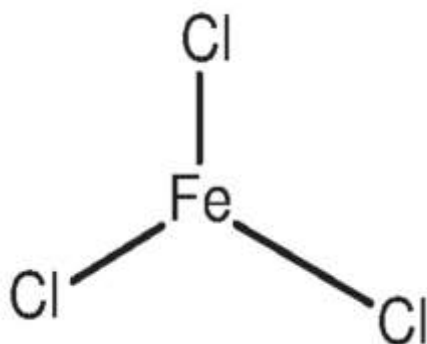
Molecular Weight: 162.204 g/mol (anhydrous) , 270.295 g/mol (hexahydrate)

Physical state: Solid.

Colour: orange to brown-black

Odour: Odourless.

Taste: Tasteless.

Melting point: 307.6 °C (585.7 °F; 580.8 K) (anhydrous); 37 °C (99 °F; 310 K) (hexahydrate)

Solubility: 912 g/L (anhydrous or hexahydrate, 25 °C in water

4.4 Ferrous sulfate [120]

Ferrous sulfate is a chemical compound with the formula $FeSO_4 \cdot x H_2O$. It is a range of salts that exist most commonly as the heptahydrate (x = 7). The hydrated form of ferrous sulfate is used medically to treat iron deficiency, and also for industrial applications.

Synonyms: Iron(II) sulfate

Chemical Structure:
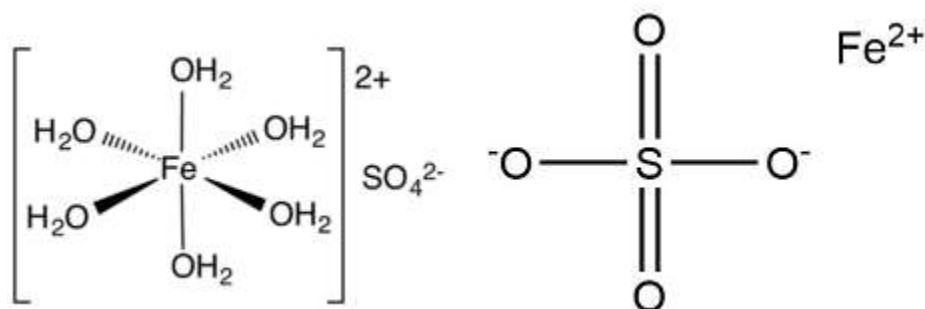
Molecular Weight: 151.91 g/mol (anhydrous), 169.93 g/mol (monohydrate), 241.99 g/mol (pentahydrate), 260.00 g/mol (hexahydrate), 278.02 g/mol (heptahydrate)

Physical state: Solid.

Colour: greenish or yellow-brown

Odour: Odourless.

Taste: Tasteless.

Melting point: 680 °C (1,256 °F; 953 K) (anhydrous) decomposes, 300 °C (572 °F; 573 K) (monohydrate) decomposes, 60–64 °C (140–147 °F; 333–337 K) (heptahydrate) decomposes)

Solubility in water: Monohydrate: 44.69 g/100 mL (77 °C) ,35.97 g/100 mL (90.1 °C)

Heptahydrate:15.65 g/100 mL (0 °C) , 19.986 g/100 mL (10 °C) 29.51 g/100   mL   (25 °C) 39.89 g/100 mL (40.1 °C) 51.35 g/100 mL (54 °C)

4.5 Sodium Hydroxide [121]

Synonyms: Caustic soda

Chemical formula: NaOH

Chemical Structure:

Na—O—H
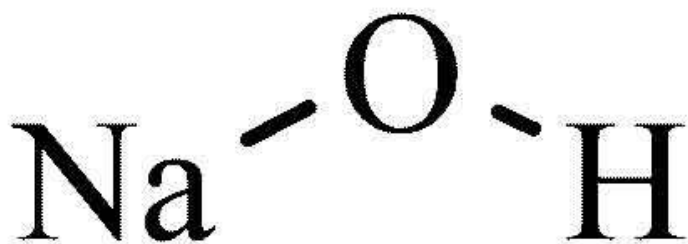
Molecular Weight: 39.9971g/mol

Physical state: Crystalline solid

Appearance: White, hard (when pure), opaque crystals

Odour: Odourless.

Taste: Tasteless.

Density: 2.13 g/cm3

Melting point: 323 °C (613 °F; 596 K)

Solubility: soluble in glycerol, negligible in ammonia, insoluble in ether, slowly soluble in propylene glycol

LD50 (median dose): 40 mg/kg (mouse, intraperitoneal)

4.6 Disodium phosphate dihydrate [122,123]

Synonyms: Disodium hydrogen phosphate dihydrate

Chemical formula: $Na_2HPO_4 \cdot 2H_2O$

Chemical Structure:
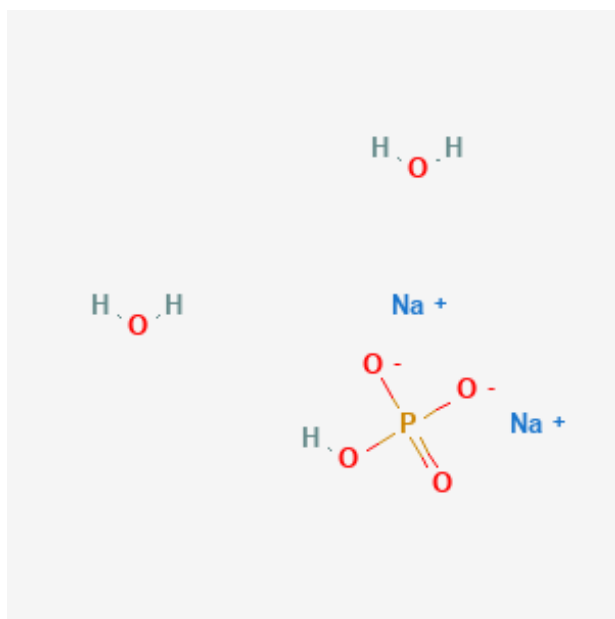
Molecular Weight: 177.99 g/mol

Physical state: Crystalline powder

ph of 2.5% in water : 8.8-9.4

Colour : White

Odour: Odourless.

Taste: Tasteless.

Density: 2.13 g/cm3

Melting point: 323 °C (613 °F; 596 K)

Solubility: highly soluble in water

Application(s): liquid formulation, parenterals, **p**harma/biopharma processes, pharmaceutical

4.7 Potassium dihydrogen orthophosphate [124,125,126]

Synonyms: Disodium hydrogen phosphate dihydrate

Chemical formula: KH_2PO_4

Chemical Structure:
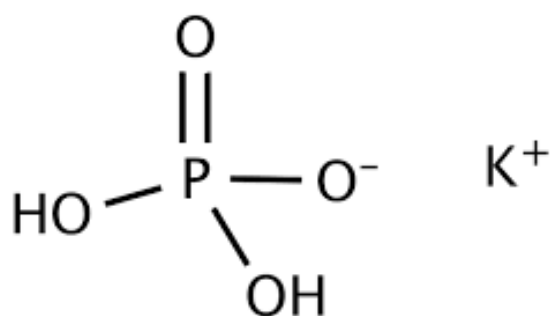
Molecular Weight: 136.09 g/mol

pH of 1% solution: 4.5-4.7

Physical state: Crystalline powder

Colour : White

Odour: Odourless.

Taste: Tasteless.

Melting point: 253 °C

Solubility: Freely soluble in water.

Application(s): Determination of pH, pharmaceutical production, urinary acidifier, paper processing, baking powder, and food), nutrient solutions, yeast foods, special liquid fertilizers, sonar systems and other electronic applications

Chapter 5

Method And Characterization.

5.0 Pre-formulation studies

5.1 Physical characterization

The physical characters like colour, texture of the drug was identified by visual examination.

5.2 Evaluation of melting point

Heating was employed to seal one end of the capillary tubes utilised for the melting point investigation. Those capillary tubes were thereafter filled with the aceclofenac. And after placing a certain quantity of the medication within the capillary tube, it was lightly tapped on the closed end in order to fill the capillary tube to a depth of 1-2 millimetres. The capillary tube was then placed in the tube holder of the device (SUNBIM®) used to determine the melting point. The knob that controls the temperature was turned to the appropriate setting. The temperature was recorded when it appeared that the drug had begun to melt. The temperature was again observed and recorded at the point of time when the drug had totally melted. The drug's melting point was determined by taking the average of the two temperatures that were recorded. In order to achieve the best possible result, the procedure was carried out thrice.

5.3 Preparation of standard curve for aceclofenac

5.3.1 Preparation of 0.01N phosphate buffer, pH 6.8

1.387 gm of Potassium dihydrogen orthophosphate and 3.508gm of Potassium dihydrogen orthophosphate was taken and dissolved in water to obtain 100ml of 0.01N phosphate buffer pH (6.8).

5.3.2 Determination of absorption maxima

The UV absorption maximum of aceclofenac (10 μg /ml) dissolved in phosphate buffer pH (6.8) was determined by scanning the solution in the region of 200-400nm with a UV Spectrophotometer (UV-1800, Shimadzu, Japan).

5.3.3 Determination of standard curve of aceclofenac

100ppm stock solution was prepared by dissolving 10 mg of aceclofenac accurately weighed in 100ml phosphate buffer 6.8 pH. From the stock solution, aliquots of 2, 4, 6, 8, 10, 12, 14, 16, 18, and 20μg/ml were scanned at 273.60nm (max) using a UV Spectrophotometer (UV-1800, Shimadzu, Japan) with spectral bandwidth of 1 nm ± 0.3 nm wavelength precision. All samples were analysed three times to reduce error.

5.4 METHOD OF PREPARATION

The coprecipitation method is a commonly used technique to prepare magnetite nanoparticles using $FeCl_3$ and $FeSO_4$ as precursors. The general procedure is as follows:

5.4.1 Magnetite preparation:

Two distinct solutions of 0.1 M $FeCl_3$ and 0.05 M $FeSO_4$ in deionized water are prepared. The two solutions are subsequently combined in a breaker after being properly mixed with a magnetic stirrer. 1M NaOH solution is dropwise added to it while the reaction mixture is subjected to constant stirring at an elevated temperature. It is further stirred for 24 hours to facilitate the formation of the magnetite nanoparticles by the coprecipitation method. The solution is then allowed to sit undisturbed for a period of two hours, which ultimately causes the precipitation of the magnetite. The supernatant (figure 8) is discarded after the solution has been thoroughly decanted. Finally, the extracted magnetite nanoparticles are dried in a hot air oven at 70°C, grinded, and sieved.
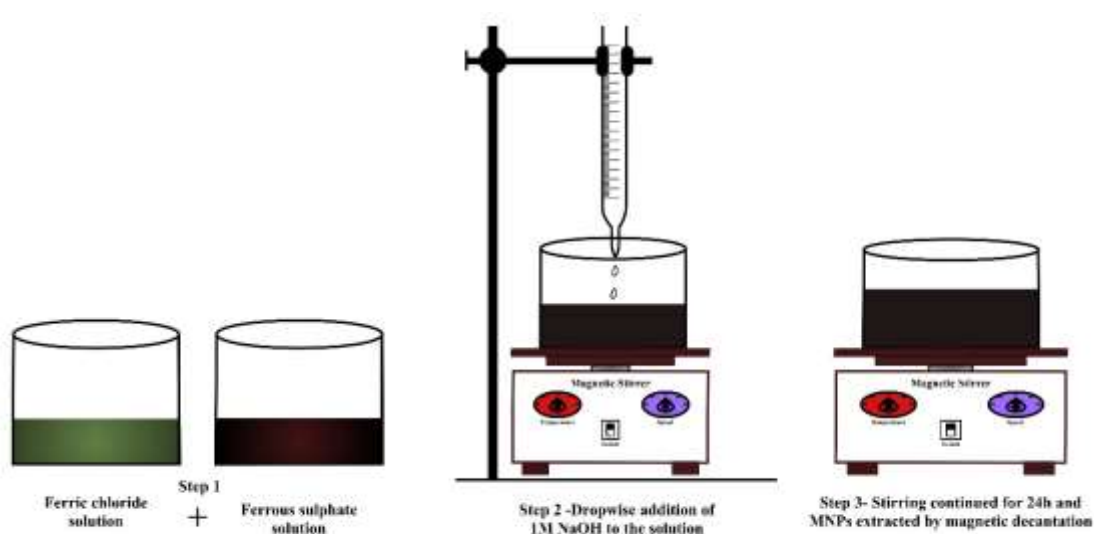

Figure 8 : Synthesis of MNPs by co-precipitation method. Step1: Mixing of $FeCl_3$ solution and $FeSO_4$, step 2: stirring the solution at 80-85°C and dropwise addition of NaOH, step 3: stirring for 24hrs and then precipitated MNPs are extracted either by magnetic decantation or centrifugation or both. Furthered the extracted MNPs are dried and grinded.

5.4.2 Preparation of magnetic nanoparticles bead

Formulation 1 (F1): 20 mg of aceclofenac (drug) is dissolved in 20ml of buffer solution of pH6.8, 0.5 g of sodium alginate is added to it. It is mixed properly with the help of magnetic stirrer. After complete dissolution remove the magnetic stirrer. 50mg of prepared magnetite is added to the beaker containing the solution and is mixed thoroughly using mechanical stirrer.

In a separate beaker, a solution of 5% $CaCl_2$ that is 5g in 100ml deionised water is prepared. After complete dissolution, the solution of $CaCl_2$ is transferred to a petri-dish. Lastly, the solution containing drug+ sodium alginate + magnetite is drop by drop added to the petri-dish form the formation of magnetic nanoparticles beads. The formed beads are then filtered and dried.

Formulation 2 (F2): In this formulation all the parameters and procedure are same as formulation 1 expect, the amount of magnetite is changed i.e., 100mg of prepared magnetite is added.

Formulation 3 (F3): Similarly in formulation 3 all the parameters are same as formulation 1, only the magnetite amount was changed to 150mg.

Formulation 4 (F4): 20 mg of aceclofenac (drug) is dissolved in 20ml of buffer solution of pH6.8, 1 g of sodium alginate is added to it. It is mixed properly with the help of magnetic stirrer. After complete dissolution remove the magnetic stirrer. 50mg of prepared magnetite is added to the beaker containing the solution and is mixed thoroughly using mechanical stirrer.

In a separate beaker, a solution of 5% $CaCl_2$ that is 5g in 100ml deionised water is prepared. After complete dissolution, the solution of $CaCl_2$ is transferred to a petri-dish. Lastly, the solution containing drug+ sodium alginate + magnetite is drop by drop added to the petri-dish form the formation of magnetic nanoparticles beads. The formed beads are then filtered and dried.

Formulation 5 (F5): All the parameters and procedure is similar to formulation 4, expect the amount of magnetite was change to 100mg.

Formulation 6 (F6): All the parameters and procedure is similar to formulation 4, expect the amount of magnetite was change to 150mg.

Formulation 7 (F7/blank): The beads prepared in this formulation is without drug. All other parameters and procedures to prepare the beads are same as formulation 5.

Table 7 summarizes the formulation of MNP beads. It shows the different components of the beads, and their concentrations used to synthesize them.

Table 7: Magnetic nanoparticles beads formulation.

Formulations	Drug	Sodium alginate	Magnetite	$CaCl_2$
F1	20mg	0.5g	50mg	5g
F2	20mg	0.5g	100mg	5g
F3	20mg	0.5g	150mg	5g
F4	20mg	1g	50mg	5g
F5	20mg	1g	100mg	5g
F6	20mg	1g	150mg	5g
F7/ blank	-	1g	100mg	5g

5.5 Characterization of prepared formulation

5.5. 1 Percentage yield

➢ Percentage yield of MNPs

The percentage yield of MNPs were determined by measuring the prepared actual weight of MNPs and the weight of chemicals used in the preparation of MNPs i.e., Weight of $FeCl_3$, $FeSO_4$ and NaOH. Percentage yield of MNPs were calculated using formula separately:

$$\% yield\ of\ MNPs = \left\{ \frac{Actual\ weight\ of\ MNPs\ prepared}{Weight\ of\ FeCl3 + FeSO4 + NaOH} \right\} * 100$$

➢ Percentage yield of MNPs beads

The percentage yield of MNPs beads were determined by measuring the prepared actual weight of beads and the initial weight of drug with excipients used in the preparation of beads, i.e., the weight of drug, polymer, and other excipients. Percentage yield of MNPs beads were calculated using formula:

$$\% yield\ of\ MNPs\ beads =$$
$$\left\{ \frac{Actual\ weight\ of\ MNPs\ beads\ prepared}{Weight\ of\ drug + MNPs + polymer + other\ exipient} \right\} * 100$$

5.5.2 Drug entrapment efficiency (%EE)

The suspension of MNP beads was filtered, leaving behind the supernatant. The supernatant was analysed at 273.60nm spectrophotometrically to determine the presence of drug in the it. The drug present in the supernatant indicates the amount of drug which is not entrapped n the **beads.**

$$\% EE = \left\{ \frac{Drug\ added - Unbound\ drug}{Drug\ added} \right\} * 100$$

5.5.3 Optical microscopy

A compound light microscope was used to obtain magnified views of the three formulations of magnetic nanoparticles beads (F2, F5, and F7). A small amount of sample from each formulation was placed on a glass slide and examined under the microscope. The optical microscopic analysis allowed for a thorough examination of the structure of the nanoparticles.

5.5.4 Scanning electron microscopy (SEM)

Scanning Electron Microscopy (SEM) is a powerful imaging technique used to observe the surface of materials at high magnifications. It provides detailed information about the morphology, topography, and composition of a sample. In SEM, the electron beam is scanned across the surface of the sample. The electrons interact with the sample and produce secondary electrons, backscattered electrons, and transmitted electrons. These electrons are collected and used to create an image of the sample surface.

Scanning electron microscopy (SEM) is a popular way to study the shape and size of MNP, MNP beads. The surface morphology of the prepared formulations of magnetic nanoparticle, F2, F5 are analysed using GeminiSEM 300, Carl Zeiss Microscopy GmbH. Scanning Electron Microscope. Small samples were positioned on a metal stub applying double sided adhesive carbon tape and they were coated with a thin layer of gold to prevent charging effects and improve image quality. The sample is then put inside the SEM apparatus, where an electron beam is directed at it. The secondary electrons produced by the interaction between the electrons and the material are detected by a detector. The resultant imagine offers a three-dimensional outlook of the surface morphology, including information on its size, shape, and surface roughness of all three formulations.

5.5.5 Transmission Electron Microscopy (TEM):

Transmission Electron Microscopy (TEM) is a powerful imaging technique used to visualize the structure, composition and morphology of magnetic nanoparticles (MNPs) at the nanoscale level. A high-energy electron beam is transmitted through the sample in TEM, where it interacts with the MNPs to produce a detailed image. Unlike SEM, in TEM, the electron beam is passed through the sample and create diffraction patterns. These diffraction patterns are utilised to generate an internal image of the sample.

For the TEM analysis, a diluted solution of F5 was prepared. A small amount of the diluted sample solution was then drop-cast onto a carbon-coated copper grid using a micropipette. The

solvent was allowed to evaporate, leaving behind a thin film of the sample on the grid. The prepared TEM grid containing the sample was carefully loaded into the TEM instrument (JEM 2100F), ensuring proper securing and alignment for imaging. The grid was exposed to a beam of electrons at an accelerated voltage of 200 kV. The electrons interacted with the sample, producing a high-resolution image that revealed the internal structure of the drug-loaded MNPs bead.

5.5.6 Atomic force microscopy (AFM)

AFM is a powerful technique for imaging and characterizing the surfaces of magnetite and MNP beads. It can be used to obtain high-resolution images of the surface of these materials, which can be used to understand their structure and properties. AFM can also be used to measure the size, shape, and surface roughness of magnetite and MNP beads, as well as their interactions with other materials. The sample of magnetite or MNP beads are typically prepared by depositing it on a substrate, such as a silicon wafer or glass slide.

AFM is an effective technique for imaging and analysing the magnetite and MNP particle surfaces. This technique enables researchers to acquire high-resolution images of these materials, which facilitates an in-depth comprehension of their surface structure. Magnetite or MNP beads are typically produced by deposition on a substrate, such as a silicon wafer or glass slide. The analysis was done using Lake shore, GMW Magnet system, electromagnet.

5.5.7 Fourier Transform Infrared Spectroscopy

Attenuated Total Reflectance Fourier Transform Infrared (ATR-FTIR) spectroscopy is a powerful analytical technique used to investigate the composition and chemical properties of various materials. It is particularly useful for analysing solid and liquid samples that may not be easily measured by traditional transmission spectroscopy. FTIR was used to ascertain if there is a relationship between a drug and a polymer. Individual IR spectra of magnetite, drug, F2, F5, and blank MNP (F7) beads were obtained to further understand the correlations. Analysis was done on a Spectrum Two FT-IR Spectrometer, Perkinelmer, using Perkinelmer spectrum software. For three minutes, scanning was done over a range of 4000-400 cm^{-1}. The samples were placed against a high refractive index prism using the attenuated total reflectance (ATR) method, and the infrared spectrum was measured using infrared light that is completely

internally reflected in the prism. The chemical bonds in the sample vibrate at various frequencies as a result of the infrared radiation's interaction with the sample. The resultant absorption spectrum is recorded and analysed in order to identify the functional groups present in the sample and to provide information about interactions between the various sample components.

5.5.8 Powder X-Ray Diffraction analysis (PXRD):

The primary purpose of XRD analysis is to ascertain the crystallographic structure of a substance. The X-Ray Diffraction analysis of magnetic nanoparticles was done by Bruker Eco D8 advance. The samples were ground into a fine powder to ensure homogeneity and increase the surface area for diffraction. Small amount of aceclofenac, magnetite, powered MNP5, powdered MNP2, powdered blank was pressed on the sample and was place in the instrument's sample stage one by one. The atoms in the sample diffract the X-rays, generating a diffraction pattern that is captured by a detector. Using X'pert Highscore XRD software, the diffraction patterns were analysed. The samples were scanned at range of 2θ from 5° to 90°.

5.5.9 Vibrating Sample Magnetometer (VSM)

Vibrating Sample Magnetometer (VSM) is a widely used technique to measure the magnetic properties of materials. It determines the magnetization of a sample as a function of an applied magnetic field. The analysis of the formulations was done using GMW Magnet system Model 3474-190 Electromagnet. The samples were weight accurately and was inserted into the probe securely. The magnetization of the sample was measure and recorded.

5.5.10 *In-vitro* drug release

In this investigation, the release of aceclofenac from the alginate-based beads was determined using a United States Pharmacopeia (USP) dissolution apparatus 1. The dissolution medium employed for this purpose had a pH of 6.8. Initially, 20mg equivalent drug content of the formulated beads was weighed and subsequently placed into a preheated basket maintained at 37 ± 0.5 °C. This basket was then immersed into 600 mL of the dissolution medium. The basket rotation was set at a speed of 100 rpm while maintaining a temperature of 37 ± 0.5 °C. At

predefined time intervals, samples were collected, and the quantity of aceclofenac released from the formulated beads was determined using a UV-VIS spectrophotometer with a λmax of 273.60 nm.

5.5.11 Kinetics of release

The pharmacokinetics of a drug delivery vector can be understood with the use of a kinetic model. Solubility, particle size, crystallinity, and amount of drug, as well as the nature of the vector that encapsulates the drug, all play a crucial role in the release pattern of the drug from the vector. Different kinetic models such as zero-order ($Q_t = K_0t + Q_0$), first-order ($Q_t = Q_0e^{-K_ft}$), Higuchi ($Q_t = K_H\sqrt{t} + Q_0$), Korsmeyer-Peppas ($Q_t/Q_\infty = K_kt^n$) and Hixon-Crowell ($Q_0^{1/3}/Q_t^{1/3} = K_st$) are used to describe the kinetics of drug release. For these equations, Q_t is the amount of drug released at time t, Q_0 is the initial amount of drug, K_0, K_f, K_H, K_s, K_k are release rate constants for Zero-order kinetics, First-order kinetics, Higuchi model, Hixon-Crowell model and Korsmeyer-Peppas model, respectively.

Chapter 6

Results and discussion

6.1 Physical Characterization of drug

The organoleptic characters such as appearance, colour, and odour of the received sample of aceclofenac was studied. It shows all the properties that comply to standards as per IP. The details have been summarized in table 8.

Table 8: Physical properties of aceclofenac

Sl no.	Property	Observation
1.	Visual appearance	powder
2.	Colour	Pale white
3.	Odour	Odourless

6.2 Melting point of drug

According to IP melting point of a substance is defined as those points of temperature at which the substance begins to melt and is completely melted except as defined otherwise for certain substances. Pure aceclofenac has a standard melting point range of 149-153°C. The recorded average melting point of aceclofenac is 151°C. As the recorded average melting pointing is within the range, it indicates the purity of the sample.

6.3 Standard curve of aclecofenac

Absorption maxima

The UV absorption maximum was recorded at λmax 273.60 nm of Aceclofenac (10 μg /ml) dissolved in phosphate buffer pH (6.8).

Calibration curve

The aliquots of aceclofenac in phosphate buffer pH 6.8 ranging from 2μg /ml to 20μg /ml showed linearity at λmax 273.60 nm. The absorbance data and its standard curve is shown intable 9 and figure 9 respectively.

Table 9: Absorbance of aliquoits of aceclofenac at λmax 273.60nm.

Concentration(μg/ml)	Absorbance
2	0.06166667
4	0.12066667
6	0.18833333
8	0.25166667
10	0.308
12	0.376
14	0.43833333
16	0.49433333
18	0.54
20	0.59933333
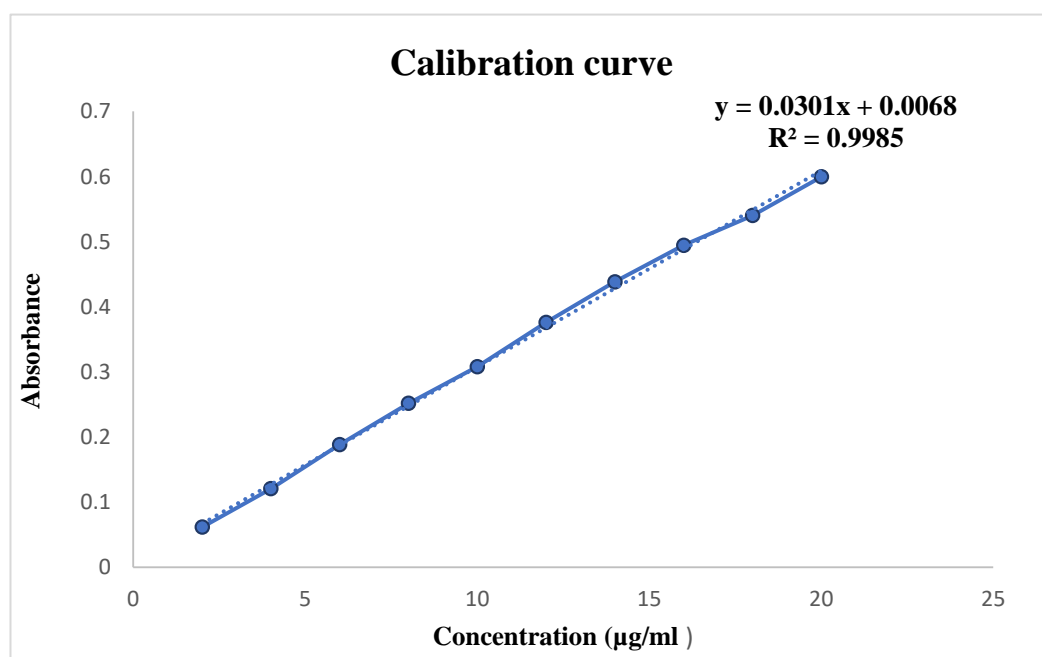
Figure 9: Standard calibration curve of aceclofenac in phosphate buffer solution of pH 6.8

.

6.4 Physical Characterization of magnetite and MNPs beads

The prepared magnetite was checked for uniformity, texture and appearance. Both magnetite and MNPs beads was found to have smooth, circular and uniform texture (figure 10)
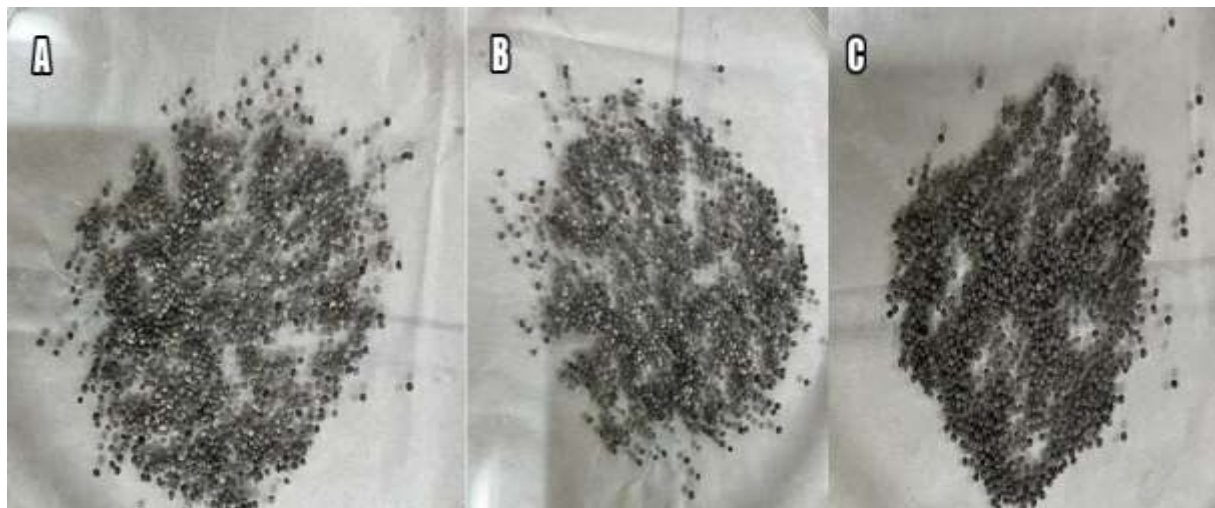
Figure 10: Dried magnetic nanoparticles beads. (A) blank, (B) F2, (C) F5.

6.5 Percentage Yield and Entrapment Efficiency

Percentage yield is the ratio of the mass of the product to the mass of the starting material. In this study, while the percentage yield of MNP beads ranged between 81-90%. This suggests that MNP beads are more efficient at entrapping magnetite than magnetite beads.

Entrapment efficiency is the ratio of the mass of the magnetite entrapped in the beads to the mass of the magnetite added to the reaction mixture. In this study, the entrapment efficiency of MNP beads ranged between 88-95 %. This suggests that MNP beads are also more efficient at entrapping magnetite than magnetite beads. Table 10 summarizes the percentage yield and entrapment efficiency of the three formulations.

Table 10: Percentage yield and entrapment efficiency result of the prepared formulations

Formulation code	Percentage yield	Entrapment efficiency %
F1	81.25	88.52
F2	89.54	94.69
F3	82.65	89.52
F4	85.33	90.10
F5	88.75	94.46
F6	82.44	89.22
F7	87.46	94.06

6.6 Optical microscopy

In order to examine the structure of the beads, optical microscopy analysis was performed at 100x. MNP beads were observed to be nearly circular (figure 10). Due to the poor magnification of the trinocular microscope, it was challenging to observe a detailed surface view of the beads. In order to obtain a greater understanding of the surface of the beads, SEM was conducted.
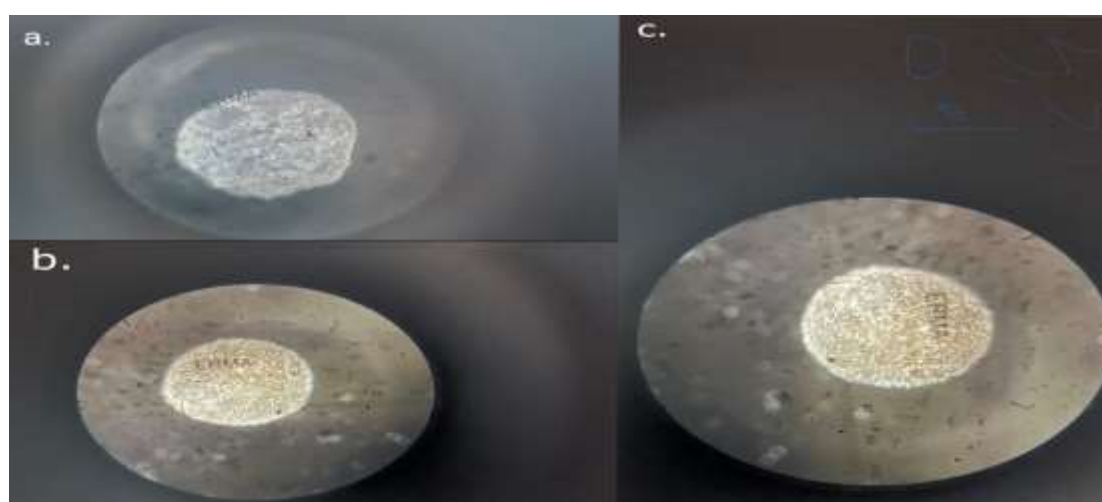
Figure 10: Images of MNPs beads from trinocular microscope, where a: F2, b:

F5, and c: F7.

6.7 SEM

The surface of magnetite and MNPs bead (F2 and F5) is rendered in exquisite detail by SEM images. The SEM images of magnetite show that the magnetite is of nano-range and has a spherical structure (figure 11). The MNPs beads also have a nearly spherical shape, with cross-sections of 1.108mm x 1.445mm for F2 and 1.100mm x 1.323mm for F5 (figure 12). The smooth surface of both MNPs beads indicates that they have been properly coated with polymer. There were no substantial fractures found in any of the beads.
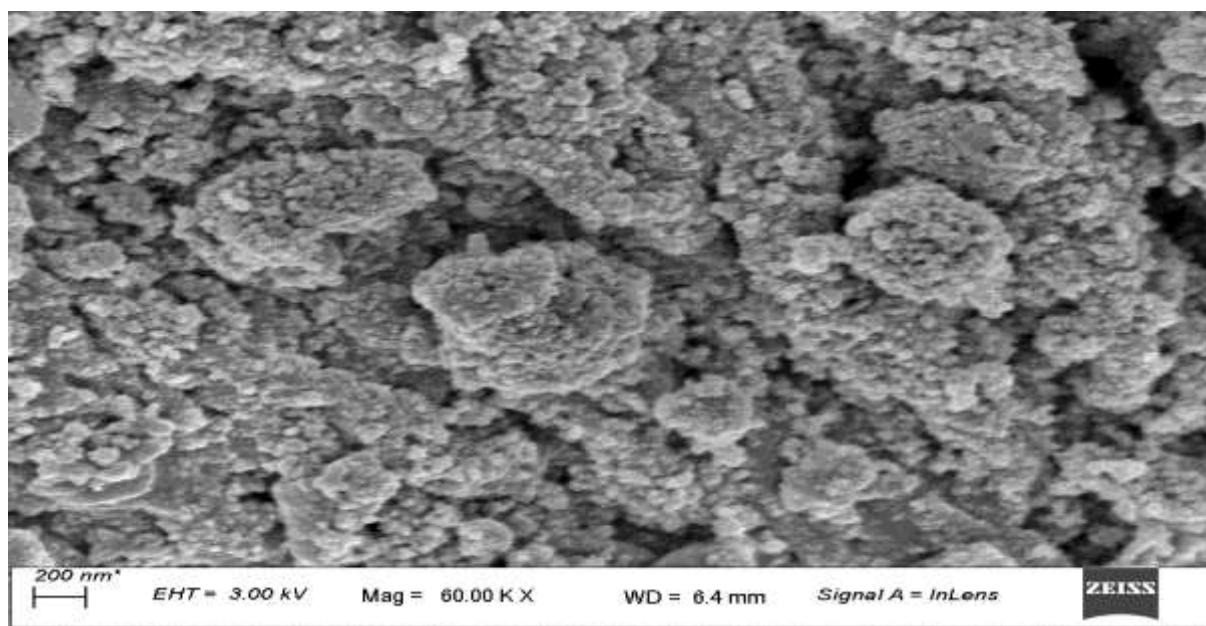
Figure 11: SEM images of synthesized magnetite.
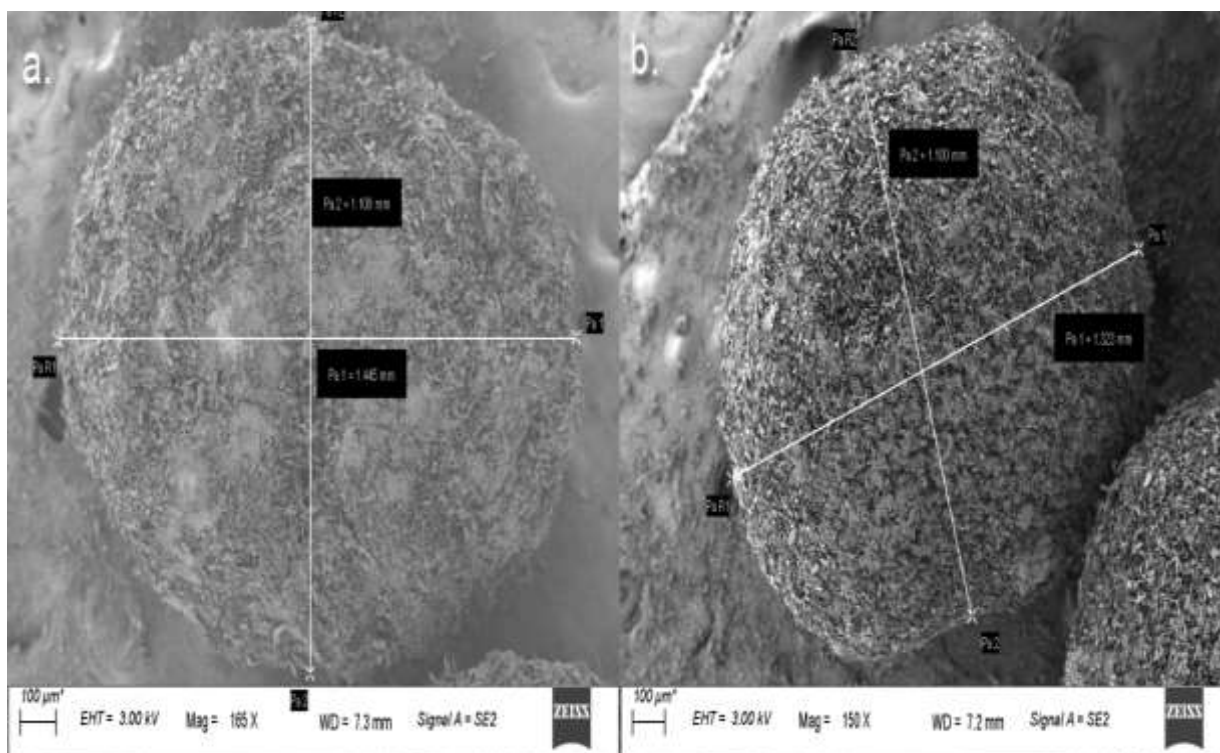
Figure 12: SEM images of MNPs beads. a - F2 and b- F5

6.8 TEM

The TEM analysis of F5 showed that the sample was composed of a matrix with ellipsoidal particles smaller than 200 nm (figure 13). Some of the particles were scattered, while others were aggregated. This indicates that the sample was stabilized [127].
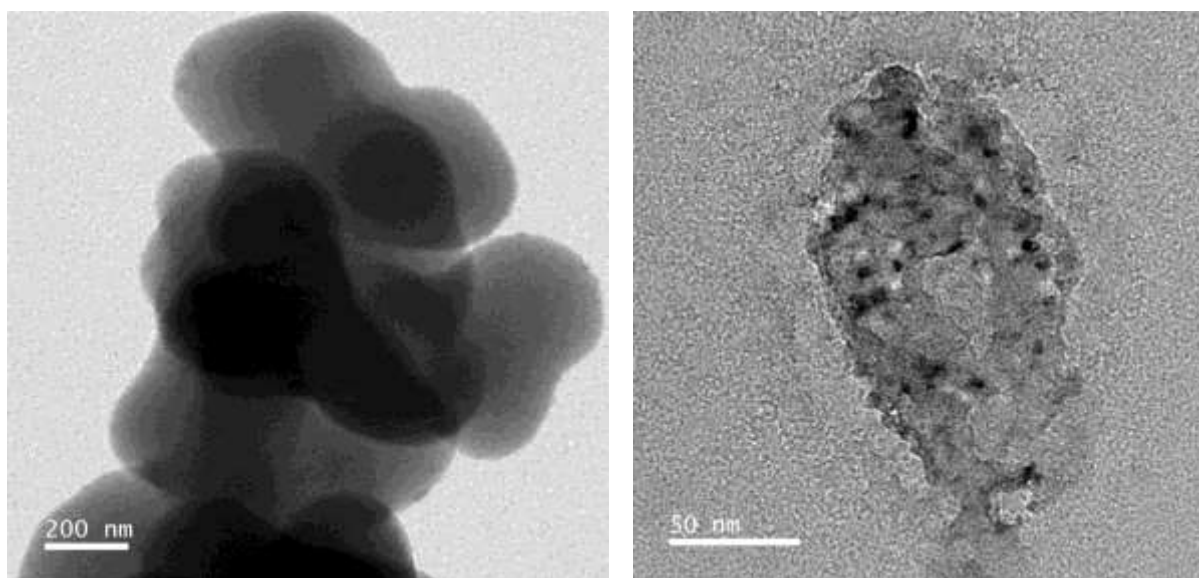
Figure 13: TEM images of F5, MNP beads, scale 200 and 50 nm

The EDX analysis, figure 14 of F5 showed the presence of C, Fe, Cl, and O peaks. These peaks correspond to the presence of aceclofenac and magnetite in the solution prepared for TEM analysis. The presence of Cl indicates that the aceclofenac was present in the sample, while the presence of Fe and O indicates that the magnetite was present in the sample.
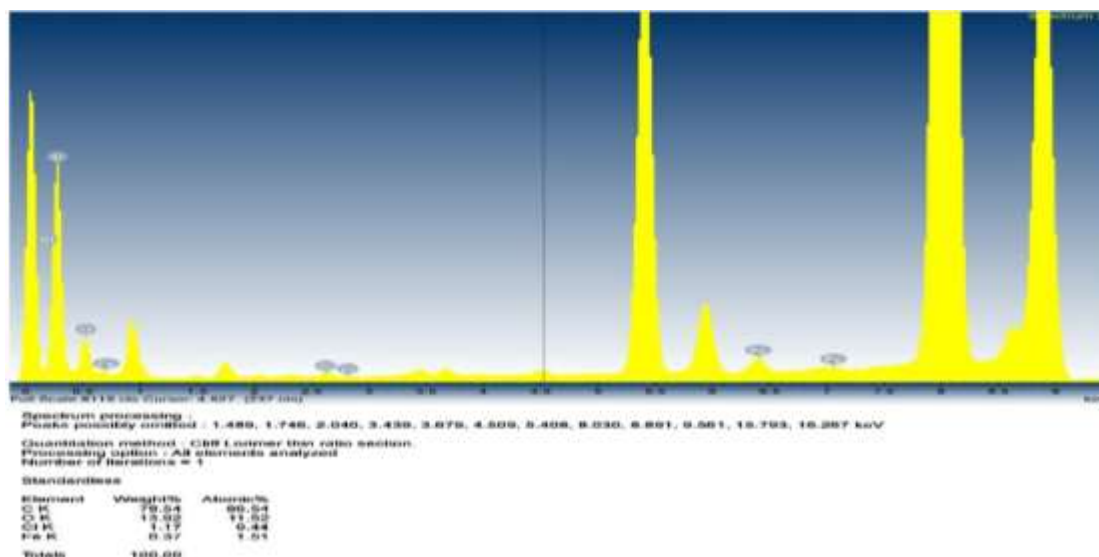
Figure 14: EDX analysis of F5 samples

6.9 AFM

The magnetite nanoparticles were deposited and dried on the glass for AFM characterization. The results were obtained to determine to the three dimensions (3D) and roughness of the samples. Figure 15 shows the resulting 3D images of the prepared samples, the maximum high of magnetite samples is 37.25, F2 is 65.19, F5 is 12.63 for a scan range of 20μm * 20μm according to histogram in figure 16 . Zakiyyu I. T. et al., stated that the knob spots yellow spot indicate the present of small agglomeration of Fe_3O_4 nanoparticles, which is also noted in the prepared F2, F5, and magnetite samples [128].
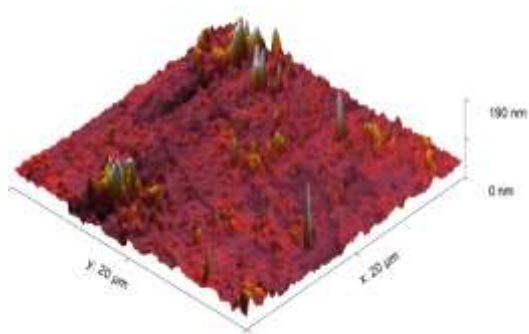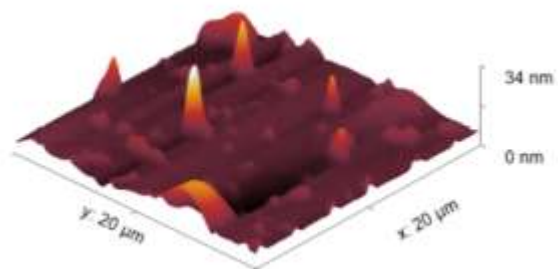
(i)   (ii)
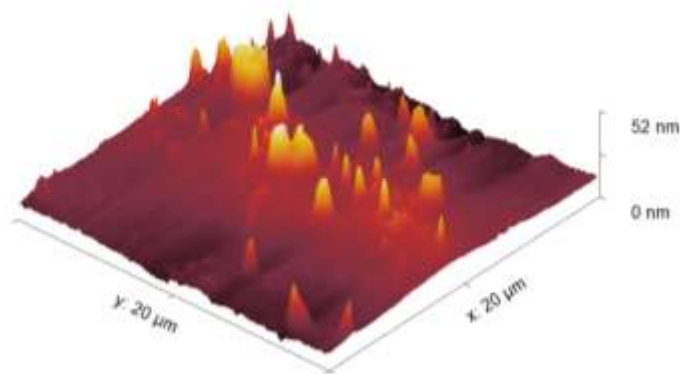
(iii)

Figure 15: AFM 3D image of prepared formulations. i) magnetite ii) F2 iii) F5

(i)

(ii)

(iii)
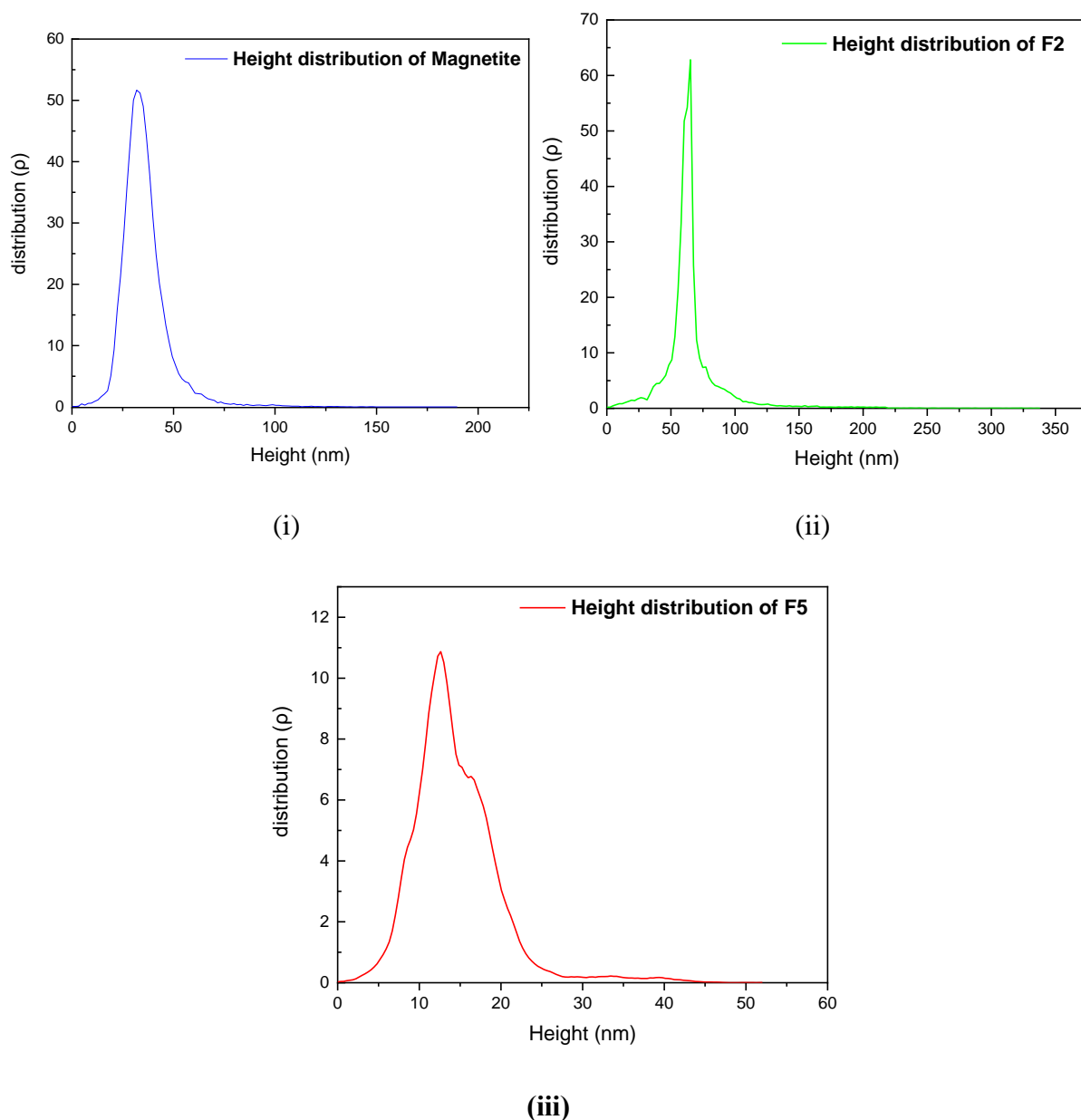
Figure 16: Histogram obtain from AFM analysis. (i) magnetite, (ii) F2. (iii) F5**.**

6.10 FTIR

Figure 17 represents the FTIR spectrum of drug, magnetite, F2, F5 and blank samples. The spectrum of aceclofenac showed characteristic bands at 3316.83 cm $^{-1}$ (N-H stretching), 1769.50 cm^{-1} and 1713.90 cm^{-1} (C=O stretching, carboxylic acid), 1581.53 cm^{-1} (Skeleton vibration of aromatic C-C stretching), 1504.59 cm^{-1} (N-O stretching, nitro compound) , 1444.20 cm^{-1} (O-H bending, carboxylic acid), 1344.28 cm^{-1} (O-H in plane bending), 1251.23 cm^{-1} (C-N stretching, aromatic amine) , 1142.37 cm^{-1}(C-O stretching, aliphatic ether), 1054.39

cm^{-1} (C-O stretching, primary alcohol) , 964.61 cm^{-1}(C=C bending, alkene), 663.73 cm^{-1} (C=C bending) indicates the presence of benzene derivative. [129, 130, 131]. The frequency range 1129–480 cm^{-1} indicated the vibration of C-X group (X= Cl, Br, I) that is halo compounds. The FTIR absorption band at observed at 850.53 cm^{-1}, 612.57 cm^{-1}, 513.43 cm^{-1} indicates C-Cl stretching [132].

In the FTIR spectrum of magnetite, strong absorption bands between 400 and 700 cm^{-1} are reported to be caused by Fe–O vibrations, which are indicative of the presence of Fe_3O_4 and $Fe_{2.67}O_4$. The strong infrared absorption peak observed at 558.25 cm^{-1} indicated stretching and banding of Fe–O bonds present in the magnetite [133]. The broad band at 3442.95 cm^{-1} and the band at 1669.98 cm^{-1} are ascribed to the vibrational mode of O–H groups adsorbed to the surface of magnetite particles [134].

The absorption spectrum of F2 showed broad and strong band at 3364.44 cm^{-1} indicated O-H stretching. The range of 3000–3600 cm^{-1} displays the vibrations of O–H bonds stretching of Na-alginate. The sudden intense broad peak at 3364.44 cm^{-1} which was absent in both drug and magnetite, signifies the presence of Na-alginate in the sample. The presence of a prominent band at 1649 cm^{-1} [135] and 1596.3 cm^{-1} [136] indicates the occurrence of asymmetric stretching vibrations of carboxylate salt ions. This particular band holds great significance and can be utilized for characterizing the structure of alginate and its derivatives [135]. A band observed at 1638.76 cm^{-1} confirm the presence of Na-alginate. The spectrum of F2 also showed strong band at 1638.76 cm^{-1} (C=C stretching), medium band at 1121.30 cm^{-1} (C-N stretching, amine), strong band at 1053.29 cm^{-1} (C-O stretching, primary alcohol) 984.64 cm^{-1}(C=C bending, alkene) medium band at 868.76 cm^{-1}(C-Cl stretching) , medium band at 783.36 cm^{-1}(C=C bending, alkene) [131]. The bands at fingerprint regions like C-N stretching band, C-Cl stretching which were noted for pure drug (aceclofenac) are also present in absorption spectrum of F2 which validates the presence of aceclofence in the sample of F2. However, there are shifting of the peaks like C-Cl stretching in drug was noted at 850.53 cm^{-1}, 612.57 cm^{-1}, 513.43 cm^{-1} whereas for F2 it was noted at 868.76 cm^{-1}. Moreover, the F2 sample did not show many characteristic bands related to aceclofenac.   This suggests that the aceclofenac is entrapped in the beads. The band observed at 570.73 cm^{-1} indicated Fe–O stretching and banding. This peak confirms the presence of magnetite in the sample F2 [133]. However, the absorption spectrum of F2 does not exactly coincide with the spectrum of magnetite or aceclofenac. This is because they are entrapped in the beads, which changes the molecular environment of the aceclofenac and causes the IR bands to shift

The IR absorption spectrum of F5 is very similar to F2, with the main difference being that the peaks are less strong in F5. This is likely due to the higher concentration of polymer (Na-alginate) in F5, which results in more cross-linking and better entrapment of the drug. As a result, the drug molecules are less able to vibrate and absorb IR radiation, which leads to weaker peaks.

The absorption spectrum of the blank sample showed peaks that were very similar to magnetite, but were comparatively less strong. This suggests that the blank sample contained magnetite and decrease in peak intensity is likely due to the entrapment of magnetite in the bead. Additionally, the blank sample did not show any significant peaks related to aceclofenac, which confirms the absence of drug in the sample.
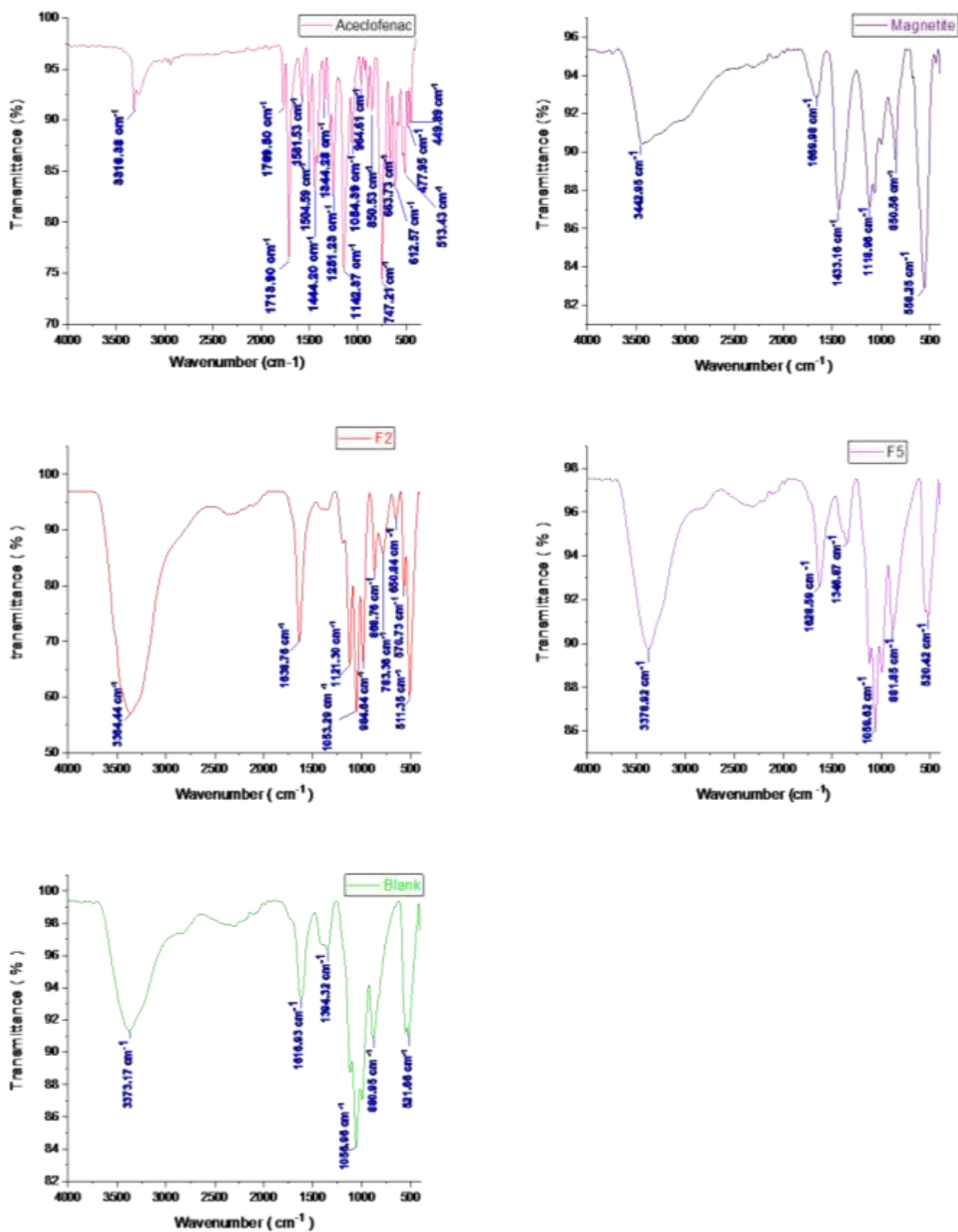
Figure 17 : FTIR spectra of aceclofenac, magnetite, F2, F5, and blank.

6.11 PXRD study

The result of a PXRD experiment typically consists of a diffraction pattern, which is a plot of the intensity of diffracted X-rays as a function of the scattering angle. This pattern contains information about the arrangement of atoms in the crystal lattice of the material, crystallinity, crystalline phase, purity, and texture. Figure 18 PXRD spectra of aceclofenac, magnetite, F2, F5, and blank.. The characteristic peak of drug (aceclofenac) at 2θ (8.46^0, 11.15^0, 14.16^0, 16.52^0, 17.20^0, 18.17^0, 19.11^0, 21.95^0, 24.17^0, 25.63^0, 31.85^0, 32.83^0, 33.51^0, 36.26^0, 37.23^0, 38.98^0, 40.21^0 were noted, amongst which 18.17^0 ,21.95^0, 24.17^0, 25.63^0, and 31.85^0 were the most sharp and distinct. Few sharp and distinct peaks of drug were missing and few that were visible were of low intensity in F5 and F2. This could possibly be due to molecular dispersion and entrapment of the drug into the beads. The XRD spectra of blank MNP beads shows no drug peak which verify the absence of drug in it. The sample of blank MNP beads shows distinctive different XRD spectra from the drug's spectra as sharp peaks are completely absent in blank formulation.

In magnetite sample, the peaks that were noted at 2θ are 30.2^0, 35.6^0, 43.2^0, 53.6^0, 57.2^0, 62.8^0. The most intense peak is observed at $311\text{-}2\theta$ ($35°$) which confirmed the existence of magnetite particles. This peak is also noted in the sample of F2, F5 and blank but of decreased intensity.

The crystalline nature of aceclofenac was confirm by sharp peak. The decrease in the diffraction pattern in F2 and F5 which is noted, is may be the result of polymer interaction. It appears that the crystalline character of pure aceclofenac changes to an amorphous form in MNP beads loaded with drug, as evidenced by a considerable decrease in the diffraction pattern.
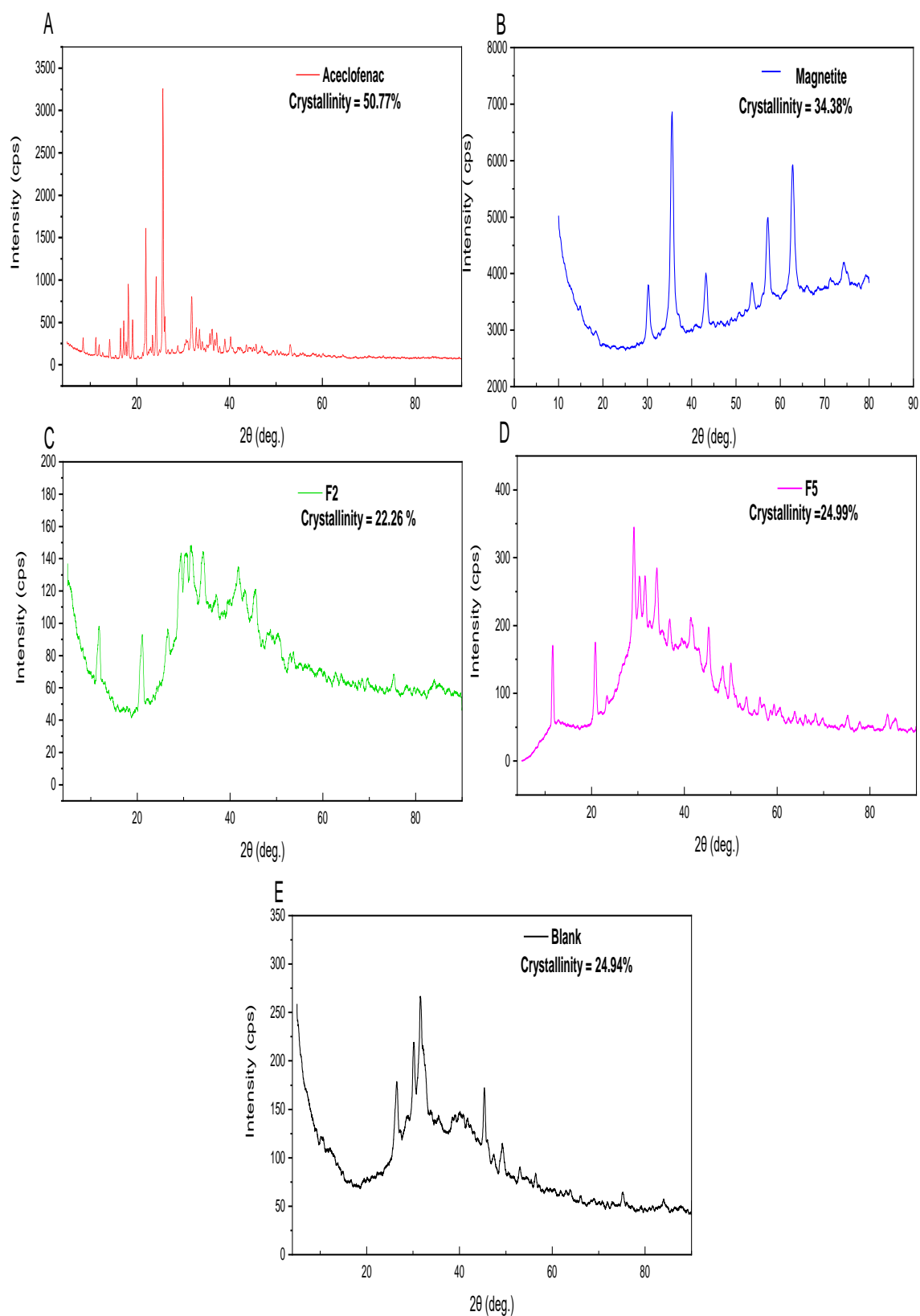
Figure 18 : XRD spectra of aceclofenac, magnetite, F2, F5, and blank.

6.12 VSM

Magnetic properties of magnetite, F2, and F5 were analysed using a VSM at atmospheric temperature. Leena Mohammed et al., suggested superparamagnetic nanoparticles (SPNPs) have higher saturation magnetization [137]. *Lorena Maldonado-Camargo et al.*, defined SPNPs as having a remanence and coercivity that are nearly negligible [138]. Figure 19 depicts the variations in magnetization property as a result of the applied magnetic field. The saturation magnetization of the magnetite is 16.53 emu/g, indicating high saturation magnetization and superparamagnetic. Moreover, the absence of hysteresis loop in the figure 19 confirms superparamagnetic nature of the samples. The saturation magnetization of F2 and F5 was noted to be in the range of 0.49 emu/g - 0.64emu/g. The decrease in saturation magnetization observed in F2 and F5 can be attributed to the presence of Na-alginate in these samples. This suggests that the Na-alginate coating lowers the magnetization of MNPs, reducing magnetic characteristics for the MNPs beads [139].

The coercivity of F2 was noted to be higher than magnetite which is due to the polymeric coating in F2. This is because the polymer coating acts as a barrier to the movement of magnetic domains within the NPs. This makes it more difficult to reverse the magnetization of the nanoparticle, which increases its coercivity. The coercive field of F5 was noted to be lesser than F2 that is due to lower proportion of magnetite with polymer than F2.

The remanent magnetization of magnetite is 0.55 emu/g, which is considered to be very low. This means that magnetite has a very weak magnetic field after withdrawal of external magnetic field. The remanent magnetization of F2 is even lower, at 0.024 emu/g. F5 has the lowest remanent magnetization of all, at 0.013 emu/g. This feature of F2 and F5 makes them suitable for targeted drug delivery. This is because it allows the nanoparticles to be easily manipulated by a magnetic field and less likely to interact with biological tissues. This could make them a safe and effective option for targeted drug delivery.
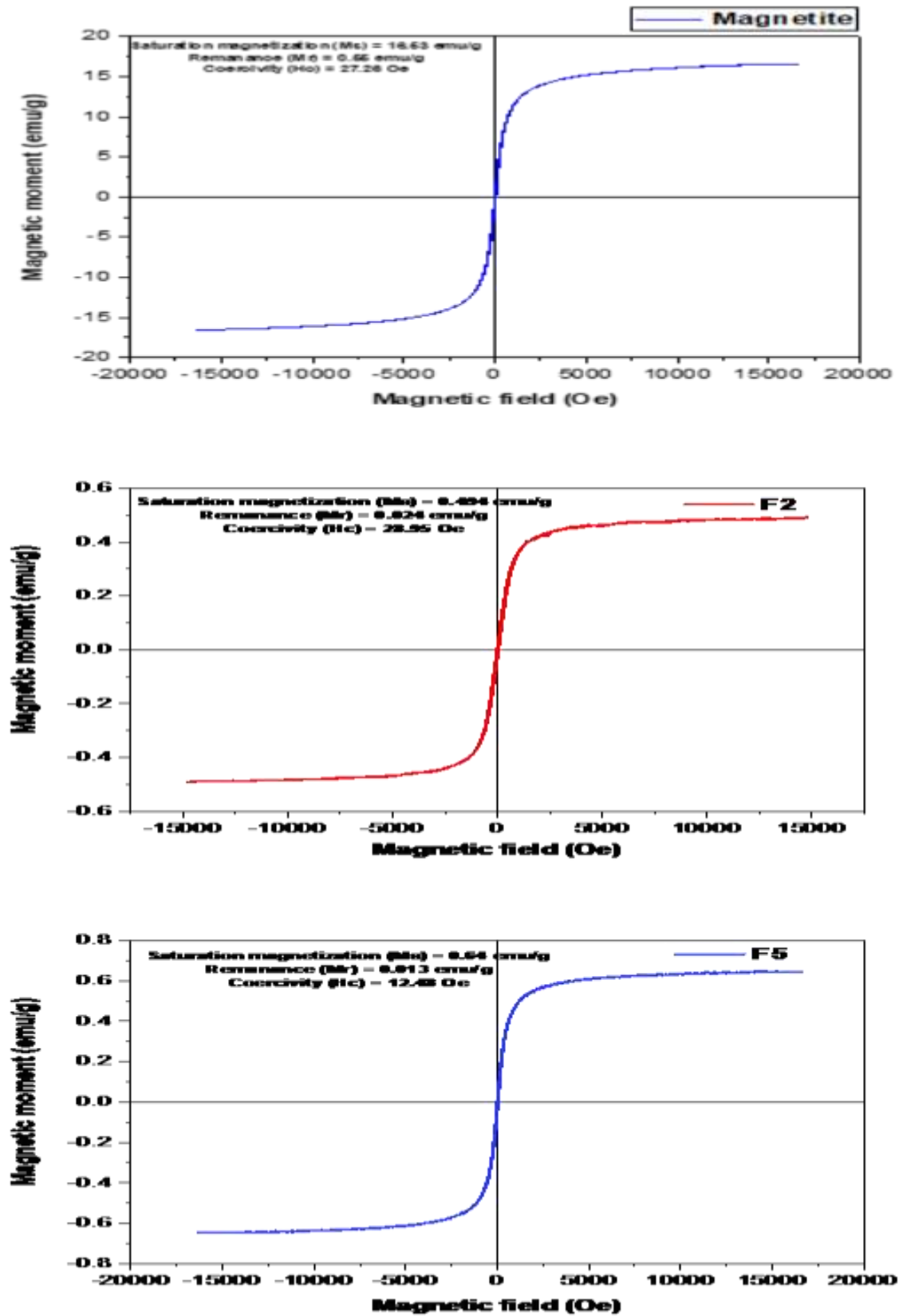
Figure 19: Variations in magnetization property as a result of the applied magnetic field.

6.13 In-vitro drug release study

We carried out in vitro release study on F1, F2, F3, F4, F5, and F6. It was noted that F1 released 37.59% drug, F2 released 34.40% drug, F3 released 33.80% drug, F4 released 28.12% drug, F5 released 25.43% drug, and F6 released 22.34% drug after 5 hrs. The study was further carried out for another 5hrs and F1, F2, F3, F4, F5 and F6 showed 74.97%, 69.28%, 68.89%, 55.53%, 49.95%, 48.85% drug release respectively after 10hrs of the study. The samples which have 1g of sodium alginate i.e., F1, F2, and F3 samples comparatively release more drug than the samples containing 0.5g of sodium alginate i.e., F4, F5 and F6 sample. Probably the ratio of polymer effects the release of drug from the beads. Increase in concentration of polymer in a sample increases cross-linkage, which would limit drug release from the beads.

The in vitro release study of formulated magnetic beads namely F1, F2, F3, F4, F5, and F6, was conducted to assess their drug release profiles (figure 20). After an initial 5-hour observation period, it was observed that F1 exhibited a drug release of 37.59%, F2 released 34.40% of the drug, F3 released 33.80%, F4 released 28.12%, F5 released 25.43%, and F6 released 22.34%.

Subsequently, the study extended for another 5 hours, totalling 10 hours of examination. At the end of this extended period, the drug release percentages were as follows: F1, 74.97%; F2, 69.28%; F3, 68.89%; F4, 55.53%; F5, 49.95%; and F6, 48.85%.

An interesting observation emerged regarding the influence of sodium alginate concentration on drug release. The formulations containing 1g of sodium alginate (F1, F2, and F3) exhibited comparatively higher drug release than those with 0.5g of sodium alginate (F4, F5, and F6). This observation suggests that the polymer-to-drug ratio plays a significant role in drug release kinetics. This is likely due to the fact that the higher concentration of sodium alginate results in increase in cross-linkage, which makes it more difficult for the drug to diffuse out of the beads.

The results of this study suggest that the amount of sodium alginate used in the formulation of magnetic beads can have a significant impact on the release of drug from the beads. Formulations with a higher concentration of sodium alginate may be more suitable for applications where a slow and sustained release of drug is desired. Individual dissolution calculations of all formulations have been summarized in table 11, 12, 13, 14,15 and 16.

Table 11: %CDR Calculation of F1 formulation

Time (hrs)	Absorbance	Concentration (μg)	Cumulative amount in 600ml	Cumulative concentration in mg	Cumulative % drug release
0.5	0.036	0.970099668	582.0598007	0.582059801	2.910299003
1	0.089	2.73089701	1638.538206	1.638538206	8.19269103
2	0.164	5.222591362	3133.554817	3.133554817	15.66777409
3	0.242	7.813953488	4688.372093	4.688372093	23.44186047
4	0.312	10.13953488	6083.72093	6.08372093	30.41860465
5	0.384	12.53156146	7518.936877	7.518936877	37.59468439
6	0.459	15.02325581	9013.953488	9.013953488	45.06976744
7	0.535	17.54817276	10528.90365	10.52890365	52.64451827
8	0.612	20.10631229	12063.78738	12.06378738	60.31893688
9	0.687	22.59800664	13558.80399	13.55880399	67.79401993
10	0.759	24.99003322	14994.01993	14.99401993	74.97009967

Table 12: %CDR Calculation of F2 formulation

Time (hrs)	Absorbance	Concentration (μg)	Cumulative amount in 600ml	Cumulative concentration in mg	Cumulative % drug release
0.5	0.031	0.803986711	482.3920266	0.482392027	2.411960133
1	0.085	2.598006645	1558.803987	1.558803987	7.794019934
2	0.149	4.724252492	2834.551495	2.834551495	14.17275748
3	0.215	6.916943522	4150.166113	4.150166113	20.75083056
4	0.284	9.209302326	5525.581395	5.525581395	27.62790698
5	0.352	11.46843854	6881.063123	6.881063123	34.40531561
6	0.42	13.72757475	8236.54485	8.23654485	41.18272425
7	0.503	16.48504983	9891.0299	9.8910299	49.4551495
8	0.571	18.74418605	11246.51163	11.24651163	56.23255814
9	0.643	21.13621262	12681.72757	12.68172757	63.40863787
10	0.702	23.09634551	13857.80731	13.85780731	69.28903654

Table 13: %CDR Calculation of F3 formulation

Time (hrs)	Absorbance	Concentration(µg)	Cumulative amount in 600ml	Cumulative concentration in mg	Cumulative % drug release
0.5	0.035	0.936877076	562.1262458	0.562126246	2.810631229
1	0.098	3.029900332	1817.940199	1.817940199	9.089700997
2	0.152	4.823920266	2894.352159	2.894352159	14.4717608
3	0.213	6.850498339	4110.299003	4.110299003	20.55149502
4	0.278	9.009966777	5405.980066	5.405980066	27.02990033
5	0.346	11.26910299	6761.461794	6.761461794	33.80730897
6	0.431	14.09302326	8455.813953	8.455813953	42.27906977
7	0.514	16.85049834	10110.299	10.110299	50.55149502
8	0.568	18.64451827	11186.71096	11.18671096	55.93355482
9	0.632	20.77076412	12462.45847	12.46245847	62.31229236
10	0.698	22.96345515	13778.07309	13.77807309	68.89036545

Table 14: %CDR Calculation of F4 formulation

Time (hrs)	Absorbance	Concentration(µg)	Cumulative amount in 600ml	Cumulative concentration in mg	Cumulative % drug release
0.5	0.03	0.77076412	462.4584718	0.462458472	2.312292359
1	0.066	1.966777409	1180.066445	1.180066445	5.900332226
2	0.134	4.225913621	2535.548173	2.535548173	12.67774086
3	0.187	5.986710963	3592.026578	3.592026578	17.96013289
4	0.243	7.84717608	4708.305648	4.708305648	23.54152824
5	0.289	9.375415282	5625.249169	5.625249169	28.12624585
6	0.343	11.16943522	6701.66113	6.70166113	33.50830565
7	0.404	13.19601329	7917.607973	7.917607973	39.58803987
8	0.459	15.02325581	9013.953488	9.013953488	45.06976744
9	0.516	16.91694352	10150.16611	10.15016611	50.75083056
10	0.564	18.51162791	11106.97674	11.10697674	55.53488372

Table 15: %CDR Calculation of F5 formulation

Time (hrs)	Absorbance	Concentration (µg)	Cumulative amount in 600ml	Cumulative concentration in mg	Cumulative % drug release
0.5	0.022	0.504983389	302.9900332	0.302990033	1.514950166
1	0.06	1.76744186	1060.465116	1.060465116	5.302325581
2	0.117	3.661129568	2196.677741	2.196677741	10.9833887
3	0.181	5.787375415	3472.425249	3.472425249	17.36212625
4	0.224	7.215946844	4329.568106	4.329568106	21.64784053
5	0.262	8.478405316	5087.043189	5.087043189	25.43521595
6	0.315	10.23920266	6143.521595	6.143521595	30.71760797
7	0.362	11.80066445	7080.398671	7.080398671	35.40199336
8	0.427	13.96013289	8376.079734	8.376079734	41.88039867
9	0.471	15.42192691	9253.156146	9.253156146	46.26578073
10	0.508	16.65116279	9990.697674	9.990697674	49.95348837

Table 16: %CDR Calculation of F6 formulation

Time	Absorbance	Concentration (µg)	Cumulative amount in 600ml	Cumulative concentration in mg	Cumulative % drug release
0.5	0.014	0.239202658	143.5215947	0.143521595	0.717607973
1	0.065	1.933554817	1160.13289	1.16013289	5.800664452
2	0.108	3.362126246	2017.275748	2.017275748	10.08637874
3	0.152	4.823920266	2894.352159	2.894352159	14.4717608
4	0.198	6.352159468	3811.295681	3.811295681	19.05647841
5	0.231	7.448504983	4469.10299	4.46910299	22.34551495
6	0.288	9.342192691	5605.315615	5.605315615	28.02657807
7	0.334	10.87043189	6522.259136	6.522259136	32.61129568
8	0.372	12.13289037	7279.734219	7.279734219	36.3986711
9	0.422	13.79401993	8276.41196	8.27641196	41.3820598
10	0.497	16.28571429	9771.428571	9.771428571	48.85714286
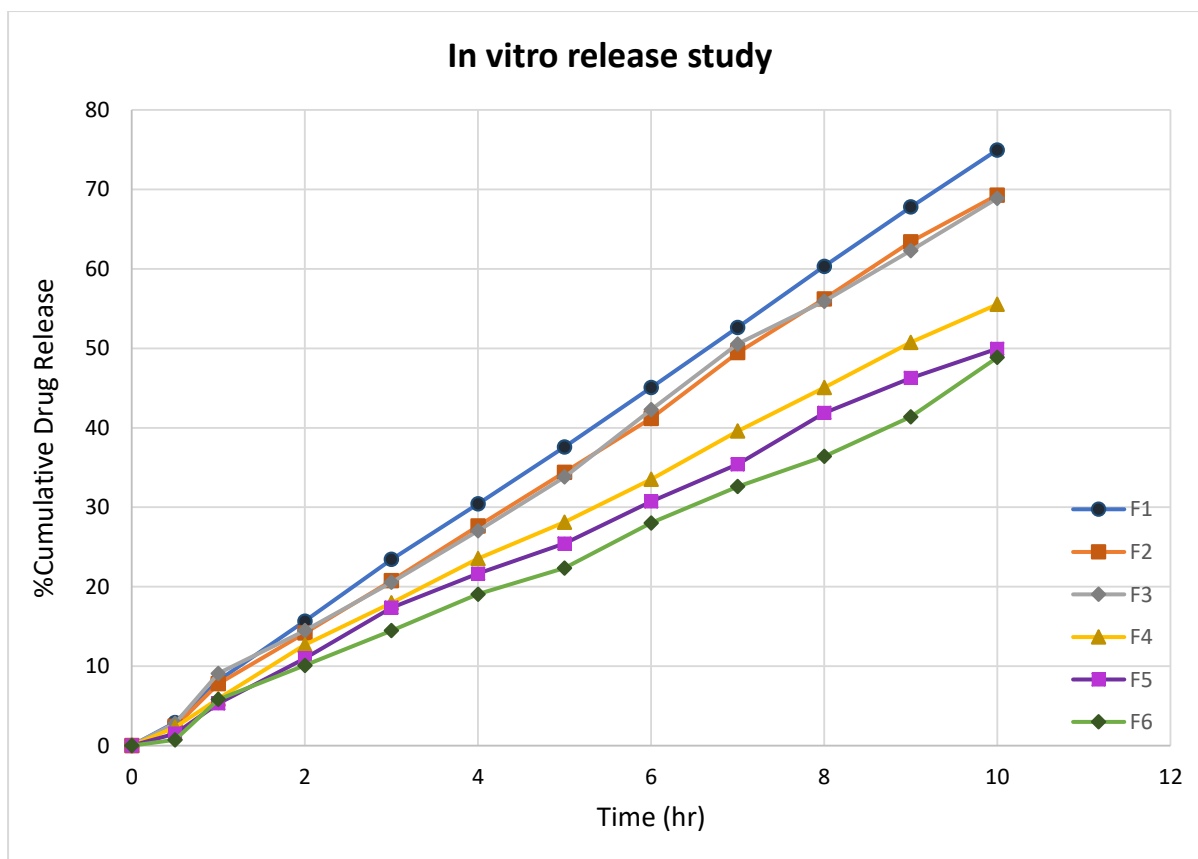
Figure 20: % Cumulative drug release vs. Time of F1, F2, F3, F4,

F5 and F6.

6.14 Release Kinetics

The release of a drug from the nanoparticle-based formulation depends on many factors including, pH, temperature, drug solubility, polymer amount, desorption of the surface-bound drug, drug diffusion through the nanoparticle matrix, nanoparticle matrix swelling and erosion, and the combination of erosion and diffusion. Magnetic nanoparticles comprise of drug, magnetic material, and polymer where the drug is physically and uniformly dispersed, and the drug is released following some mechanism. Korsmeyer-Peppas model describes drug release from a polymeric system considering non-Fickian mechanisms transport (0.45<n< 0.89) which occurs when the diffusion is entirely controlled by stress-induced relaxations of polymer chains. The release mechanism approaches zero order when exponent n =0.89-1 (case II transport).

After analyzing data obtained from Korsmeyer Peppas it was observed that n values in all formulations are from 0.917 to 0.965 which fall in the range of 0.89-1 indicating Case II transport and it complies with zero order. Data obtained by using Zero order equation (table 18, figure 21) we observed R^2 values of release profiles of all formulations as 0.9951 to 0.9996 confirming the linearity of profiles. The mechanism of drug release conforms to that of zero

order too. The profiles obtained from the Hixon- Crowell model are linear as supported by the R2 values (0.9951- 0.9996). The release mechanism conforms to that of the Hixon- Crowell model if it is assumed that the structure of particles gradually decreases keeping the shape of initial particles. The profiles obtained by using the Higuchi model and First-order model show less linearity compared to that of other models Korsmeyer Peppas, Zero order, and Hixon-Crowell model. Table 17 presents the summary of r^2 value of various models. Table 19, 20, 21, 22 represent summary of 1st order kinetic, Higuchi model, Hixon-Crowell model, Korsmeyer Peppas respectively and figure 22,23,24, and 25 presents

Table 17: Summary of r^2 value of various models

Code	Zero order	First order	Higuchi	Hixson-Crowell	Korsmeyer-Peppas	
	r2	r2	r2	r2	r2	n
F1	0.9996	0.9676	0.9733	0.9996	0.9998	0.963
F2	0.9993	0.9757	0.9699	0.9933	0.9986	0.965
F3	0.9978	0.9772	0.9677	0.9978	0.9919	0.924
F4	0.9988	0.9904	0.9767	0.9988	0.9985	0.957
F5	0.9968	0.9936	0.9799	0.9968	0.9973	0.963
F6	0.9951	0.9816	0.9656	0.9951	0.9959	0.917

Table 18: Calculation of zero-order kinetics.

Zero order: cumulative % drug release vs. Time						
	2.5% Polymer				5% Polymer	
Time	F1	F2	F3	F4	F5	F6
0.5	2.910299	2.41196	2.810631	2.312292	1.51495	0.717608
1	8.192691	7.79402	9.089701	5.900332	5.302326	5.800664
2	15.66777	14.17276	14.47176	12.67774	10.98339	10.08638
3	23.44186	20.75083	20.5515	17.96013	17.36213	14.47176
4	30.4186	27.62791	27.0299	23.54153	21.64784	19.05648
5	37.59468	34.40532	33.80731	28.12625	25.43522	22.34551
6	45.06977	41.18272	42.27907	33.50831	30.71761	28.02658
7	52.64452	49.45515	50.5515	39.58804	35.40199	32.6113
8	60.31894	56.23256	55.93355	45.06977	41.8804	36.39867
9	67.79402	63.40864	62.31229	50.75083	46.26578	41.38206
10	74.9701	69.28904	68.89037	55.53488	49.95349	48.85714
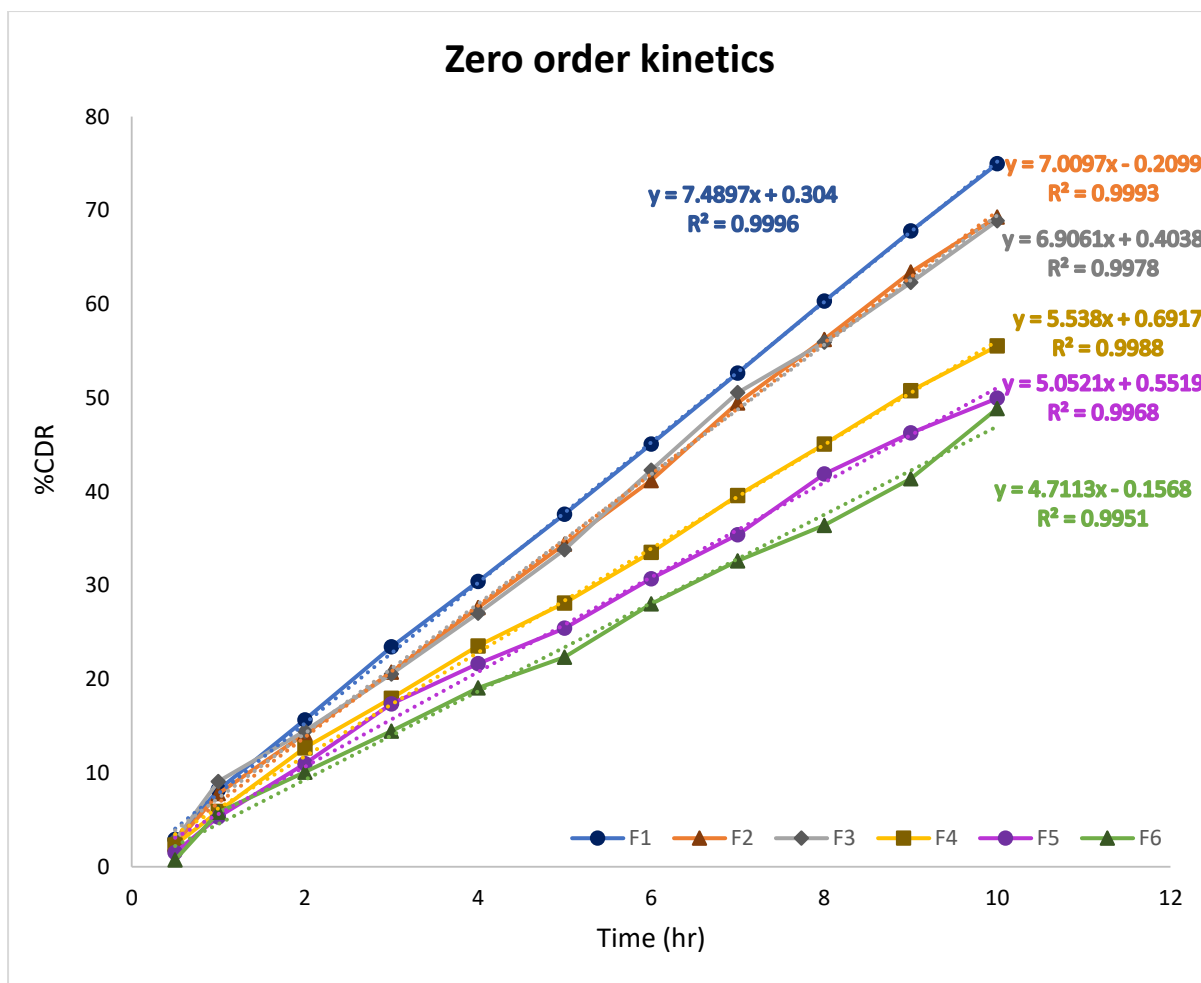
Figure 21: Zero-order release kinetics.

Table 19: Calculation of first-order kinetics

Time	2.5% Polymer			5% Polymer		
	F1	F2	F3	F4	F5	F6
0.5	1.987173	1.989397	1.987619	1.98984	1.99337	1.996872
1	1.962877	1.964759	1.958613	1.973588	1.976339	1.974048
2	1.925994	1.933625	1.93211	1.941125	1.949471	1.953825
3	1.883991	1.898995	1.900086	1.914025	1.917179	1.93211
4	1.842493	1.859571	1.863145	1.883426	1.894051	1.908182
5	1.795222	1.816869	1.82081	1.85657	1.872534	1.890167
6	1.739811	1.769505	1.761333	1.822767	1.840623	1.857172
7	1.67537	1.703677	1.694153	1.781123	1.810219	1.828587

8	1.598583	1.641151	1.644108	1.739811	1.764323	1.803466
9	1.507937	1.563379	1.5762	1.692399	1.730251	1.768031
10	1.398459	1.487293	1.492895	1.648019	1.699374	1.708785

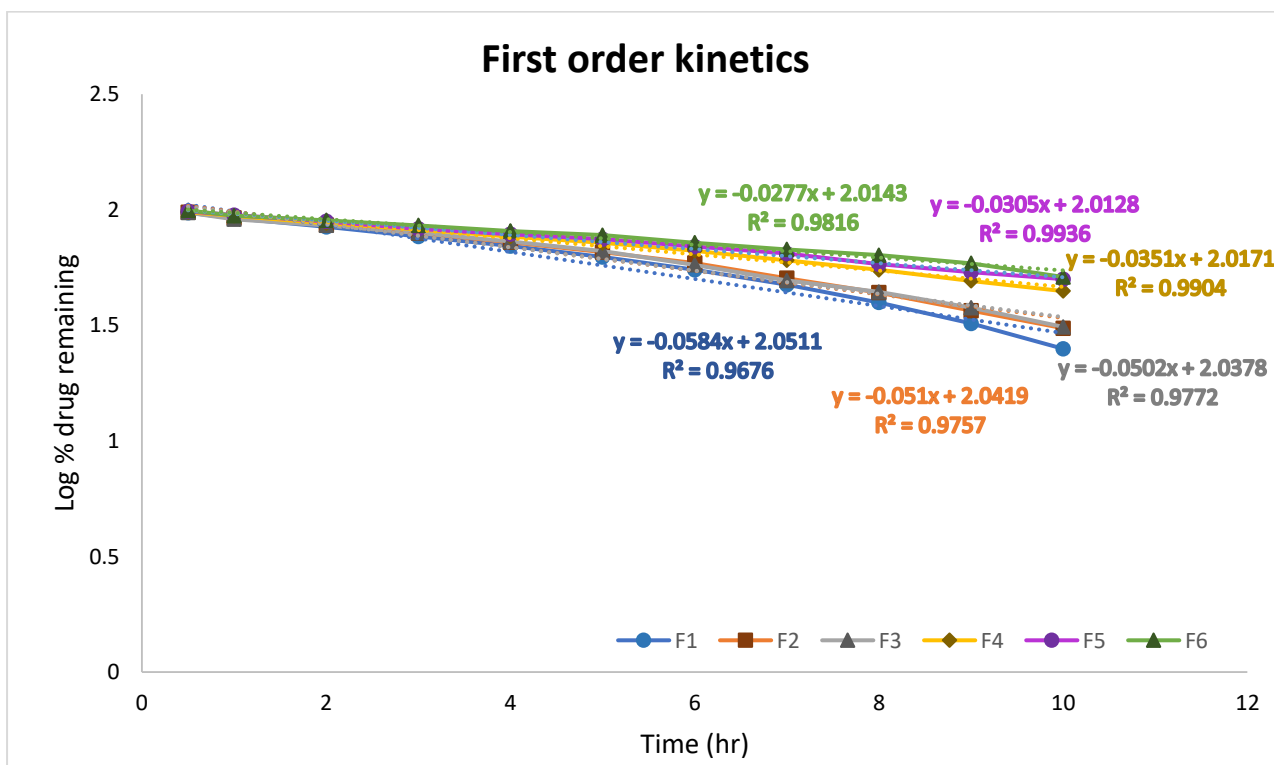**Figure 22:** First-order release kinetics.

Table 20: Calculation of Higuchi model

Higuchi: %CDR vs. sq. root of time						
				2.5% Polymer		5% Polymer
Time (hrs)	Sq root of time	F1	F2	F3	F4	F5	F6
0.5	0.707106781	2.910299	2.41196	2.810631	2.312292	1.51495	0.717608
1	1	8.192691	7.79402	9.089701	5.900332	5.302326	5.800664
2	1.414213562	15.66777	14.17276	14.47176	12.67774	10.98339	10.08638
3	1.732050808	23.44186	20.75083	20.5515	17.96013	17.36213	14.47176
4	2	30.4186	27.62791	27.0299	23.54153	21.64784	19.05648
5	2.236067977	37.59468	34.40532	33.80731	28.12625	25.43522	22.34551
6	2.449489743	45.06977	41.18272	42.27907	33.50831	30.71761	28.02658
7	2.645751311	52.64452	49.45515	50.5515	39.58804	35.40199	32.6113

| 8 | 2.828427125 | 60.31894 | 56.23256 | 55.93355 | 45.06977 | 41.8804 | 36.39867 |
| 9 | 3 | 67.79402 | 63.40864 | 62.31229 | 50.75083 | 46.26578 | 41.38206 |
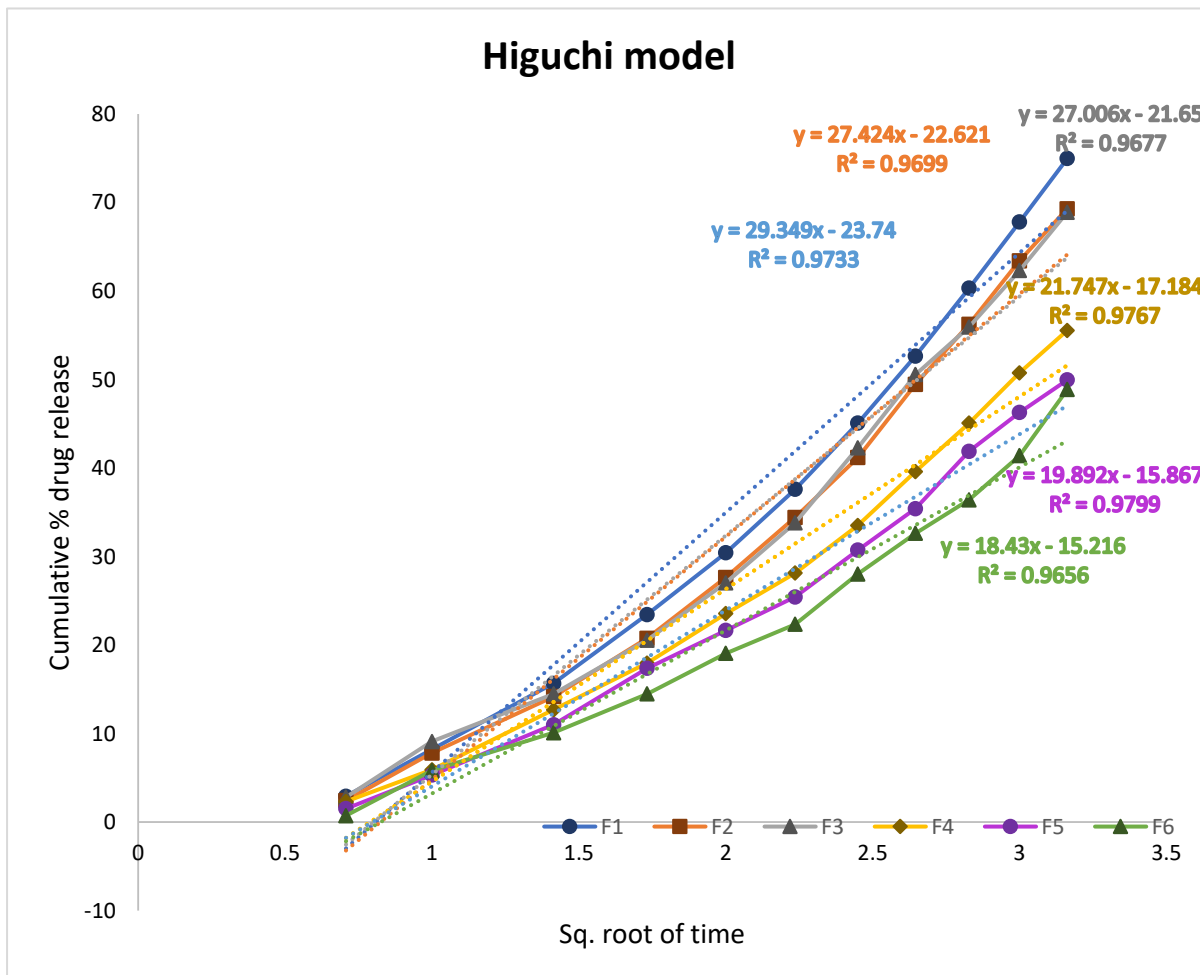
Figure 23: Higuchi release kinetics.

Table 21: Calculation of Hixon-Crowell model

Time (hrs)	Cube root of % drug released.					
	F1	F2	F3	F4	F5	F6
0.5	32.36323	32.52935	32.39646	32.56257	32.82835	33.09413
1	30.60244	30.73533	30.30343	31.36656	31.56589	31.39978
2	28.11074	28.60908	28.50941	29.10742	29.6722	29.97121
3	25.51938	26.41639	26.48283	27.34662	27.54596	28.50941
4	23.1938	24.12403	24.32337	25.48616	26.11739	26.98117

5	20.80177	21.86489	22.06423	23.95792	24.85493	25.88483
6	18.31008	19.60576	19.24031	22.1639	23.09413	23.99114
7	15.78516	16.84828	16.48283	20.13732	21.53267	22.4629
8	13.22702	14.58915	14.68882	18.31008	19.3732	21.20044
9	10.73533	12.19712	12.56257	16.41639	17.91141	19.53931
10	8.3433	10.23699	10.36988	14.82171	16.68217	17.04762
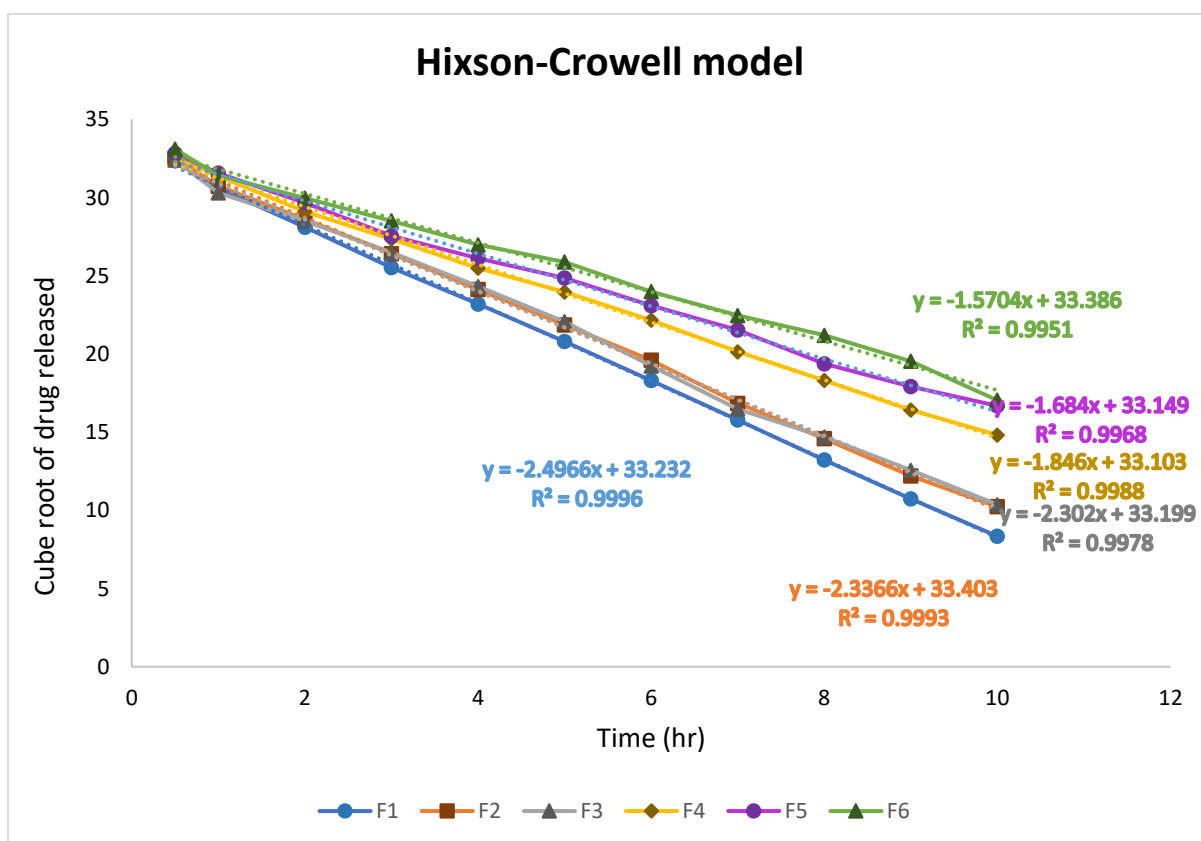
Figure 24: Hixon-Crowell Kinetics.

Table 22: Calculation of Korsmeyar-Peppas model

Log time	F1	F2	F3	F4	F5	F6
-0.30103	0.463938	0.38237	0.448804	0.364043	0.180398	-0.14411
0	0.913427	0.891762	0.95855	0.770876	0.724466	0.763478
0.30103	1.195007	1.151454	1.160521	1.103042	1.040736	1.003735
0.477121	1.369992	1.317035	1.312843	1.25431	1.239603	1.160521

| 0.60206	1.483139	1.441348	1.431844	1.371835	1.335415	1.280043
0.69897	1.575126	1.536626	1.529011	1.449112	1.405435	1.34919
0.778151	1.653885	1.614715	1.626125	1.525152	1.487387	1.44757
0.845098	1.721353	1.694212	1.703734	1.597564	1.549028	1.513368
0.90309	1.780454	1.749988	1.747672	1.653885	1.622011	1.561086
0.954243	1.831191	1.802148	1.794574	1.705443	1.66526	1.616812
1	1.874888	1.840665	1.838158	1.744566	1.698566	1.688928
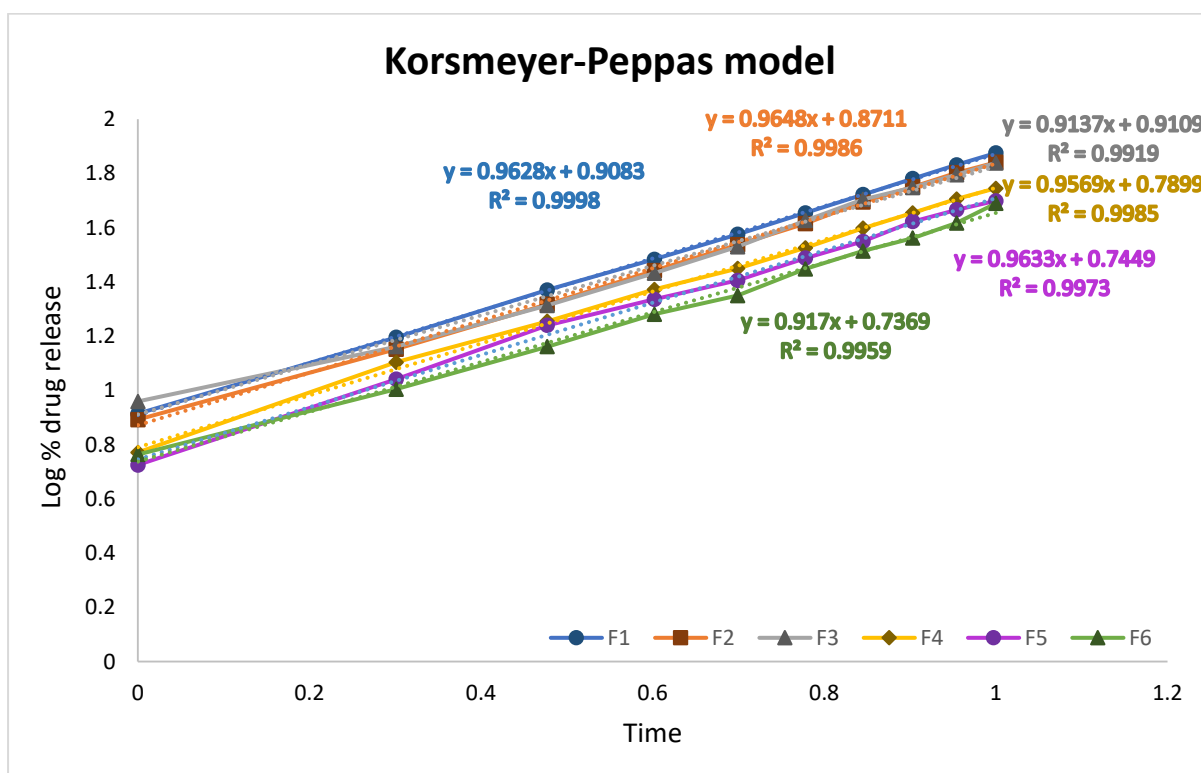
Figure 25: Korsmeyar-Peppas kinetics.

Chapter 7

Summary and Conclusion

7.0 Summary and conclusion

Magnetic nanoparticles have emerged as a promising tool in the field of targeted drug delivery, biosensing, and MRI. The efficiency of these nanoparticles in capturing and delivering drugs to specific targets depends on several physical parameters, including their magnetic properties, size, field strength, and field geometry. The size of MNP beads and release rate of drug can be adjusted by altering ratio of polymer. Magnetic property, field strength can be altered according to need by altering the concentration of magnetite in the bead. Magnetic property of the beads can be also be affected by altering the external field strength. MNP beads, because of their diminutive size and round shape, can be formulated into a variety of dosage forms, including parenteral, aerosol, topical, tablets, and capsules. Additionally, physiological parameters such as the depth to target, rate of blood flow, vascular supply, and body weight must also be taken into consideration when designing a magnetic nanoparticle-based targeting system. The synthesis of magnetic nanoparticles involves several methods, including co-precipitation, sol-gel, microemulsion, and thermal decomposition. These methods can be used to produce nanoparticles of different sizes and shapes, which can be further modified by tagging them with specific molecules to interact with biological entities. The surface chemistry of these nanoparticles can also be altered by applying various coating materials, but the advantages and disadvantages of each coating material must be weighed before selection. The functional group of MNPs prevents them from aggregating and allows for the attachment of drugs and other ligands for specific targeting. Ultrasmall superparamagnetic iron oxide nanoparticles (USPIONs) are smaller than superparamagnetic iron oxide nanoparticles (SPIONs) and can remain in the bloodstream for a longer period of time, making them less likely to be attacked by the immune system. Several types of SPIONs and USPIONs have been authorized for usage in the past. Furthermore, magnetic nanoparticles have shown potential in theragnostic applications, where they can be used for both diagnosis and therapy. The ability of these nanoparticles to act as contrast agents in MRI and to deliver drugs to specific targets makes them a promising tool in the field of medicine.

The synergistic effect localized magnetic hyperthermia shows promising results in treating diseases. The MNPs have great importance and are widely used in targeted drug delivery. As compared to conventional drug delivery, MNPs based drug delivery administration can minimize the doses of drugs and subsequently reduce the side effects.

Before preparation of drug loaded MNPs bead for targeted drug delivery, pre-formulation studies are necessary for drug and polymers used in formulation. For the drug candidate melting point was determined and its solubility was assessed. The physical characteristics, melting point of aceclofenac were examined. The λmax of aceclofenac was determined and standard curve was plotted. Instrumental analysis (FTIR, and PXRD) was performed for drug, magnetite, blank MNPs beads (having only polymers and magnetite) and drug loaded MNPs beads (drug + magnetite + polymer) to check any interaction among ingredients. Particle size, and morphology were also assessed for the MNPs beads by SEM, TEM, and AFM. VSM was carried out to study the magnetic characteristic of the prepared samples.

- SEM and TEM analysis provided insights into the surface morphology and dimensions of MNPs beads. The smooth surface of these beads suggests effective polymer coating, with no notable fractures observed.

- AMF analysis revealed magnetite, F2, and F5 exhibited some small agglomeration of Fe3O4 nanoparticles, as revealed by height distribution studies.

- From FTIR spectra, it was concluded that there was no chemical interference between drug and polymers. Some of the peaks of drug are not visible in the FTIR spectrum of prepared formulation. It suggests that some functional groups of drugs form weak Vander Waals force with that of polymers. Due to drug entrapment, the characteristic peaks of the polymers also have reduced in intensity of drug loaded MNPs beads when compared with blank MNPs beads spectra. The characteristic peaks noted for magnetite samples have also reduced in intensity in MNPs beads. The blank sample did not show any significant peaks related to aceclofenac, which confirms the absence of drug in the sample.

- From PXRD data, the crystalline nature of aceclofenac was confirm by sharp peak. The decrease in the diffraction pattern in F2 and F5 which is noted, is may be the result of polymer interaction. It appears that the crystalline character of pure aceclofenac changes to an amorphous form in drug loaded MNP beads, as evidenced by a considerable decrease in the diffraction pattern.

- From VSM, it is confirmed that the magnetite samples have high saturation magnetization and very low remanent magnetization. This means that they can be easily magnetized and demagnetized. The polymeric coating on F2 and F5 samples increases their coercivity. This means that it is more difficult to reverse the magnetization of these samples. The remanent magnetization of F2 and F5 were negligible which makes them suitable for targeted drug

delivery. This means that these samples will not retain any magnetization after being exposed to a magnetic field, which is important for targeted drug delivery.

Chapter 8

References

References

1. Deore, P. and Hnawate, R.M., 2017. Nanoparticle-novel drug delivery system: A Review. PharmaTutor, 5(5), pp.9-23.

2. Laurent, S., Forge, D., Port, M., Roch, A., Robic, C., Vander Elst, L. and Muller, R.N., 2008. Magnetic iron oxide nanoparticles: synthesis, stabilization, vectorization, physicochemical characterizations, and biological applications. Chemical reviews, 108(6), pp.2064-2110.

3. Anik, M.I., Hossain, M.K., Hossain, I., Mahfuz, A.M.U.B., Rahman, M.T. and Ahmed, I., 2021. Recent progress of magnetic nanoparticles in biomedical applications: A review. *Nano Select*, *2*(6), pp.1146-1186.

4. An-Hui Lu Dr., E. L. Salabas Dr., Ferdi Schüth Prof. Dr. (2007) 'Magnetic Nanoparticles: Synthesis, Protection, Functionalization, and Application'. *Angewandte Chemie International Edition* 46(8):1222-1244 https://doi.org/10.1002/anie.200602866

5. Dagmar Högemann, Vasilis Ntziachristos, Lee Josephson et al (2002) 'High throughput magnetic resonance imaging for evaluating targeted nanoparticle probes'. *Bioconjug. Chem*. 13(1):116–121.

6. Fortin JP, Gazeau F, Wilhelm C. (2008) 'Intracellular heating of living cells through Néel relaxation of magnetic nanoparticles'. *European Biophysics J*. 37(2):223-8. DOI: 10.1007/s00249-007-0197-4. Epub 2007 Jul 20. PMID: 17641885.

7. Billotey C, Wilhelm C, Devaud M, Bacri JC, Bittoun J, Gazeau F. (2003) 'Cell internalization of anionic maghemite nanoparticles: quantitative effect on magnetic resonance imaging'. *Magnetic Resonance in Medicine*. 49(4):646-54. doi: 10.1002/mrm.10418. PMID: 12652535.

8. Moroz P, Jones SK, Gray BN. (2002) 'Magnetically mediated hyperthermia: current status and future directions'. *Int J Hyperthermia*. 18(4):267-84. doi: 10.1080/02656730110108785. PMID: 12079583.

9. Dürr, S., Janko, C., Lyer, S., Tripal, P., Schwarz, M., Zaloga, J., Tietze, R. and Alexiou, C. (2013) 'Magnetic nanoparticles for cancer therapy'. *Nanotechnology Reviews*, 2 (4):395-409. https://doi.org/10.1515/ntrev-2013-0011

10. Flores-Rojas GG, López-Saucedo F, Vera-Graziano R, Mendizabal E, Bucio E.(2022) 'Magnetic Nanoparticles for Medical Applications: Updated Review'. *Macromol*. 2(3):374-390. https://doi.org/10.3390/macromol2030024

11. Wong Joanna, Prout Jeremy and Seifalian Alexander. 'Magnetic Nanoparticles: New Perspectives in Drug Delivery'. *Current Pharmaceutical Design* 2017; 23(20):2908-2917. https://dx.doi.org/10.2174/1381612823666170215104659

12. S.P. Vyas, R.K. Khar. Targeted and Controlled Drug Delivery – Novel Carrier Systems: Molecular Basis of Targeted Drug Delivery. CBS Publishers and Distributors; New Delhi: 2012: 38-40.

13. Q A Pankhurst, J Connolly, S K Jones and J Dobson. 'Applications of magnetic nanoparticles in biomedicine'. Journal of Physics D: Applied Physics. 2003; 36(13):167-181

14. Jon Dobson. 'Magnetic nanoparticles for drug delivery' *Drug Development Research.* 2006; 67(1):55–60

15. Abolfazl Akbarzadeh, Mohammad Samiei and Soodabeh Davaran. 'Magnetic nanoparticles: preparation, physical properties, and applications in biomedicine'.Nanoscale Research Letters 2012, 7(144):1-13 http://www.nanoscalereslett.com/content/7/1/144

16. Alejandra Sabín López, María Paredes Ramos, Roberto Herrero et al. 'Synthesis of magnetic green nanoparticle – Molecular imprinted polymers with emerging contaminants templates'. Journal of Environmental Chemical Engineering 2020, 8(4):103889 https://doi.org/10.1016/j.jece.2020.103889

17. Ghosal, K., Chatterjee, S., Thomas, S. et al. A Detailed Review on Synthesis, Functionalization, Application, Challenges, and Current Status of Magnetic Nanoparticles in the Field of Drug Delivery and Gene Delivery System. AAPS PharmSciTech 24, 25 (2023). https://doi.org/10.1208/s12249-022-02485-5.

18. Ahmadi S, Fazilati M, Nazem H, Mousavi SM. 'Green Synthesis of Magnetic Nanoparticles Using Satureja hortensis Essential Oil toward Superior Antibacterial/Fungal and Anticancer Performance'. Biomed Res Int. 2021 Jan 19;2021:8822645. doi: 10.1155/2021/8822645. PMID: 33542927; PMCID: PMC7840253.

19. Yen Pin Yew, Kamyar Shameli et al. 'Green Synthesis of Magnetite (Fe3O4) Nanoparticles Using Seaweed (Kappaphycus alvarezii) Extract'. Nanoscale Research Letters. 2016, 11(1):1-7.

20. Dhar, P. K., Saha, P., Hasan, M. K., Amin, M. K., & Haque, M. R. (2021). Green synthesis of magnetite nanoparticles using Lathyrus sativus peel extract and evaluation

of their catalytic activity. Cleaner Engineering and Technology, 3, 100117. doi:10.1016/j.clet.2021.100117

21. Lunge, S., Singh, S., & Sinha, A. (2014). Magnetic iron oxide (Fe3O4) nanoparticles from tea waste for arsenic removal. Journal of Magnetism and Magnetic Materials, 356, 21–31. doi:10.1016/j.jmmm.2013.12.008

22. Karade, V. C., Waifalkar, P. P., Dongle, T. D., Sahoo, S. C., Kollu, P., Patil, P. S., & Patil, P. B. (2017). Greener synthesis of magnetite nanoparticles using green tea extract and their magnetic properties. Materials Research Express, 4(9), 096102. doi:10.1088/2053-1591/aa892f

23. Kombaiah, K., Vijaya, J. J., Kennedy, L. J., Bououdina, M., Ramalingam, R. J., & Al-Lohedan, H. A. (2018). Okra extract-assisted green synthesis of CoFe 2 O 4 nanoparticles and their optical, magnetic, and antimicrobial properties. Materials Chemistry and Physics, 204, 410–419. doi:10.1016/j.matchemphys.2017.10

24. M., S., K., R. D., R., R., & T., T. (2020). Green synthesis of magnetic nanoparticles via Cinnamomum verum bark extract for biological application. Journal of Environmental Chemical Engineering, 104420. doi:10.1016/j.jece.2020.104420

25. Ahmad Fadli, Komalasari, Arisman Adnan et al. 'Synthesis of Magnetite Nanoparticles via Co-precipitation method.' IOP Conference Series: Materials Science and Engineering 622 (2019) 012013 IOP Publishing doi:10.1088/1757-899X/622/1/012013

26. K. Petcharoen a, A. Sirivat. 'Synthesis and characterization of magnetite nanoparticles via the chemical co-precipitation method.' Materials Science and Engineering: B 25 March 2012, 177(5):421-427 https://doi.org/10.1016/j.mseb.2012.01.003

27. Baker, I. (2018). Magnetic nanoparticle synthesis. Nanobiomaterials, 197–229. doi:10.1016/b978-0-08-100716-7.00009-x

28. Walid M Daoush. Co-Precipitation and Magnetic Properties of Magnetite Nanoparticles for Potential Biomedical Applications Journal of Nanomedecine Research 5(3): 00118. DOI: 10.15406/jnmr.2017.05.00118

29. Yazdani, F., & Seddigh, M. (2016). Magnetite nanoparticles synthesized by co-precipitation method: The effects of various iron anions on specifications. Materials Chemistry and Physics, 184, 318–323. doi: 10.1016/j.matchemphys.2016.09

30. Mohammadi, H., Nekobahr, E., Akhtari, J., Saeedi, M., Akbari, J., & Fathi, F. (2021). Synthesis and characterization of magnetite nanoparticles by co-precipitation method coated with biocompatible compounds and evaluation of in-vitro cytotoxicity. Toxicology Reports, 8, 331–336. doi:10.1016/j.toxrep.2021.01.012

31. Khalil, M. I. (2015). Co-precipitation in aqueous solution synthesis of magnetite nanoparticles using iron(III) salts as precursors. Arabian Journal of Chemistry, 8(2), 279–284. doi:10.1016/j.arabjc.2015.02.008

32. Nguyen, T. A., Nguyen, L. T. T., Bui, V. X., Nguyen, D. H. T., Lieu, H. D., Le, L. M. T., & Pham, V. (2020). Optical and magnetic properties of HoFeO3 nanocrystals prepared by a simple co-precipitation method using ethanol. Journal of Alloys and Compounds, 155098. doi:10.1016/j.jallcom.2020.155098

33. Jesus, A. C. B., Jesus, J. R., Lima, R. J. S., Moura, K. O., Almeida, J. M. A., Duque, J. G. S., & Meneses, C. T. (2020). Synthesis and magnetic interaction on concentrated Fe3O4 nanoparticles obtained by the co-precipitation and hydrothermal chemical methods. Ceramics International, 46(8), 11149–11153. doi:10.1016/j.ceramint.2020.01.13

34. Lassalle, V. L., Zysler, R. D., & Ferreira, M. L. (2011). Novel and facile synthesis of magnetic composites by a modified co-precipitation method. Materials Chemistry and Physics, 130(1-2), 624–634. doi:10.1016/j.matchemphys.2011.07

35. Sarah Belaid, Sophie Laurent et al (2013). 'A new approach to follow the formation of iron oxide nanoparticles synthesized by thermal decomposition.' Nanotechnology.24(5):1-8. DOI 10.1088/0957-4484/24/5/055705

36. Mythreyi Unni, Amanda M. Uhl et al. 'Thermal Decomposition Synthesis of Iron Oxide Nanoparticles with Diminished Magnetic Dead Layer by Controlled Addition of Oxygen'ACS Nano 2017, 11(2):2284–2303

37. P. Tartaj, M.P. Morales et al. 'Advances in magnetic nanoparticles for biotechnology applications' Journal of Magnetism and Magnetic Materials April 2005 290–291(1):28-34 https://doi.org/10.1016/j.jmmm.2004.11.155

38. Maity, D., Kale, S. N., Kaul-Ghanekar, R., Xue, J.-M., & Ding, J. (2009). Studies of magnetite nanoparticles synthesized by thermal decomposition of iron (III) acetylacetonate in tri(ethylene glycol). Journal of Magnetism and Magnetic Materials, 321(19), 3093–3098. doi:10.1016/j.jmmm.2009.05.020

39. Maity, D., Choo, S.-G., Yi, J., Ding, J., & Xue, J. M. (2009). Synthesis of magnetite nanoparticles via a solvent-free thermal decomposition route. Journal of Magnetism and Magnetic Materials, 321(9), 1256–1259. doi:10.1016/j.jmmm.2008.11.013

40. Maity, d., ding, j., & xue, j.-m. (2008). Synthesis of magnetite nanoparticles by thermal decomposition: time, temperature, surfactant and solvent effects. Functional Materials Letters, 01(03), 189–193. doi:10.1142/s1793604708000381

41. Hu, P., Kang, L., Chang, T., Yang, F., Wang, H., Zhang, Y., … Yang, Z. (2017). High saturation magnetization Fe 3 O 4 nanoparticles prepared by one-step reduction method in autoclave. Journal of Alloys and Compounds, 728, 88–92. doi:10.1016/j.jallcom.2017.08.290

42. Vuong, T. K. O., Tran, D. L., et . (2015). Synthesis of high-magnetization and monodisperse Fe 3 O 4 nanoparticles via thermal decomposition. Materials Chemistry and Physics, 163, 537–544. doi:10.1016/j.matchemphys.2015.08

43. J. A. López Pérez, M. A. López Quintela et al. 'Advances in the Preparation of Magnetic Nanoparticles by the Microemulsion Method' J. Phys. Chem. B 1997, 101(41):8045–8047

44. Ang Bee Chin, Iskandar Idris Yaacob. 'Synthesis and characterization of magnetic iron oxide nanoparticles via w/o microemulsion and Massart's procedure.' Journal of Materials Processing Technology. 1 August 2007, 191(1–3):235-237 https://doi.org/10.1016/j.jmatprotec.2007.03.011

45. Maqsood Ahmad Malik, Mohammad Younus Wani et al. 'Microemulsion method: A novel route to synthesize organic and inorganic nanomaterials: 1st Nano Update' Arabian Journal of Chemistry October 2012 5(4):397-417 https://doi.org/10.1016/j.arabjc.2010.09.027

46. María Salvador, Gemma Gutiérrez et al. 'Microemulsion Synthesis of Superparamagnetic Nanoparticles for Bioapplications.' International Journal of Molecular Science 2021 Jan 4;22(1):427. doi: 10.3390/ijms22010427

47. Pedro Tartaj, Maria del Puerto Morales et al. 'The preparation of magneticnanoparticles for applications in biomedicine.' Journal Of Physics D: Applied Physics July 2003, 36(13):R182-R197DOI:10.1088/0022-3727/36/13/202

48. Veronica I. Shubayev, Thomas R. Pisanic et al. 'Magnetic nanoparticles for theragnostics.' Advanced Drug Delivery Reviews 21 June 2009, 61(6):467-477 https://doi.org/10.1016/j.addr.2009.03.007

49. Kaarjel K. Narayanasamy, Joshua C. Price et al. 'Cytotoxic effect of PEI-coated magnetic nanoparticles on the regulation of cellular focal adhesions and actin stress fibres.' MaterialiaSeptember 2020, volume 13, 100848https://doi.org/10.1016/j.mtla.2020.100848

50. Cîrcu M, Nan A, Borodi G, Liebscher J, Turcu R. Refinement of Magnetite Nanoparticles by Coating with Organic Stabilizers. Nanomaterials. 2016; 6(12):228. https://doi.org/10.3390/nano6120228

51. Andra Mihaela Predescu, Ecaterina Matei et al. 'Synthesis and characterization of dextran-coated iron oxide nanoparticles.' R. Soc. open sci. March 20085(3): 171525. http://dx.doi.org/10.1098/rsos.171525

52. Isa Karimzadeh, Mustafa Aghazadeh et al. 'Superparamagnetic Iron Oxide (Fe3O4) Nanoparticles Coated with PEG/PEI for Biomedical Applications: A Facile and Scalable Preparation Route Based on the Cathodic Electrochemical Deposition Method', Advances in Physical Chemistry, vol. 2017, Article ID 9437487:1-7 2017. https://doi.org/10.1155/2017/9437487

53. Nan Zhu, Haining Ji et al. 'Surface Modification of Magnetic Iron Oxide Nanoparticles' Nanomaterials 2018, 8(10), 810; https://doi.org/10.3390/nano8100810

54. Muhammad Nadeem,Munir Ahmad et al. 'Magnetic Properties of Polyvinyl Alcohol and Doxorubicine Loaded Iron Oxide Nanoparticles for Anticancer Drug Delivery Applications' PLoS One. 2016; 11(6): e0158084. doi: 10.1371/journal.pone.0158084

55. Vicennati, P.; Giuliano, A.; Ortaggi, G.; Masotti, A. 'Polyethylenimine in medicinal chemistry.' Curr. Med. Chem. 2008, 15, 2826–2839.

56. Maria Camilla Operti, Alexander Bernhardt et al. 'PLGA-based nanomedicines manufacturing: Technologies overview and challenges in industrial scale-up.' International Journal of Pharmaceutics Volume 605, 10 August 2021, 120807 https://doi.org/10.1016/j.ijpharm.2021.120807

57. Lü JM, Wang X, Marin-Muller C, Wang H, Lin PH, Yao Q, Chen C. 'Current advances in research and clinical applications of PLGA-based nanotechnology'. Expert Rev Mol Diagn. 2009 May;9(4):325-41. doi: 10.1586/erm.09.15. PMID: 19435455; PMCID: PMC2701163

58. Yan Sheng a, Changsheng Liu et al. 'Long-circulating polymeric nanoparticles bearing a combinatorial coating of PEG and water-soluble chitosan' Biomaterials, April 2009,30(12):2340-2348

59. Jun Wang a b, Baolin Zhang et al. 'One-pot synthesis of water-soluble superparamagnetic iron oxide nanoparticles and their MRI contrast effects in the mouse brains.'Materials Science and Engineering: C March 2015, 48(1):416-423 https://doi.org/10.1016/j.msec.2014.12.026

60. Li, J.; Zhou, Y.; Li, M.; Xia, N.; Huang, Q.; Do, H.; Liu, Y.N.; Zhou, F. 'Carboxymethylated dextran-coated magnetic iron oxide nanoparticles for regenerable bioseparation'. J. Nanosci. Nanotechnol. 2011, 11(11):10187–10192

61. Rivera-Hernández, G.; Antunes-Ricardo, M.; Martínez-Morales, P.; Sánchez, M.L. 'Polyvinyl alcohol based-drug delivery systems for cancer treatment.' Int. J. Pharm. 2021, 600, 120478

62. Salunkhe, A.B.; Khot, V.M.; Thorat, N.D.; Phadatare, M.R.; Sathish, C.I.; Dhawale, D.S.; Pawar, S.H. 'Polyvinyl alcohol functionalized cobalt ferrite nanoparticles for biomedical applications.' Appl. Surf. Sci. 2013, 264:598–604

63. Wiseman, J., Goddard, C., McLelland, D. et al. 'A comparison of linear and branched polyethylenimine (PEI) with DCChol/DOPE liposomes for gene delivery to epithelial cells in vitro and in vivo'. Gene Ther 10, 1654–1662 (2003). https://doi.org/10.1038/sj.gt.3302050

64. : Abbas Zakeri, Mohammad Amin Jadidi Kouhbanani. et al. (2018) Polyethylenimine-based nanocarriers in co-delivery of drug and gene: a developing horizon, Nano Reviews & Experiments, 9:1, 1488497, DOI: 10.1080/20022727.2018.1488497

65. Wang, J.J.; Zeng, Z.W.; Xiao, R.Z.; Xie, T.; Zhou, G.L.; Zhan, X.R.; Wang, S.L. 'Recent advances of chitosan nanoparticles as drug carriers.'Int. J. Nanomed. 2011(6):765–774. DOI https://doi.org/10.2147/IJN.S17296

66. Song, G.; Cheng, L.; Chao, Y.; Yang, K.; Liu, Z. 'Emerging nanotechnology and advanced materials for cancer radiation therapy.'Adv. Mater. 2017, 29, 1700996.

67. Safari, A.; Sarikhani, A.; Shahbazi-Gahrouei, D.; Alamzadeh, Z.; Beik, J.; Dezfuli, A.S.; Mahabadi, V.P.; Tohfeh, M.; Shakeri-Zadeh, A. 'Optimal scheduling of the nanoparticle-mediated cancer photo-thermo-radiotherapy.' Photodiagn. Photodyn. Ther. 2020, 32, 102061

68. Sander Langereis, Tessa Geelen, Holger Grüll, Gustav J. Strijkers, Klaas Nicolay. 'Paramagnetic liposomes for molecular MRI and MRI-guided drug delivery.' NMR in Biomedicine 26(9):1195-1195 https://doi.org/10.1002/nbm.2971

69. Kamaly, N.; Miller, A.D. 'Paramagnetic liposome nanoparticles for cellular and tumour imaging.' Int. J. Mol. Sci. 2010, 11(4), 1759-1776; https://doi.org/10.3390/ijms1104175

70. Al-Jamal, W.T.; Kostarelos, K. 'Liposomes: From a clinically established drug delivery system to a nanoparticle platform for theranostic nanomedicine.'Acc. Chem. Res. 2011, 44, 1094–1104.

71. Mikhaylov, G.; Mikac, U.; Magaeva, A.A.; Itin, V.I.; Naiden, E.P.; Psakhye, I.; Babes, L.; Reinheckel, T.; Peters, C.; Zeiser, R.; et al. 'Ferri-liposomes as an MRI-visible drug-

delivery system for targeting tumours and their microenvironment.' Nat. Nanotechnol. 2011, 6, 594–602

72. Amnon Bar-Shir, Liat Avram, Shani Yariv-Shoushan, Debbie Anaby, Smadar Cohen, Niva Segev-Amzaleg, Dan Frenkel, Ofer Sadan, Daniel Offen, Yoram Cohen. 'Alginate-coated magnetic nanoparticles for noninvasive MRI of extracellular calcium' NMR in Biomedicine. 27(7):774-784 https://doi.org/10.1002/nbm.3117

73. Elsa M. Materón, Celina M. Miyazaki, Olivia Carr, Nirav Joshi, Paulo H.S. Picciani, Cleocir J. Dalmaschio, Frank Davis, Flavio M. Shimizu. 'Magnetic nanoparticles in biomedical applications: A review.'Applied Surface Science Advances1 December 2021, 6:100163 https://doi.org/10.1016/j.apsadv.2021.100163

74. Muzahidul I. Anik, M. Khalid Hossain, Imran Hossain, A. M. U. B. Mahfuz, M. Tayebur Rahman, Isteaque Ahmed. 'Recent progress of magnetic nanoparticles in biomedical applications: A review.' *Nano select* June 2021, 2(6): 1146-1186 https://doi.org/10.1002/nano.202000162

75. McBain SC, Yiu HH, Dobson J. Magnetic nanoparticles for gene and drug delivery. Int J Nanomedicine. 2008;3(2):169-80. doi: 10.2147/ijn.s1608. PMID: 18686777; PMCID: PMC2527670

76. Harry M. Williams. 'The application of magnetic nanoparticles in the treatment and monitoring of cancer and infectious diseases.' *Bioscience Horizons: The International Journal of Student Research,* Volume 10, 2017, hzx009, https://doi.org/10.1093/biohorizons/hzx009

77. Avasthi A, Caro C, Pozo-Torres E, Leal MP, García-Martín ML. 'Magnetic Nanoparticles as MRI Contrast Agents.' *Topics in Current Chemistry (Cham)*. 2020 May 7;378(3):40. doi: 10.1007/s41061-020-00302-w. Erratum in: Top Curr Chem (Cham). 2021 Jun 14;379(4):30. PMID: 32382832; PMCID: PMC8203530.

78. Nina Kostevšek. 'A Review on the Optimal Design of Magnetic Nanoparticle-Based T2 MRI Contrast Agents.' *Magnetochemistry* 2020, 6(1), 11; https://doi.org/10.3390/magnetochemistry6010011

79. K. Salimi, D. D. Usta, İ. Koçer, E. Çelik, A. Tuncel, Int. J. Biol. Macromol. 2018, 111, 178

80. A. Gómez Pérez, E. González-Martínez, C. R. Díaz Águila, D. A. González-Martínez, G. González Ruiz, A. García Artalejo, H. Yee-Madeira, Colloids Surfaces A Physicochem. *Eng. Asp.* 2020, 591, 124500.

81. Hei, A.L. and Cai, J.P., 2005. Development of a method for concentrating and purifying SARS coronavirus RNA by a magnetic bead capture system. *DNA and cell biology*, 24(8), pp.479-484.

82. Schwaminger, S.P., Blank-Shim, S.A., Scheifele, I., Pipich, V., Fraga-García, P. and Berensmeier, S., 2019. Design of interactions between nanomaterials and proteins: a highly affine peptide tag to bare iron oxide nanoparticles for magnetic protein separation. *Biotechnology journal*, *14*(3), p.1800055.

83. Blank, S.S.F.G.P., 2019. Shim SA Straub T. *Haslbeck M. Muraca F. Dawson KA Berensmeier S. ACS Omega*, *4*, pp.3790-3799.

84. Xie, X., Hu, Q., Ke, R., Zhen, X., Bu, Y. and Wang, S., 2019. Facile preparation of photonic and magnetic dual responsive protein imprinted nanomaterial for specific recognition of bovine hemoglobin. *Chemical Engineering Journal*, *371*, pp.130-137.

85. Xie, X., Hu, Q., Ke, R., Zhen, X., Bu, Y. and Wang, S., 2019. Facile preparation of photonic and magnetic dual responsive protein imprinted nanomaterial for specific recognition of bovine hemoglobin. *Chemical Engineering Journal*, *371*, pp.130-137.

86. Magnefy™ | Bangs Laboratories, Inc. (bangslabs.com), accessed on 7 May 2023.

87. ProMag® Particle Lines | Bangs Laboratories, Inc. (bangslabs.com), accessed on 7 May 2023.

88. COMPEL™ | Bangs Laboratories, Inc. (bangslabs.com), accessed on 7 May 2023.

89. BioMag® & BioMag®Plus Unconjugated Particles | Bangs Laboratories, Inc. (bangslabs.com), accessed on 7 May 2023.

90. BioMag® & BioMag®Plus Binding Proteins | Bangs Laboratories, Inc. (bangslabs.com), accessed on 7 May 2023.

91. Magnetic Separators | Bangs Laboratories, Inc. (bangslabs.com), accessed on 7 May 2023.

92. Magnefy™ COOH (polysciences.com), accessed on 8 May 2023.

93. ProMag® Microspheres - Polysciences, accessed on 8 May 2023.

94. BioMag® Amine Magnetic Immobilization Kit | Polysciences, Inc., accessed on 8 May 2023.

95. BioMag®Plus Carboxyl | Polysciences, Inc., accessed on 8 May 2023.

96. BioMag® Goat anti-Human IgG (Fc Specific) | Polysciences, Inc., accessed on 8 May 2023.

97. Magnetic particles – micromod Partikeltechnologie GmbH, accessed on 8 May 2023.

98. [Fluoreszente Magnetpartikel – micromod Partikeltechnologie GmbH](#), accessed on 8 May 2023.

99. [Magnetic Particles - Ademtech](#), accessed on 9 May 2023.

100. [MagMAX™ Plant DNA Isolation Kit (thermofisher.com)](#), accessed on 9 May 2023.

101. [MagMAX™ Cell-Free DNA Isolation Kit (thermofisher.com)](#), accessed on 9 May 2023.

102. [Magnetite Iron Oxide Nanoparticles-Polyimethylsiloxane - Nanorh](#), accessed on 9 May 2023.

103. Joseph Kost; Jackie Wolfrum; Robert Langer (1987). Magnetically enhanced insulin release in diabetic rats. , 21(12), 1367–1373. doi:10.1002/jbm.820211202

104. Liu, T.Y., Hu, S.H., Liu, K.H., Liu, D.M. and Chen, S.Y., 2008. Study on controlled drug permeation of magnetic-sensitive ferrogels: effect of Fe3O4 and PVA. Journal of Controlled Release, 126(3), pp.228-236.

105. Sulaiman, N.H., Ghazali, M.J., Majlis, B.Y., Yunas, J. and Razali, M., 2015. Superparamagnetic calcium ferrite nanoparticles synthesized using a simple sol-gel method for targeted drug delivery. Bio-medical materials and engineering, 26(s1), pp.S103-S110.

106. Kim, D.H., Nikles, D.E. and Brazel, C.S., 2010. Synthesis and characterization of multifunctional chitosan-MnFe2O4 nanoparticles for magnetic hyperthermia and drug delivery. *Materials*, *3*(7), pp.4051-4065.

107. Wu, H., Liu, G., Wang, X., Zhang, J., Chen, Y., Shi, J., Yang, H., Hu, H. and Yang, S., 2011. Solvothermal synthesis of cobalt ferrite nanoparticles loaded on multiwalled carbon nanotubes for magnetic resonance imaging and drug delivery. Acta biomaterialia, 7(9), pp.3496-3504.

108. Kamaraj, S., Palanisamy, U.M., Mohamed, M.S.B.K., Gangasalam, A., Maria, G.A. and Kandasamy, R., 2018. Curcumin drug delivery by vanillin-chitosan coated with calcium ferrite hybrid nanoparticles as carrier. *European journal of pharmaceutical sciences*, *116*, pp.48-60

109. Wang, G., Zhao, D., Ma, Y., Zhang, Z., Che, H., Mu, J., Zhang, X. and Zhang, Z., 2018. Synthesis and characterization of polymer-coated manganese ferrite nanoparticles as controlled drug delivery. *Applied surface science*, *428*, pp.258-263.

110. Ghanbari, M., Davar, F. and Shalan, A.E., 2021. Effect of rosemary extract on the microstructure, phase evolution, and magnetic behavior of cobalt ferrite

nanoparticles and its application on anti-cancer drug delivery. *Ceramics International*, *47*(7), pp.9409-9417.

111.   Amiri, M., Gholami, T., Amiri, O., Pardakhti, A., Ahmadi, M., Akbari, A., Amanatfard, A. and Salavati-Niasari, M., 2020. The magnetic inorganic-organic nanocomposite based on ZnFe2O4-Imatinib-liposome for biomedical applications, in vivo and in vitro study. *Journal of Alloys and Compounds*, *849*, p.156604.

112.   Arshadi, S. and Pishevar, A.R., 2021. Magnetic drug delivery effects on tumor growth. *Informatics in Medicine Unlocked*, *27*, p.100789.

113.   https://pubchem.ncbi.nlm.nih.gov/compound/Aceclofenac, accessed on 22 Aug 2023.

114.   https://go.drugbank.com/drugs/DB06736, accessed on 22 Aug 2023.

115.   Raza K, Kumar M, Kumar P, Malik R, Sharma G, Kaur M, Katare OP: Topical delivery of aceclofenac: challenges and promises of novel drug delivery systems. Biomed Res Int. 2014;2014:406731. doi: 10.1155/2014/406731. Epub 2014 Jun 18.

116.   Dooley M, Spencer CM, Dunn CJ: Aceclofenac: a reappraisal of its use in the management of pain and rheumatic disease. Drugs. 2001;61(9):1351-78.

117.   Sodium Alginate - Pharmacognosy (pharmacy180.com), accessed on 22 Aug 2023.

118.   https://pubchem.ncbi.nlm.nih.gov/compound/Ferric-chloride, accessed on 22 Aug 2023

119.   Haynes, William M., ed. (2011). CRC Handbook of Chemistry and Physics (92nd ed.). Boca Raton, FL: CRC Press. p. 4.69. ISBN 1-4398-5511-0.

120.   FERROUS SULFATE | CAMEO Chemicals | NOAA, accessed on 22 Aug 2023

121.   https://pubchem.ncbi.nlm.nih.gov/compound/Sodium-hydroxide#section=Related-Records, accessed on 24 Aug 2023.

122.   di-Sodium hydrogen phosphate dihydrate EMPROVE EXPERT Ph Eur,BP,USP 10028-24-7 (sigmaaldrich.com), accessed on 24 Aug 2023.

123.   https://pubchem.ncbi.nlm.nih.gov/compound/Disodium-phosphate-dihydrat, accessed on 24 Aug 2023

124.   Potassium dihydrogen phosphate/ di-sodium hydrogen phosphate certified reference material, traceable to NIST (SRM), traceable to PTB | Sigma-Aldrich (sigmaaldrich.com), accessed on 24 Aug 2023.

125.   https://pubchem.ncbi.nlm.nih.gov/compound/Potassium-dihydrogen-phosphate, accessed on 24 Aug 2023.

126. [Potassium Dihydrogen Orthophosphate | Uses, Dosage, Side Effects, FAQ - MedicinesFAQ](), accessed on 24 Aug 2023.

Lilhare, S., Mathew, S.B., Singh, A.K. and Carabineiro, S.A., 2021. Calcium alginate beads with entrapped iron oxide magnetic nanoparticles functionalized with methionine—A versatile adsorbent for arsenic removal. *Nanomaterials*, *11*(5), p.1345.

127. Shaker, S., Zafarian, S., Chakra, C.S. and Rao, K.V., 2013. Preparation and characterization of magnetite nanoparticles by sol-gel method for water treatment. International journal of innovative research in science, engineering and technology, 2(7), pp.2969-2973.

128. Rajbanshi, K., Bajracharya, R., Shrestha, A. and Thapa, P., 2014. Dissolution enhancement of aceclofenac tablet by solid dispersion technique. *International Journal of Pharma Sciences and Research*, *5*(4), pp.127-139.

129. Sevukarajan, M., Parveen, S.S., Nair, R. and Badivaddin, T.M., 2011. Preparation and characterization of aceclofenac salt by using triethanolamine. *Journal of Pharmaceutical Sciences and Research*, *3*(6), p.1280.

130. [IR Spectrum Table (sigmaaldrich.com)](), accessed on 25 Aug 2023.

131. Suresh, S., Gunasekaran, S. and Srinivasan, S., 2014. Studies of the molecular geometry, vibrational spectra, Frontier molecular orbital, nonlinear optical and thermodynamics properties of Aceclofenac by quantum chemical calculations. Spectrochimica Acta Part A: Molecular and Biomolecular Spectroscopy, 125, pp.239-251.

132. Namduri, H. and Nasrazadani, S., 2008. Quantitative analysis of iron oxides using Fourier transform infrared spectrophotometry. *Corrosion Science*, *50*(9), pp.2493-2497.

133. Ivashchenko, O., Jurga-Stopa, J., Coy, E., Peplinska, B., Pietralik, Z. and Jurga, S., 2016. Fourier transform infrared and Raman spectroscopy studies on magnetite/Ag/antibiotic nanocomposites. *Applied Surface Science*, *364*, pp.400-409.

134. Daemi, H. and Barikani, M., 2012. Synthesis and characterization of calcium alginate nanoparticles, sodium homopolymannuronate salt and its calcium nanoparticles. Scientia Iranica, 19(6), pp.2023-2028.

135. Papageorgiou, S.K., Kouvelos, E.P., Favvas, E.P., Sapalidis, A.A., Romanos, G.E. and Katsaros, F.K., 2010. Metal–carboxylate interactions in metal–alginate complexes studied with FTIR spectroscopy. *Carbohydrate research*, *345*(4), pp.469-473.

136. Mohammed, L., Gomaa, H.G., Ragab, D. and Zhu, J., 2017. Magnetic nanoparticles for environmental and biomedical applications: A review. *Particuology*, *30*, pp.1-14.

137. Maldonado-Camargo, L., Unni, M. and Rinaldi, C., 2017. Magnetic characterization of iron oxide nanoparticles for biomedical applications. *Biomedical Nanotechnology: Methods and Protocols*, pp.47-71.

138. Abdo, N.I., 2021. Comparative study between magnetite nanoparticles and magnetite/silver as a core/shell nanostructure. *Advances in Nanoparticles*, *10*(04), pp.115-122.

Chapter 9

Recent Publications

Main publications

1. Amrita Das, Prateep Sengupta, Jasmina Khanam, Kajal Ghosal, **Magnetic Nanoparticles (MNP), A Novel Drug Delivery and Diagnostic Platform: A review on its Basic Concepts, Synthesis, Surface Coating and Applications. (under review).**

2. Shreya Chatterjee1, Ankita Das, Amrita Das, Poulomi Roy, Pallab Datta, Sabu Thomas, Kajal Ghosal, **Synthesis, Evaluation, and Biocompatibility Study of Magnetite Nano Particles in Normal Cells and Cancer Cells for Health Care Application. (under review).**

Related Publications

1. Prateep Sengupta, Amrita Das, Debaldeb Datta, Jasmina Khanam, Kajal Ghosal, **Nanosponge: A New Platform for Antifungal Drug Delivery. Reactive and Functional Polymer (under review).**

2. Prateep Sengupta, Amrita Das, Jasmina Khanam, Pranab Kumar Mondal, Avirup Biswas, Jesil Mathew Arjan, Kajal Ghosal, **Griseofulvin loaded nanoporous scaffolds for topical antifungal drug delivery for extended duration. (patent under process).**